


Review

Ruby Deposits: A Review and Geological Classification

Gaston Giuliani^{1,*}, Lee A. Groat², Anthony E. Fallick³ , Isabella Pignatelli⁴ and Vincent Pardieu⁵

¹ Géosciences Environnement, Université Paul Sabatier, GET/IRD et Université de Lorraine, C.R.P.G./C.N.R.S., 15 rue Notre-Dame-des-Pauvres, BP 20, 54501 Vandœuvre, France

² Earth, Ocean and Atmospheric Sciences, University of British Columbia, Vancouver, BC V6T 1Z4, Canada; groat@mail.ubc.ca

³ Isotope Geosciences Unit, Scottish Universities Environmental Research Centre (S.U.E.R.C.), Rankine Avenue, East Kilbride, Glasgow G75 0QF, UK; anthony.fallick@glasgow.ac.uk

⁴ Georessources, Université de Lorraine, UMR 7539 CNRS-UL, BP 70239 Vandœuvre, France; isabella.pignatelli@univ-lorraine.fr

⁵ Field gemmologist & Consultant at VP Consulting, Manama, Bahrain; vince@fieldgemology.org

* Correspondence: giuliani@crpg.cnrs-nancy.fr; Tel.: +33-3-83594238

Received: 30 March 2020; Accepted: 23 June 2020; Published: 30 June 2020



Abstract: Corundum is not uncommon on Earth but the gem varieties of ruby and sapphire are relatively rare. Gem corundum deposits are classified as primary and secondary deposits. Primary deposits contain corundum either in the rocks where it crystallized or as xenocrysts and xenoliths carried by magmas to the Earth's surface. Classification systems for corundum deposits are based on different mineralogical and geological features. An up-to-date classification scheme for ruby deposits is described in the present paper. Ruby forms in mafic or felsic geological environments, or in metamorphosed carbonate platforms but it is always associated with rocks depleted in silica and enriched in alumina. Two major geological environments are favorable for the presence of ruby: (1) amphibolite to medium pressure granulite facies metamorphic belts and (2) alkaline basaltic volcanism in continental rifting environments. Primary ruby deposits formed from the Archean (2.71 Ga) in Greenland to the Pliocene (5 Ma) in Nepal. Secondary ruby deposits have formed at various times from the erosion of metamorphic belts (since the Precambrian) and alkali basalts (from the Cenozoic to the Quaternary). Primary ruby deposits are subdivided into two types based on their geological environment of formation: (Type I) magmatic-related and (Type II) metamorphic-related. Type I is characterized by two sub-types, specifically Type IA where xenocrysts or xenoliths of gem ruby of metamorphic (sometimes magmatic) origin are hosted by alkali basalts (Madagascar and others), and Type IB corresponding to xenocrysts of ruby in kimberlite (Democratic Republic of Congo). Type II also has two sub-types; metamorphic deposits *sensu stricto* (Type IIA) that formed in amphibolite to granulite facies environments, and metamorphic-metasomatic deposits (Type IIB) formed via high fluid-rock interaction and metasomatism. Secondary ruby deposits, i.e., placers are termed sedimentary-related (Type III). These placers are hosted in sedimentary rocks (soil, rudite, arenite, and silt) that formed via erosion, gravity effect, mechanical transport, and sedimentation along slopes or basins related to neotectonic motions and deformation.

Keywords: ruby deposits; classification; typology; magmatism; metamorphism; sedimentary; metasomatism; fluids; stable and radiogenic isotopes; genetic models; exploration

1. Introduction

Ruby is the red gem variety of the mineral corundum. The name corundum was introduced in the early 19th century by French mineralogist De Bournon when gemmological terminology was transformed

from a rather confusing system mainly based on color and origin into a system based on a new science: mineralogy. The term “corundum” likely originated from the Sanskrit *kuruvinda* meaning “hard stone”, which became *kurund* in vernacular. It was the name used by the native people met during the field expedition sent by De Bournon to describe the stones they were mining in Southern India.

If the name “corundum” originates from Sanskrit, in Sanskrit rubies were called *ratnaraj*, queen of precious stones and symbol of permanent internal fire. In Greco-Roman times, the reference to fire was also common; in 400 before Christ Theophrastus [1] related ruby to anthrax (coal). Two thousand years ago Pliny [2] called all red stones *carbunculus* (diminutive of *carbo*), which became *escarboucle* in old French. In the 11th century, the Arab scholar Al Biruni separated different types of rubies based on specific gravity and hardness, but his work remained unknown in Europe for centuries except possibly for a few scholars like French bishop Marbode [3] who, a few years later, also separated carbuncles into three different types.

The term “ruby” appeared in European languages during the Middle Ages. How and why it was introduced is not clear but it was used by [4]. It is derived from the Latin *ruber*, meaning red. It became popular and then, until the introduction of the word *corundum* in the 19th century, most red stones were just called rubies. Experts and authors commonly separated different types based on their origin: “Oriental Ruby” was used for stones mined from Burma or Ceylon (ruby), “Balas Ruby” for gems mined from the modern-day Tajikistan (spinel), and “Bohemian ruby” was used for gems coming traditionally from the modern-day Czech Republic (“red garnet”, either *pyrope*, *almandine*, and/or *spessartite*). However, as rubies, spinels, and garnets are often found in association and as new deposits were discovered, the system became very confusing. Ironically, the majority of the most famous rubies (like the “Black Prince Ruby” and the “Timur Ruby” of the British Crown Jewels or the “Cote de Bretagne Ruby” of the French Crown Jewels) that contributed significantly to the public recognition of the word “ruby” would actually, according to the new terminology based on mineralogy, be spinels. As gemmology is not simply about science, but also about history, art, and trade, these gems are still called by their historic “ruby” name, maintaining the taste for either curiosity, controversy, or confusion among many authors, particularly those with a non-scientific and/or historical background.

Currently we know that ruby is the chromium (Cr)-rich variety of corundum, but other chromophores such as vanadium (V) and iron (Fe) may be present in the structure of the mineral. The ideal formula of corundum is Al_2O_3 and it crystallizes in the trigonal system, with a hardness of 9 on the Mohs scale (while spinel and garnets crystallize in the cubic system and are softer with a hardness of 8). Unlike spinel and garnet, ruby is a dichroic mineral, which will show a different color (either purplish- or orangey-red) depending on which direction light travels inside the gem. In gemmology this is of critical importance because lapidaries, wishing to optimize the color from a rough stone by cutting it, can produce a red, a pinkish red, a purplish red, or an orangey-red stone, depending on how they decide to orientate and cut the gem.

The ruby industry is very lucrative [5] but it is far more complex than many ore industries such as iron, silver, or gold because the values of ruby do not depend only on weight or purity. The value depends on a much more complex quality, with grading systems including many artistic, subjective, and cultural aspects. In addition to the well-known and rather comprehensive system established by the diamond trade based on the 4Cs (i.e., color, clarity, cut, and carat weight of the gem) in the middle of the 20th century, with colored stones such as rubies additional factors have a critical importance for market value.

First, it has to be established that the gem was actually mined and was not produced from a factory. Synthetic rubies created either by flux, flame fusion, or some hydrothermal process appeared at the end of the 19th century. If the arrival of synthetics created some initial scandals and panic, the trade answered by establishing gemmological laboratories that were able to identify natural gems versus synthetics and thus re-establish the necessary confidence for the trade to grow.

Second, enhancements and treatments are also of importance to the final evaluation. To satisfy the strong demand for large clean rubies, some very efficient heat treatment techniques were developed in the 1990s in Thailand. These were different from the traditional blow-pipe technique used in Sri

Lanka for centuries and described by many travellers beginning with Al Burini in the 10–11th centuries. Whilst the blow pipe was used to remove the purplish aspect in some rubies, the new technique went further: using borax as a flux additive it could heal fractures in rubies and thus enable the cutting of larger stones. Due to this new treatment technique and the ones that followed, new deposits, such as Mong Hsu in eastern Myanmar, started to dominate the ruby trade in the early 1990s and Thailand increased its importance as the World's main ruby trading centre [6]. In the early 1990s, in Bangkok, it was very rare to find gem corundum that had not been heat-treated [7]. Drucker in [8], at the end of 1990, explained that the average price of ruby fell after controversy over its treatments. However, if the average price for rubies fell, prices for fine untreated rubies have exploded, particularly since the early 2000s (as observed in the reports from auction houses, many available online).

As the auction results show, not only did the prices for unheated rubies increase, but also the prices for unheated Myanmar rubies. Geographic origin is the last important factor to consider in establishing the value of a fine ruby (Figure 1). At this point it is critical to understand that, as fine rubies are both very rare but also very durable products, they usually survive for centuries after being mined, passing from one owner to another. As a consequence, the few very fine gems coming from existing mines are actually in competition with all the fine gems mined in the past, which are mainly from Myanmar (formerly known as Burma). Due to this, modern ruby traders are actually acting more like antique dealers than exploration geologists or Indiana Jones [9]. Public recognition and romance are very important factors contributing to demand for fine gemstones [10].

The assignment of a commercial value to ruby and other gems is carried out by gem merchants with the help of a few specialized gemmological laboratories providing independent third-party opinions. These labs provide answers for the following key questions [11]: (1) Is the gem the ruby variety of corundum? (2) Is it natural or synthetic ruby? (3) Has it been enhanced? (4) Where is it from (geographic origin)? If for most of these laboratories the answer to the first question is more or less routine work, the question about origin determination remains a great challenge [11]. The geographic origin is often controversial as in many cases it is based on expert opinion more than on provable facts [12–15]. Origin determination was introduced by Eduard Gübelin who worked on inclusions in gems using mainly microscopy [16,17], but also Raman and infrared spectroscopy. Such techniques are usually suitable for high value large rubies (that are usually never really free of mineral inclusions) but find their limits in the case of small clean stones or for heated stones (with inclusions that have been altered or even melted by heat treatment). Currently, these techniques are combined with the analysis of trace elements using energy dispersive X-ray fluorescence (EDXRF) and more especially since the early 2000s laser ablation-inductively coupled plasma-mass spectroscopy (LA-ICP-MS). To be able to produce origin reports, gemmological laboratories require sophisticated instrumentation, an experienced and qualified team, and a solid and very reliable reference collection.

The pricing of natural ruby is unique in terms of color and weight in carats. Currently if factory-grown synthetic rubies are cheap, if carving- or bead-grade treated rubies of low transparency and either dark or light color can be worth only a few dollars per kilo, a natural untreated ruby is still perhaps the world's most expensive gemstone. The best Myanmar rubies are more highly valued than an equivalent-sized flawless colorless diamond. The world record price for a single ruby sold at auction currently belongs to the Sunrise ruby, sold in 2015 for US\$32.42 million (US\$1.27 million per carat at 25.59 ct) [18]. In December 2015, the 15.04 ct Crimson Flame ruby was sold for US\$18.3 million (US\$1.21 million per ct). Another notable ruby is the 10.05 ct Ratnaraj, sold for US\$10.2 million (just over US\$1 million per ct) in November 2017. Fine-quality unheated rubies from the recently discovered Didy mine in Madagascar also command high prices [19]. A set of eight faceted rubies, ranging from seven to more than 14 cts in weight, had an estimated market value of US\$10 million [20]. The discovery of the Montepuez ruby deposits in Mozambique in May 2009 [21–23] and their exploitation by various companies including Gemfields Group Ltd. [24,25] changed the international ruby market [6,26]. A recent Competent Persons Report by SRK Consulting forecast production of 432 million carats from Montepuez over 21 years [27]. The resource at Montepuez is

divided into primary reserves of 253 million cts (projection of 115 cts per ton) and secondary (mainly colluvial) reserves of 179 million cts (projection of 7.07 cts per ton). Twelve Montepuez auctions held since June 2014 have generated US\$512 million in aggregate revenue (see Gemfields website). The auction by Gemfields Group Ltd. in June 2018 yielded a record sale of US\$71.8 million with an average price of US\$122 per ct. The success of the Gemfields ruby auctions are due to product from the Mugloto colluvial deposit, which provided clean and very high-quality red stones with typical sizes between one and 10 cts, and occasionally larger crystals [24].



Figure 1. Rubies worldwide. (A) Ruby crystal (1.7 cm × 1.7 cm × 0.5 cm) in marble from Bawpadan, Mogok, Myanmar. Photo: Louis-Dominique Bayle © le Règne Minéral; (B) rubies (from left to right: 2.1 cm × 1.3 cm × 1.3 cm and 1.7 cm × 1 cm × 1 cm) from Ambohimandrosoa, Antsirabe area, Madagascar. Collection: L. Thomas; Photo: Louis-Dominique Bayle © le Règne Minéral; (C) rubies from the Montepuez mine, Mozambique. Vincent Pardieu © Gemmological Institute of America; (D) Barrington Tops alluvial ruby concentrate, crystals up to 9 mm in size, New South Wales, Australia. Photo: Australian Museum Collection, courtesy Gayle Webb; (E) ruby crystal (6 cm × 4.8 cm × 1 cm) extracted from amphibolite rocks at Ampanihy, Southern Madagascar. Collection: J. Béhier. Photo: Louis-Dominique Bayle © le Règne Minéral; (F) rubies in phlogopite matrix with plagioclase (white) and minor kyanite (blue) hosted in between leucogabbro and meta-ultramafic rocks affected by fluid circulation and metamorphic metasomatism, Aappaluttoq deposit, southwest Greenland. Photo: Courtesy True North Gems Inc. (Vancouver, BC, Canada).

Over the last decade, knowledge on the formation of ruby deposits has improved significantly as their origin determination using a variety of new methods and analytical procedures. The present article synthesizes the state of knowledge on the geology and genesis of ruby deposits. The different issues focused on their location on the planet, their physical and chemical properties, pressure–temperature conditions of crystallization, the source of the constituent elements (viz. aluminum, chromium, vanadium, and iron), their age of formation, and finally the different proposed genetic models.

In this review we propose a geological classification scheme for ruby based on scientific works and own experience. The classification typology should open a new framework for mineral exploration guidelines and geographic determination for gemmological laboratories.

2. Worldwide Ruby Deposits

The distribution of major and minor commercial, industrial, scientific, and historical world sources of ruby is shown in Figure 2.

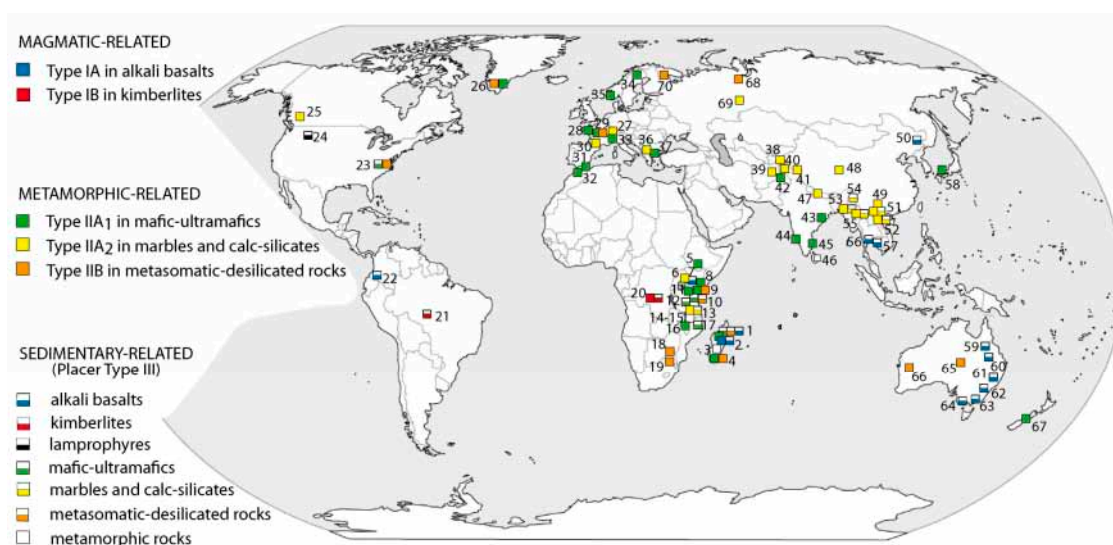


Figure 2. Main major and minor world sources of ruby plotted according to their geological types. Madagascar: (1) Andilamena, Ambodivoangy-Zahamena, Didy, Vatomandry; (2) Andriba; Ankaratra (Antsirabe-Antanifotsy region, Soamiakatra-Ambohimandroso; Ambohibary); (3) Zazafotsy; Ilakaka-Sakaraha; (4) Bekily-Vohibory area (Ambatomena; Ianapera; Fotadrevo; Anavoaha; Maniry; Gogogogo; Vohitany; Ejeda). Ethiopia: (5) Kibre mengist, Dilla. Kenya: (6) West Pokot; (7) Baringo; (8) Kitui; (9) Mangare (Rockland-formerly John Saul mine; Penny Lane; Aqua, Hard Rock). Tanzania: (10) Uмба valley; (11) Longido, Lossogonoi; (12) Winza; Loolera (Kibuko); (13) Morogoro (Mwalazi; Visakazi; Nyama, Kibuko, etc.); Mahenge (Lukande; Mayote; Kitwaro; Ipanko; (14) Songea; (15) Tunduru. Malawi: (16) Chimwadzulu. Mozambique: (17) Montepuez (Namahumbire/Namahaca), M'sawize, Ruambeze. Zimbabwe: (18) O'Briens (verdites). South Africa: (19) Barberton (verdites). Democratic Republic of Congo: (20) Mbuji-Mayi. Brazil: (21) São Luis-Juina River. Colombia: (22) Mercaderes-Rio Mayo. United States: (23) North Carolina (Corundum Hill; Cowee Valley; Buck Creek); (24) Montana (Rock Creek). Canada: (25) Revelstoke. Greenland: (26) South of Nuuk region (Fiskenæsset district-Aappaluttoq); North of Nuuk (Storø; Kangerdluarssuk). Switzerland: (27) Campo Lungo. France: (28) Brittany (Champtoceaux); (29) French Massif Central (Haut-Allier-Chantel; Peygerolles; Lozère-Aveyron-Marvejols; Vialat-du-Tarn); (30) Pyrenées (Arignac). Spain: (31) Alboran sea; Marrocos: (32) Beni Bousera. It aly: (33) Piedmont. Norway: (34) Froland. Finland: (35) Kittilä. Macedonia: (36) Prilep. Greece: (37) Gorgona-Xanthi; Paranesti-Drama. Tajikistan: (38) Snezhnoe, Turakuloma, Badakhshan. Afghanistan: (39) Jegdalek, Kash. Pakistan: (40) Hunza valley; (41) Batakundi, Nangimali; (42) Dir. India: (43) Orissa, Kalahandi; (44) Karnakata (Mysore); (45) Andhra Pradesh (Salem district). Sri Lanka: (46) Ratnapura, Polonnaruwa; Elahera. Nepal: (47) Chumar, Ruyil. China: (48) Qinghai; (49) Yuan Jiang. (50) Muling. Vietnam: (51) Luc Yen-Yen Bai; (52) Quy Chau. Myanmar: (53) Mogok, (54) Namya; (55) Mong Hsu. Thailand: (56) Chanthaburi-Trat (Bo Waen, Bo Na Wong, Wat Tok Phrom, Bo Rai, Nong Bon). Cambodia: (57) Pailin, Samlaut. Japan: (58) Ida. Australia: (59) Lava Plains; (60) Anakie fields-Rubyvale; (61) New England fields (Inverell); (62) Macquarie-Cudgegong, Barrington Tops-Yarrowitch; (63) Tumberumba; (64) Western Melbourne fields; (65) Harts range; (66) Poona. New Zealand: (67) Westland (Hokitika). Russia: (68) Polar Urals (Hit Island); (69) Ural mountains (Kuchin-Chuksin-Kootchinskoye); (70) Karelia.

High-value rubies are important mineral resources that contribute significantly to the gross domestic product of many countries. In 2005, Africa was officially (statistics are rare on the production of most ruby deposits) responsible for around 90% of world ruby production (in weight, not in quality; 8000 tons [28]; Figure 3) and this was before 2009 when the Montepuez ruby deposits were discovered in Mozambique [21–23].

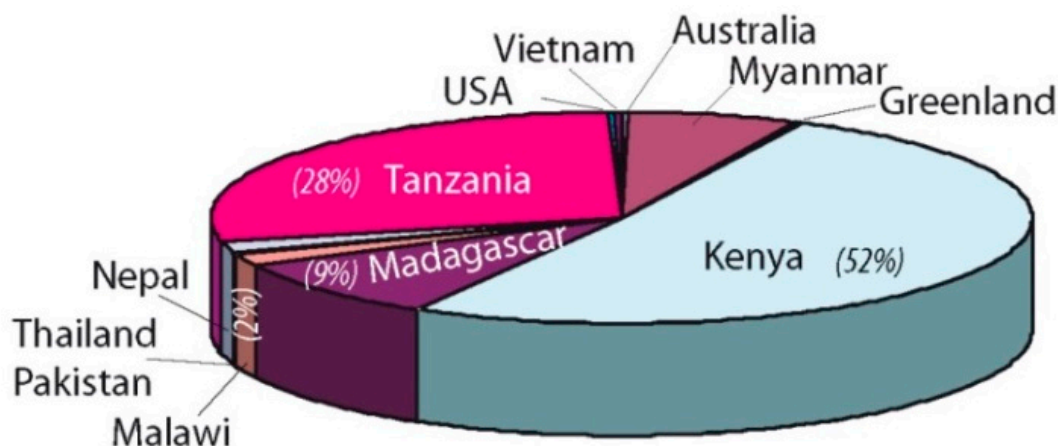


Figure 3. Ruby production worldwide in 2005 showing the production (in %) of some African countries, and others; modified from [28].

The highest-quality ruby crystals come from Central and South-East Asia and Eastern Africa ([27]; see Figure 1C). Myanmar, with the Mogok Stone Tract (see Figure 1A), is famous for having produced rubies of the finest quality since 600 CE [5,29,30]. These are often called “pigeon blood”, a term of Myanmar origin popularized by English traders in the 19th century [31]. Other Asian producers including Thailand (Chanthaburi-Trat mines) and Cambodia (Pailin and Samlaut) emerged as serious players in the 1970s, but their production has declined dramatically over the past 20 years [6]. Ruby deposits in Vietnam (Luc Yen, Yen Bai, and Quy Chau areas), Afghanistan (Jegdalek), Pakistan (Hunza valley), Azad-Kashmir (Batakundi and Nangimali), and Tajikistan (Kukurt, Turakoluma, and Badakshan) have become significant producers since the end of the 1980s, but their production remains limited. In the early 1990s Mong Hsu in Eastern Myanmar emerged as a major deposit but its production has declined since the early 2000s [6].

Today the high production and quality of rubies from Mozambique (and to a lesser extent Madagascar) has changed the way rubies are traded and with the arrival of these new players, the production of many other deposits collapsed [6]. Production from the Winza deposit diminished to the point of essentially disappearing, and the Rockland (former John Saul) mine in Kenya stopped producing. In Africa (Figure 4) gem rubies are mined in Kenya (Mangare and Baringo), Tanzania (Umba-Kalalani, Morogoro, Mahenge, and Loolera), Malawi (Chimwadzulu), Madagascar (Vatomandry, Andilamena, Didy, Zahamena, and Ilakaka), and Mozambique (Montepuez, Ruambeze, and M’sawize). The Montepuez mine is the most highly mechanized ruby mine worldwide [6,26]. In Southern Greenland True North Gems Inc. started working on the Aappaluttoq deposit near Fiskenæsset in 2005 (see Figure 1F) [32–37] and a mine (operated by “Greenland Ruby”) entered into production in 2017.

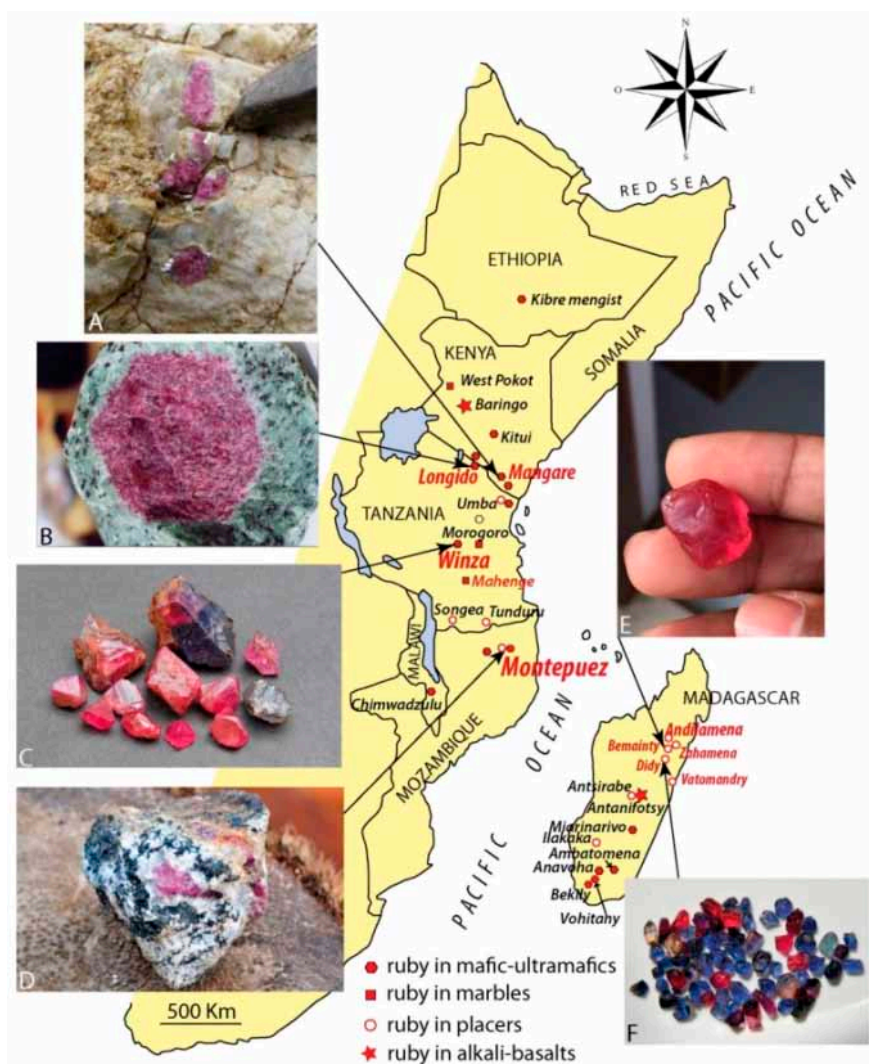


Figure 4. In East Africa and Madagascar rubies have been and are produced from both primary and secondary deposits. The most important deposits are those located in the Neoproterozoic Metamorphic Mozambique Belt. Of much lesser importance are deposits in which the ruby is entrained as xenocrysts in Cenozoic alkali basalts; these are the Baringo and Antanifotsy (Soamiakatra) deposits in Kenya and Madagascar, respectively. (A) Desilicated pegmatite in ultramafic rocks of the Rockland (ex-John Saul) mine in the Mangare area. Photo width 7 cm. Photo: Gaston Giuliani; (B) a ruby hexagonal prism (5 cm across) in anyolite rock (with green zoisite and black amphibole) from Longido, Tanzania. Photo: Gaston Giuliani; (C) rubies and two colored sapphires (3 cm across) from the Winza deposit in Tanzania, which occurs in metamorphosed leucogabbro and amphibolite. Photo: Vincent Pardieu; (D) ruby (5 cm long) in metasomatized amphibolite at M'sawize. Photo: Vincent Pardieu © GIA; (E) pink corundum (1 cm across) from placer at Bemainty, Madagascar. Photo: Vincent Pardieu © GIA; and (F) ruby and sapphires recovered from placer at Didy, Madagascar. Photo: Vincent Pardieu.

3. The Mineralogical, Physical, and Chemical Properties of Ruby

3.1. Mineralogical and Physical Properties

Corundum ($\alpha\text{-Al}_2\text{O}_3$) is trigonal and crystallizes in space group $R\bar{3}c$ with approximate unit-cell parameters $a = 4.76 \text{ \AA}$ and $c = 12.99 \text{ \AA}$ [38]. In corundum the oxygen atoms are in a hexagonal close packing arrangement corresponding to an ABAB stacking of alternate anion layers (Figure 5). This arrangement creates octahedral sites of which 2/3 are occupied by Al as suggested by the cation-anion ratio in the formula. Each Al atom is coordinated by three oxygen atoms from layer A and

three from layer B. The structure is thus based on pairs of edge-sharing octahedra in sheets parallel to {0001}. In each pair, one octahedron shares a face with an octahedron in the sheet below, while the other octahedron has a shared face with an octahedron in the sheet above [39].

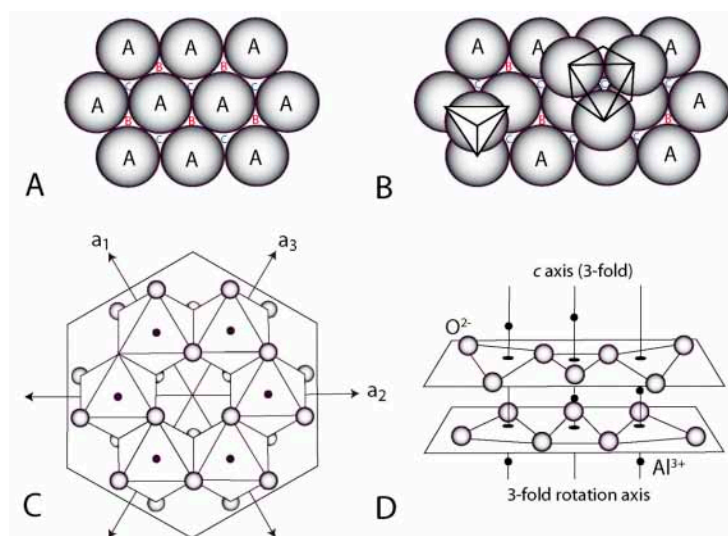


Figure 5. The crystal structure of corundum. (A) A single layer of spheres representing oxygen atoms in hexagonal close packed coordination. In a second layer the spheres would be oriented over the B locations, and a third layer would be over the first (A locations); (B) six oxygen atoms coordinate Al atoms at the C positions forming an octahedron (the tetrahedral coordinated site is vacant). Only two out of every three Al sites are occupied in the Al layers; (C) the crystal structure of corundum looking down c ; and (D) perspective view of the crystal structure of corundum [5,40].

If there are no cation substitutions in the structure, corundum is colorless. However when chromophorous elements replace aluminum in the octahedral site, the crystal is colored. The substitution of Al^{3+} by Cr^{3+} results in pink to red colors, depending on the Cr content. The pink corundum variety is called “pink sapphire” or “pink ruby”, and the red variety, with higher Cr contents ($0.1 < \text{Cr}_2\text{O}_3 < 3.0$ wt %; [5]), is called “ruby”. However, the distinction between these two varieties is not yet well defined and is debated by gem dealers and laboratories. As such, in the present work, pink corundum crystals that are associated with deep red ruby in some deposits worldwide will be considered rubies from here onward. Concentrations of 9.4 wt % Cr_2O_3 were measured in ruby from Karelia in Russia [41] and up to 13 and 13.4 wt % respectively, in ruby from Westland in New Zealand [42], and in ruby inclusions in diamond from placers associated with the Juina kimberlite [43].

The optical absorption spectrum of ruby shows two large absorption bands (Figure 6) with transmission windows at 480 nm (blue visible light) and at 610 nm (red visible light).

The most desired color for rubies is known in the trade as “pigeon’s blood”. While there is no globally accepted definition for it, it is usually used for stones with a vivid red color with sometimes a small amount of blue (just enough to balance the yellow from the gold on which the stone might be set). The presence of Cr at the octahedral site also gives rise to strong fluorescence when the stone is exposed to ultraviolet light (365 nm). The intensity of fluorescence is a function of Cr concentration and the Cr/Fe ratio [43], because the presence of Fe or an excess of Cr tends to eliminate or quench the fluorescence in ruby. In some stones, the fluorescence can even be seen when exposed to the ultraviolet component in sunlight, and this makes the ruby’s color more intense, increasing its value. This fluorescence is sometimes observed in small pinkish rubies, from marble deposits, that contain little to no iron, including those traditionally from Myanmar (Mogok, Mong Hsu, and Namya), and recently from Vietnam and Afghanistan [44]. Some rubies from amphibolite (Mozambique) and alkali-basalts (Thailand) have also been described as “pigeon’s blood” in laboratory reports but this is controversial because most reputable laboratories limit their use of the term to strongly fluorescent

rubies (which means the low-iron type, which is typically from marble-type deposits). The intensity of fluorescence is a function of the Fe content of ruby and three categories are distinguished: Burma Pigeon’s Blood Strong Fluorescent, Mozambique Type I Pigeon’s Blood Fluorescent, and Mozambique Type II Pigeon’s Blood Fluorescent [44] (Figure 7).

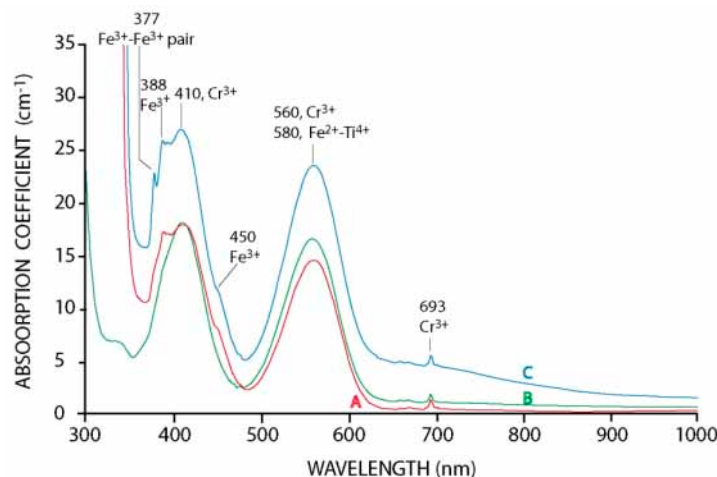


Figure 6. Ultraviolet, visible, and near infrared (UV-Vis-NIR) spectra of rubies from the Maninge Nice and Mugloto deposits, Mozambique; modified from [26]. The three spectra show the Cr³⁺ absorption bands at 410 and 560 nm, and the Cr³⁺ “doublet” at 694 nm. Spectrum (A) of a ruby from Mugloto also shows the shoulder at 330 nm but in addition a single Fe³⁺ feature at 377, 388, and 450 nm that reflects a higher Fe content in this ruby. Spectrum (B) of a ruby from Maninge Nice shows a shoulder at 330 nm caused by Fe³⁺ pairs. Spectrum (C) of a ruby from Mugloto differs from the others mainly by a Fe²⁺ → Ti⁴⁺ charge transfer band centered at 580 nm and increasing absorption above 600 nm.

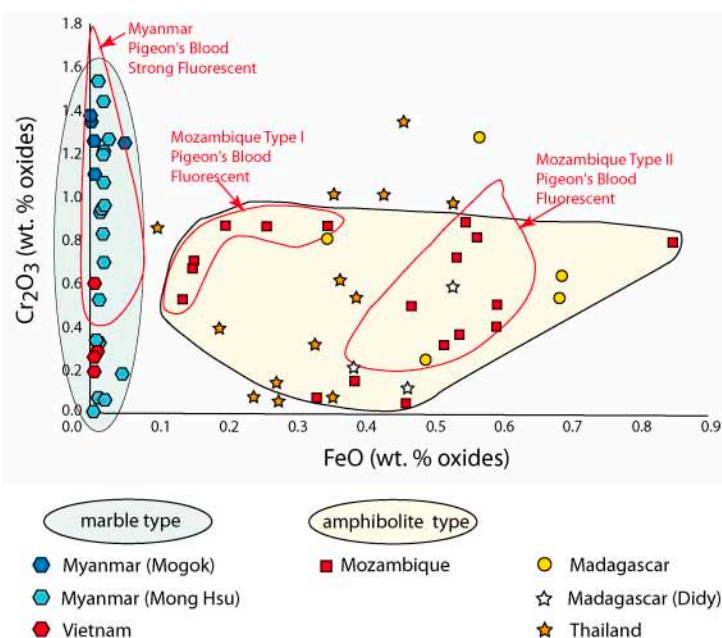


Figure 7. FeO versus Cr₂O₃ diagram of different pigeon’s blood color of rubies worldwide (modified from [44]). The color of the gem is defined as vivid with high intensity and low tone. The distinction of rubies between Myanmar Pigeon’s Blood Strong Fluorescent (in marble from Myanmar and Vietnam), Mozambique Type I Pigeon’s Blood Fluorescent, and Mozambique II Pigeon’s Blood Fluorescent (both in amphibolite) is correlated with the amount of Fe in the ruby, respectively FeO < 0.1 wt %; 0.1 < FeO < 0.35 wt %; and 0.35 < FeO < 0.6 wt % (data from [44]).

Euhedral crystals of ruby can exhibit several faces (Figure 8) that correspond to the following crystalline forms [38]: pinacoid $\{0001\}$, first-order hexagonal prism $\{10\bar{1}0\}$, second-order hexagonal prism $\{11\bar{2}0\}$, hexagonal dipyramid $\{hh\bar{2}hl\}$, rhombohedron $\{h0hl\}$, and ditrigonal scalenohedron $\{hkil\}$.

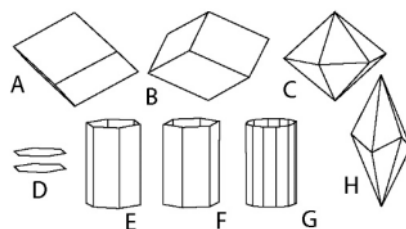


Figure 8. Crystalline forms of the $\bar{3}2/m$ class of the rhombohedral system, after [38]. (A) positive rhombohedron; (B) negative rhombohedron; (C) hexagonal dipyramid; (D) pinacoid; (E) first-order hexagonal prism; (F) second-order hexagonal prism; (G) dihexagonal prism; and (H) ditrigonal scalenohedron.

Rubies from Mong Hsu in Myanmar show a number of different habits (Figure 9) [30,45] and are bounded by pinacoidal $\{0001\}$ faces and hexagonal dipyramidal faces $\{hh\bar{2}hl\}$, sometimes associated with small rhombohedral $\{10\bar{1}1\}$ faces. Second-order prism $\{10\bar{2}0\}$ faces are also observed in some rubies. The smaller dipyramidal faces are $\{22\bar{4}3\}$, whereas the larger dipyramidal ones are often reported as $\{44\bar{8}1\}$ or $\{14\ 14\ \bar{2}8\ 3\}$, or less commonly $\{22\bar{4}1\}$ or $\{11\bar{2}1\}$. The $\{14\ 14\ \bar{2}8\ 3\}$ indices are too high for smooth faces, and it could be possible that they consist of alternating microsteps between $\{11\bar{2}0\}$ and $\{0001\}$ faces [46,47]. Rubies from Mogok are generally tabular with predominant pinacoids and rhombohedral $\{10\bar{1}1\}$ and dipyramidal $\{11\bar{2}1\}$ faces. Other habits (Figure 9) have been reported for marble-hosted rubies from Morogoro in Tanzania as flattened to tabular pseudo-cubes, pseudocubes according to the relative size of the six rhombohedral faces and six additional prism faces $\{10\bar{2}1\}$ with a lath-like form [48], and Jegdalek in Afghanistan [5]. Rubies in alkali basalt from Thailand and Cambodia are tabular and have combinations of rhombohedral $\{10\bar{1}1\}$ and pinacoid $\{0001\}$ faces (Figure 9).

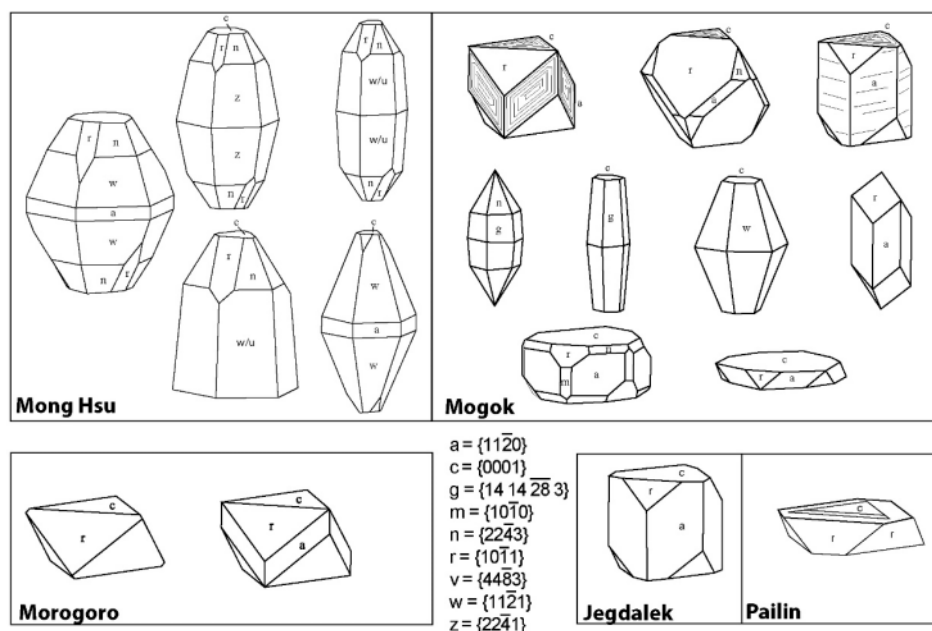


Figure 9. Main habits of ruby from different marble-hosted deposits: Mong Hsu and Mogok in Myanmar, Morogoro in Tanzania, and Jegdalek in Afghanistan. The rubies from the Pailin deposit (Cambodia) are from alkali-basalt placer deposits. From [5,30,45,48].

To explain these morphological differences, Sorokina et al. [49] introduced the concept of crystal “ontogeny” that encompasses nucleation, growth, and alteration of single crystals. According to their data, the variations of crystal habits in rubies from deposits in Africa and South-East Asia can be directly correlated with Cr and Fe contents and changes in P–T conditions during crystal growth.

3.2. The Trapiche Texture of Ruby

The conditions under which the ruby grows can give rise to a particular texture called ‘trapiche’ (Figure 10A). This texture was first described by [50] for an unusual Colombian emerald that resembles the spokes of a milling wheel used to process sugar cane. The term “trapiche” was used exclusively for emeralds until the 1990s, when trapiche rubies appeared in the Thai and Burmese gem markets [47,51,52].

The trapiche texture is composed of growth sectors separated by more or less sharp boundaries of inclusions [53,54], known as “sector boundaries”. These boundaries separate a central “core” (corresponding to the pinacoidal growth sectors) from the surrounding growth sectors. The boundaries are generally inclined with respect to the *c* axis. This texture should not be confused with that seen in purple-pink and blue sapphires (Figure 10B) and resulting from the distribution of different inclusions in alternating portions of the crystal and called “trapiche-like” [55,56].

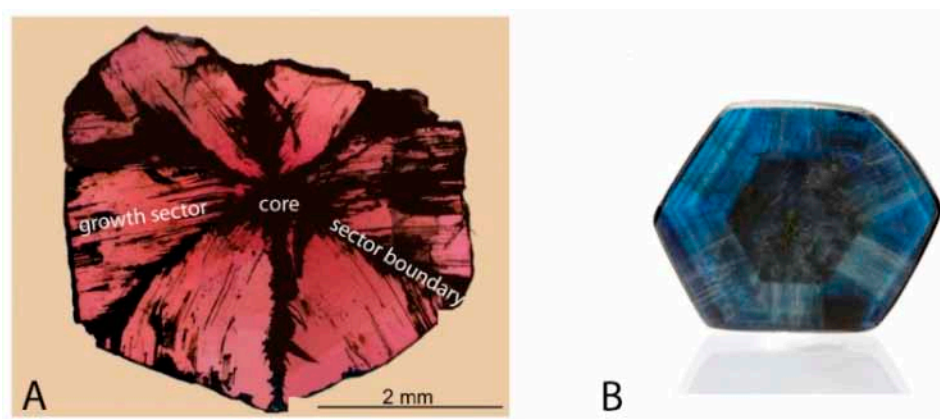


Figure 10. The trapiche texture of corundum. (A) Photomicrograph in transmitted light of a trapiche ruby from Mong Hsu, Myanmar (Photo: Virginie Garnier) and (B) aspect of a “trapiche-like” sapphire from southern Africa (2 cm × 1.8 cm × 0.2 cm, 13.46 cts). Photo: Louis-Dominique Bayle © le Règne Minéral.

The trapiche texture is best seen in cross-sections perpendicular to the *c* axis. The presence and size of the core depends on the orientation of the cross-section in the crystal [57] (Figure 11A). Thus, two cross-section appearances are possible: (1) the core is present and the sector boundaries surround it and develop from its edges to the rim of the crystal, separating six trapezoidal growth sectors (Figure 11B) and (2) the core is absent and the sector boundaries intersect at a central point, giving rise to triangular growth sectors (Figure 11C).

Variable contents of chromophores, in particular Cr but also Ti and V have been detected in different rubies as well as within the same samples [52,58,59]. This can explain why the core can be red (Cr > Ti) or black (Ti > Cr) [60], although the core is sometimes yellowish/white-to-brown like the sector boundaries. For both core and sector boundaries, the yellowish/white-to-brown color is due to the presence of calcite, dolomite, corundum, unidentified silicate inclusions containing K-Al-Fe-Ti, and Fe-bearing minerals. Iron oxides/hydroxides formed during late weathering that was favored by the high porosity of the sector boundaries (Figure 12) [52,57]. The sector boundaries develop along the $\langle 110 \rangle$ directions and can contain other solid inclusions such as plagioclase, rutile, titanite, margarite, zircon, etc. [57–59], but they do not contain matrix material from the host rock. This absence is an important feature differentiating trapiche rubies from trapiche emeralds [61].

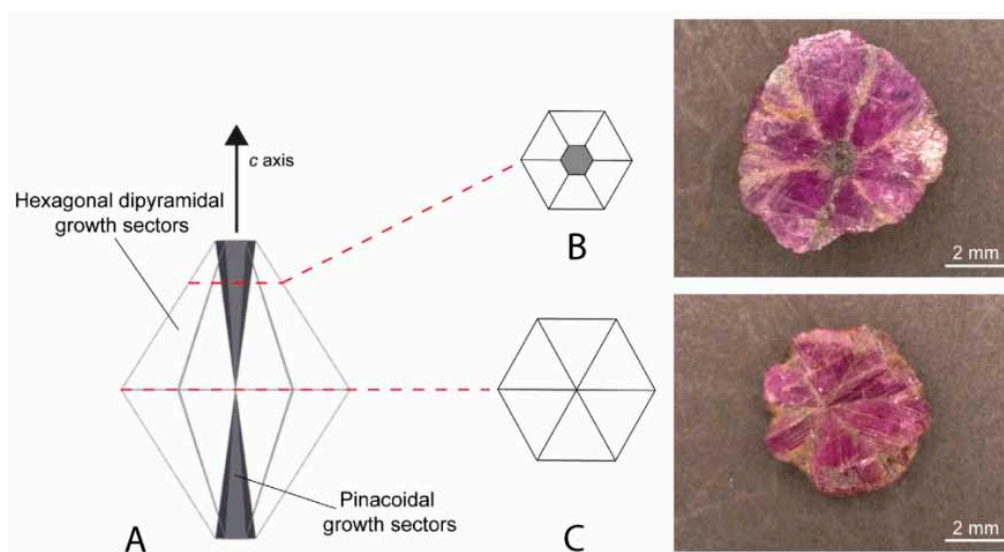


Figure 11. Variations of the ruby trapiche texture. (A) Variation of the core, which corresponds to the pinacoidal growth sectors (in grey). These sectors have a tapered shape and the core size varies as a function of the orientation of the cross-section; (B) aspect of the section near the vertex of the pyramid; and (C) aspect of the section if cut in the vertex plane. Photos by Isabella Pignatelli of two trapiche rubies from Mong Hsu, Myanmar.

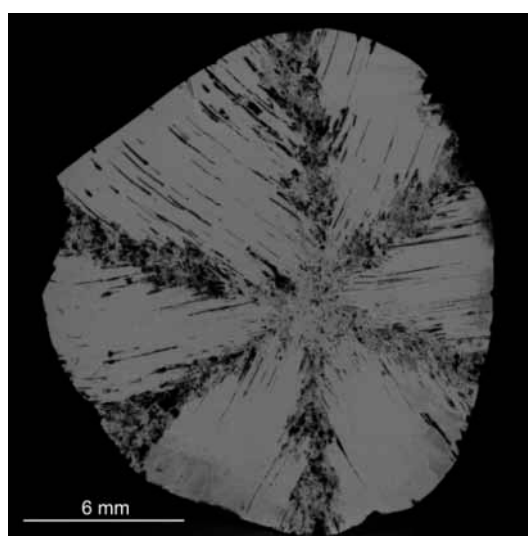


Figure 12. X-ray computed tomography image showing the high porosity (in black) of a trapiche ruby from Luc Yen, North Vietnam [57]. The porosity corresponds to 0.6% of the ruby volume and is developed in the sector boundaries. Photo: Christophe Morlot.

Tube-like voids filled with carbonates, liquid, and/or gas may be observed in the growth sectors (Figure 13) [51,57,62]. These can develop from the core or sector boundaries and extend into the growth sectors, running perpendicular to the sectors with an inclination of 5° relative to the {0001} ruby faces. Sometimes the tube-like voids can be parallel to the *c* axis.

Garnier et al. [58,59] found single-phase (liquid), two-phase (liquid + gas), and three-phase (liquid + gas + solid) inclusions between the tube-like voids and/or their extensions into the sector boundaries. Microthermometry and Raman spectrometry indicate that these inclusions correspond to the trapping of two immiscible fluids during the ruby formation: a carbonic fluid in the $\text{CO}_2\text{-H}_2\text{S-COS-S}_8\text{-AlO(OH)}$ system and molten salts [62–64]. These fluids are considered the product of metamorphism of evaporites during the devolatilization of carbonates and thermochemical-sulfate reduction.

Trapiche rubies are found in Myanmar, Vietnam, Tajikistan, Pakistan, and Nepal, but have never been described by geologists *in situ* in primary deposits. The trace element contents of the Myanmar and Vietnamese trapiche rubies prove that they originated from marble-type deposits [57–59]. Moreover, similar mineralogical and chemical features have been observed for trapiche and non-trapiche rubies from Mong Hsu in Myanmar and Luc Yen in Vietnam, confirming that they formed in the same geological context, i.e., marble-hosted ruby deposits [57,58,62,65]. The rubies formed in the amphibolite facies, during retrograde metamorphism at $620 < T < 670$ °C and $2.6 < P < 3.3$ kbar [65,66].

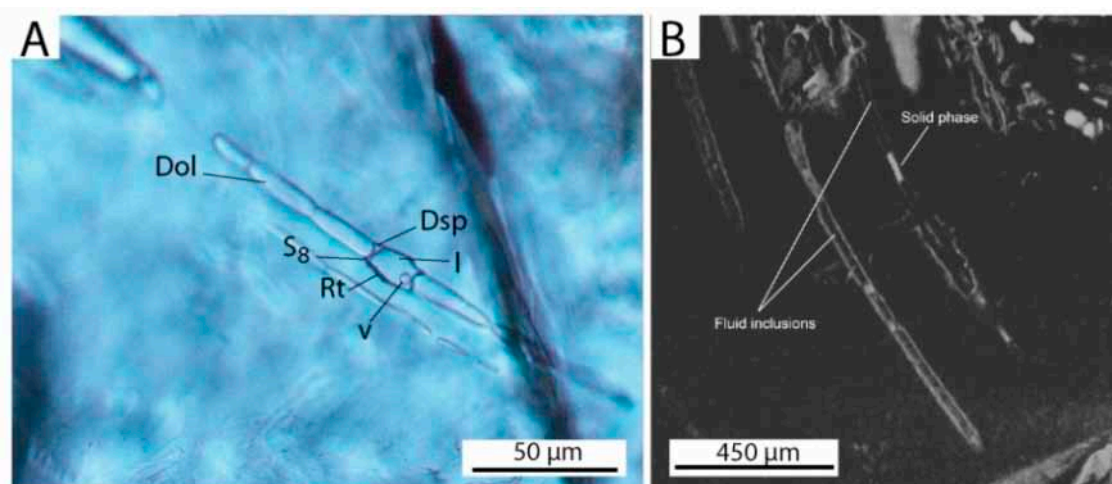


Figure 13. Solid and fluid inclusions trapped by trapiche rubies. (A) Primary fluid inclusions trapped along the sector boundary of a trapiche ruby from Mong Hsu, Myanmar. The fluid inclusion was trapped within tube-like structures formed by dolomite (Dol). It is a multi-phase fluid inclusion containing a two-phase (liquid + vapor) $\text{CO}_2\text{-H}_2\text{S-S}_8$ -bearing fluid and minerals including diaspore (Dsp) and rutile (Rt). V = vapor phase, l = liquid phase; from [62]. Photo: Gaston Giuliani; (B) X-ray computed tomography image of a trapiche ruby from Luc Yen, north Vietnam, showing tube-like voids that contain solid and fluid inclusion cavities; from [57]. Photo: Christophe Morlot.

In this geological context, the trapiche texture developed very quickly, as witnessed by the trapping of several solid and fluid inclusions and the formation of tube-like voids. The growth episodes in minerals are due to changes in the driving-force conditions [47]. In solution growth, mass transfer plays a key role. The driving force is defined by the difference in concentration between the bulk and subsurface supersaturation, i.e., the concentration gradient within the boundary layer [46]. Three growth episodes due to changes in driving force conditions were identified by [47] (Figure 14). Firstly, the core formed under low driving-force conditions via layer-by-layer growth (Step 1). Its development was hindered by the rapid formation of sector boundaries, which enveloped it and constitute the “skeleton” of the trapiche ruby (Step 2). These boundaries formed when the driving-force conditions increased and adhesive-type growth took place. Finally, a decrease in the driving-force conditions allowed the formation of growth sectors and the corresponding crystal faces through ordinary layer-by-layer growth (Step 3). The growth sectors filled the interstices left by the sector boundary, completing the trapiche texture.

3.3. Chemical Composition and Geographic Origin of Ruby

Currently, the accurate chemical composition of rubies can be determined by several analytical techniques, such as X-ray fluorescence (XRF), electron microprobe analysis (EMPA), laser ablation-inductively coupled plasma-mass spectrometry (LA-ICP-MS), and secondary ion mass spectrometry (SIMS). Chemical data facilitate the differentiation between natural and synthetic rubies [67] (Figure 15) and help to determine their geological origin worldwide [11,68–72].

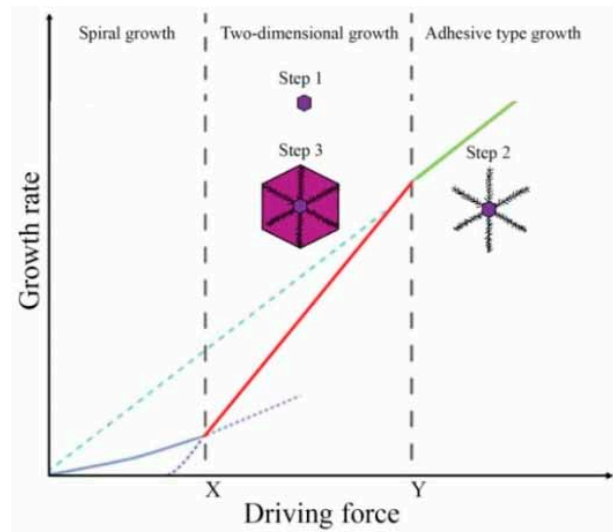


Figure 14. Schematic diagram showing growth rate versus driving force of the three development stages of trapiche ruby. The diagram shows the different types of crystal growth mechanisms, modified from [47]: spiral growth, two-dimensional growth, and adhesive-type growth. The increasing intensity of the driving force is presented between the critical points X and Y, where nucleation occurred. The curves represent growth rate versus driving force relations for the three mechanisms. The curve (in blue) shows the spiral growth mechanism; the curve (in red) represents the two-dimensional nucleation growth mechanism; the curve (in green) denotes the adhesive-type mechanism. A rough interface is expected above point Y and it corresponds to the dendritic stage of trapiche-ruby formation. The nucleation occurred between X and Y domains where the growth sectors formed in trapiche texture. Finally, a smooth interface is expected below X where nucleation by dislocation occurred either for non-trapiche ruby or in overgrowth zone in trapiche ruby.

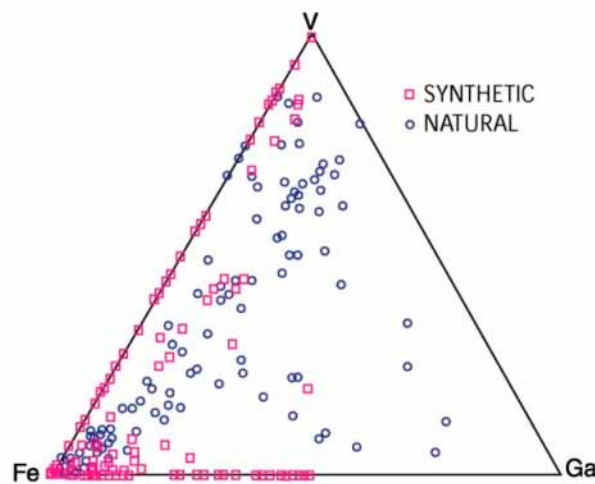


Figure 15. Gallium (Ga)-vanadium (V)-iron (Fe) ternary showing the distinction between natural and synthetic rubies, modified from [67].

Sutherland et al. [73–75] used a Fe_2O_3/TiO_2 versus Cr_2O_3/Ga_2O_3 diagram to decipher the metamorphic versus magmatic origin of corundum. This diagram is commonly used for the separation of blue sapphires from several deposits worldwide [76]. The corundum crystals termed “metamorphic” have pastel (blue, pink, and orange) to red colors, and are rich in chromium and poor in gallium (Cr_2O_3/Ga_2O_3 ratio > 3). The corundum crystals defined as “magmatic” are xenocrysts of blue-green-yellow (BGY) sapphires with a Cr_2O_3/Ga_2O_3 ratio < 1. The diagram was applied to rubies and sapphires related to alkali basalt from the provinces of Antananarivo (the Soamiakatra, Kianjanakanga, and Ambatomainty deposits) and

Toamasina (the Vatomandry and Andilamena deposits) in Madagascar [77,78] (Figure 16). Note that all of the points related to rubies plot in the metamorphic field. They overlap data for rubies from Andilamena, which is located in the north of the Vatomandry area, and where the corundum is hosted in different types of rocks (viz. metamorphosed mafic and ultramafic rocks (M-UMR) and plumasites in M-UMR). The majority of the sapphires plot in the magmatic domain. The distribution of sapphires from the Vatomandry area is heterogeneous, and while most are located in the magmatic domain yet others are in the metamorphic one. The latter corresponds to colorless, light to dark green, and light to purplish blue sapphires with significant Cr_2O_3 contents ($150 \text{ ppm} < \text{Cr}_2\text{O}_3 < 2100 \text{ ppm}$).

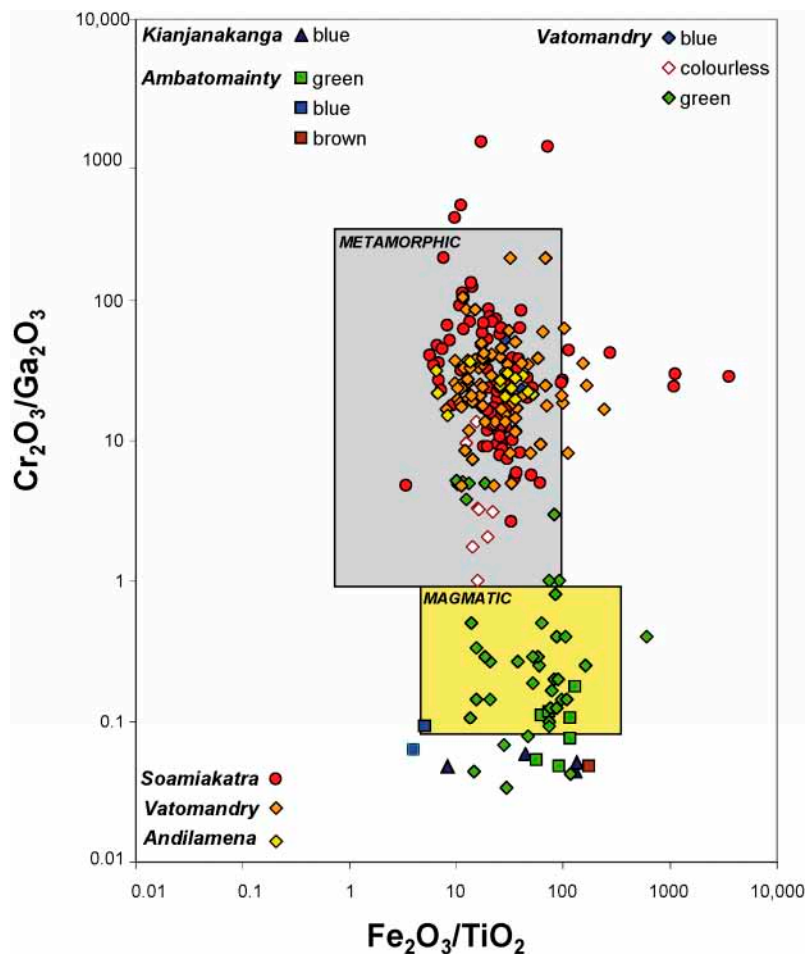


Figure 16. $\text{Cr}_2\text{O}_3/\text{Ga}_2\text{O}_3$ versus $\text{Fe}_2\text{O}_3/\text{TiO}_2$ diagram for rubies and sapphires associated with alkali basalts from the Antananarivo and Toamasina Provinces in Madagascar. The metamorphic and magmatic boxes defined for Australian sapphires are from [68,75].

Giuliani et al. [72] and Uher et al. [79] proposed a new chemical classification diagram for gem corundum based on the different types of primary corundum deposits worldwide (see [40,80]). It used a database of 2000 EMPA analyses of ruby and sapphire that were obtained under the same analytical conditions. The $\text{FeO} + \text{TiO}_2 + \text{Ga}_2\text{O}_3$ versus $\text{FeO}-\text{Cr}_2\text{O}_3-\text{MgO}-\text{V}_2\text{O}_3$ diagram in Figure 17 uses: (1) the FeO content to discriminate between iron-poor rubies in marbles and iron-rich rubies in M-UMR and (2) the second discriminator between ruby and sapphire is the addition to (Y-axis parameter) or subtraction from (X-axis parameter) FeO of trace elements associated preferentially with sapphire (TiO_2 and Ga_2O_3) or ruby (Cr_2O_3 , V_2O_5 , and MgO). The fields of the different gem corundum deposits are: for rubies, (R1) marble; (R2) John Saul mine-type; (R3) M-UMR; (R4) metasomatites; for sapphires, (S1) syenitic rocks; (S2) metasomatites; and (S3) alkali-basalt and lamprophyre. Finally, the chemical diagram permits a clear separation with limited overlap of the main types of deposit found worldwide.

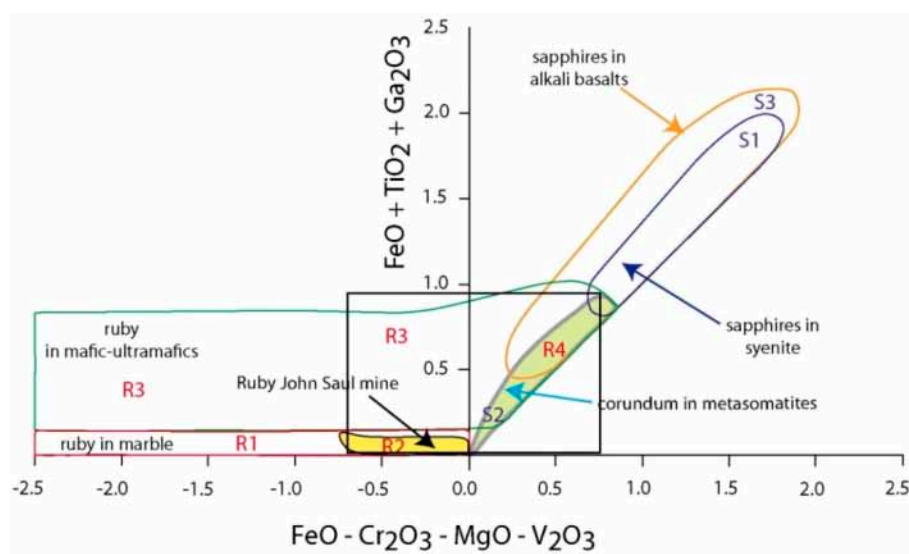


Figure 17. FeO-Cr₂O₃-MgO-V₂O₃ versus FeO + TiO₂ + Ga₂O₃ diagram based on a database of 2000 electron microprobe analysis (EMPA) analyses (in wt % oxides) showing the main chemical fields defined for different types of corundum deposits worldwide [72]. Different geochemical domains are defined (see text).

The chemical diagram provides sufficient discrimination to distinguish between the different types of corundum deposits for the following reasons: (1) the database contains more than 2000 EMPA analysis representative of all of the types of primary deposits and (2) the magmatic sapphire domain (S1) is defined by the geology and chemistry of corundum. The sapphires are hosted in syenitic rocks or occur as megacrysts in syenitic xenoliths carried by alkali basalts. Most of the sapphires in placers linked to the erosion of alkali basalts (domain S2) overlap the domain S1. The main superposition of geological domains is for ruby of metasomatic (-metamorphic) origin that overlaps the domain of ruby associated with M-UMR (strictly metamorphic); (3) the diagram uses Ga and Mg despite their high detection limits, and the two elements are opposed: Ga is added to Ti while Mg is added to Cr and V. This choice corresponds with the fact that Ga and Ti are concentrated in magmatic sapphires (syenitic rocks) while Mg, Cr, and V are concentrated in metamorphic rubies hosted in Mg-Cr(V)-rich protoliths.

A statistical classification by discriminant factors analysis using oxide concentrations (Ti, Mg, V, Cr, Fe, and Ga) of more than 900 corundum crystals from the main primary deposits worldwide was proposed by [72]. The deposits were classified into different types: (1) for ruby as marble, M-UMR, and metasomatites and (2) for sapphires as syenitic rocks, metasomatites, plumasites, and skarns.

The discriminating factors F1 and F2 calculated for the different types of ruby deposits (known classes) with their respective centroid for each class are as follows:

$$\begin{aligned} \text{Factor 1} = & 0.271691 \times (\text{Cr}_2\text{O}_3 - 0.294456)/0.376245 + 0.796762 \times (\text{FeO} - 0.26294)/0.224015 \\ & + 0.0206904 \times (\text{Ga}_2\text{O}_3 - 0.0112047)/0.0124095 + 0.136135 \times (\text{MgO} - \\ & 0.00545581)/0.00526035 - 0.124367 \times (\text{TiO}_2 - 0.0274651)/0.0539087 - 0.108332 \times (\text{V}_2\text{O}_3 \\ & - 0.0102233)/0.0111099 \end{aligned}$$

$$\begin{aligned} \text{Factor 2} = & 0.124957 \times (\text{Cr}_2\text{O}_3 - 0.294456)/0.376245 - 0.121871 \times (\text{FeO} - 0.26294)/0.224015 \\ & - 0.287007 \times (\text{Ga}_2\text{O}_3 - 0.0112047)/0.0124095 - 0.0527783 \times (\text{MgO} - \\ & 0.00545581)/0.00526035 + 0.0584802 \times (\text{TiO}_2 - 0.0274651)/0.0539087 - 0.439517 \times (\text{V}_2\text{O}_3 \\ & - 0.0102233)/0.0111099 \end{aligned}$$

The discriminating factors F1 and F2 calculated for the different types of sapphire deposits (known classes) with their respective centroid for each class are as follows:

$$\begin{aligned} \text{Factor 1} = & 0.23095 \times (\text{Cr}_2\text{O}_3 - 0.0613814)/0.0596296 - 0.723839 \times (\text{FeO} - \\ & 0.489593)/0.372367 - 0.0403934 \times (\text{Ga}_2\text{O}_3 - 0.0159195)/0.00946033 + 0.0767757 \times \\ & (\text{MgO} - 0.00613983)/0.0040002 - 0.00901195 \times (\text{TiO}_2 - 0.0236271)/0.0567399 + \\ & 0.0791335 \times (\text{V}_2\text{O}_3 - 0.00402119)/0.00329669 \end{aligned}$$

$$\begin{aligned} \text{Factor 2} = & -0.530426 \times (\text{Cr}_2\text{O}_3 - 0.0613814)/0.0596296 - 0.638704 \times (\text{FeO} - \\ & 0.489593)/0.372367 - 0.00893226 \times (\text{Ga}_2\text{O}_3 - 0.0159195)/0.00946033 - 0.200622 \times (\text{MgO} \\ & - 0.00613983)/0.0040002 + 0.296868 \times (\text{TiO}_2 - 0.0236271)/0.0567399 - 0.165072 \times (\text{V}_2\text{O}_3 - \\ & 0.00402119)/0.00329669 \end{aligned}$$

Finally, prediction diagrams were proposed for the different types of deposits and applied to placers of alkali basalt-related deposits [72]. Figure 18 shows how such a diagram can be used to determine the most probable deposit type for ruby from the Soamiakatra deposit in Madagascar.

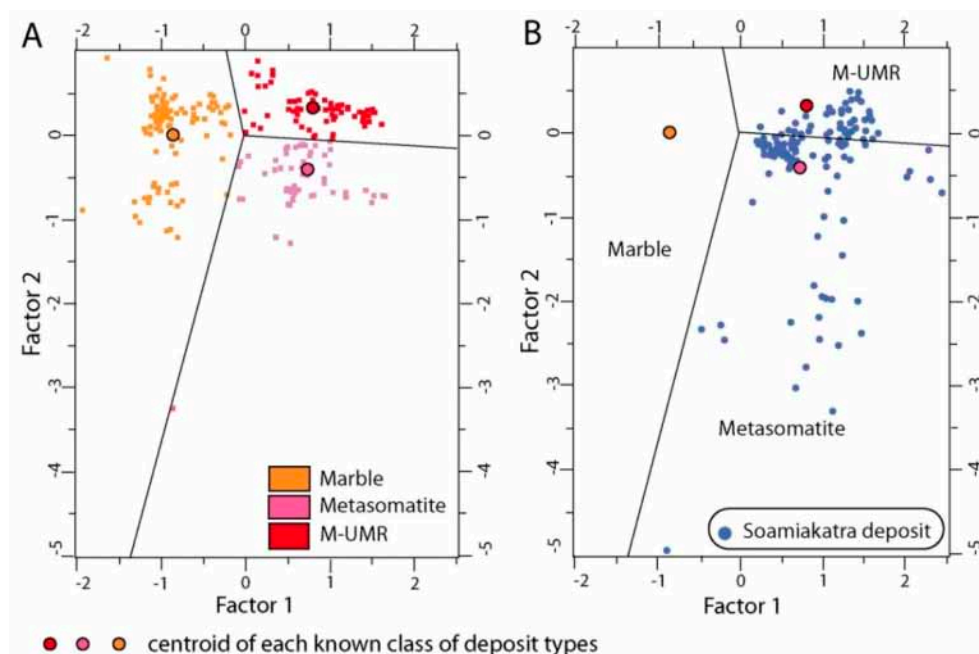


Figure 18. Discriminant factors analysis using oxide concentrations in ruby; modified from [72]. (A) Diagram used to distinguish between the different types of ruby deposit (marble, metamorphosed mafic and ultramafic rocks (M-UMR), and metasomatite) with the centroids of the known deposit classes and (B) prediction of the geologic origin of rubies from the Soamiakatra deposit in the Antanarivo province of Madagascar.

Peucat et al. [70] obtained LA-ICP-MS analyses of corundum from different geological settings and suggested using their Fe, Ti, Cr, Ga, and Mg contents and chemical ratios such as Ga/Mg, Fe/Ti, Fe/Mg, and Cr/Ga to determine their geological origins. The Ga/Mg ratio versus the Fe content has proven to be an efficient tool for discriminating between some metamorphic and magmatic blue sapphires, even if some localities overlap and are difficult to discriminate. Natural rubies have normally limited Ga (<200 ppm) and low Ga/Mg ratios (<10) and in some cases their trace-element contents are unusual and they plot in the field for sapphire [81].

The use of Fe versus Ga/Mg for ruby is presented here for different types of deposits (Figure 19). The main types of deposits are discriminated as a function of the Fe content of the ruby: (1) range 10,000–1000 (ppm) for ruby in M-UMR (metamorphism sensu stricto and metamorphic metasomatic) with

the example of different ruby deposits in Southern Madagascar (Vohitany, Anavoaha, and Andriba), Greenland (Aappaluttoq), Mozambique (Maninge Nice at Montepuez), ruby as xenocrysts in alkali basalts (examples include Pailin, Macquarie River, New England, and Chanthaburi-Trat) and kimberlite (Mbuji-Mayi) or alluvial from kimberlites (Juina, Brazil); (2) range 1000–10 ppm for ruby in marbles (Lu Yen-Yen Bai and Quy Chau in Vietnam, Mogok and Mong Hsu in Myanmar); and (3) less than 10 ppm for metasomatites as plumasites (John Saul mine, Kenya).

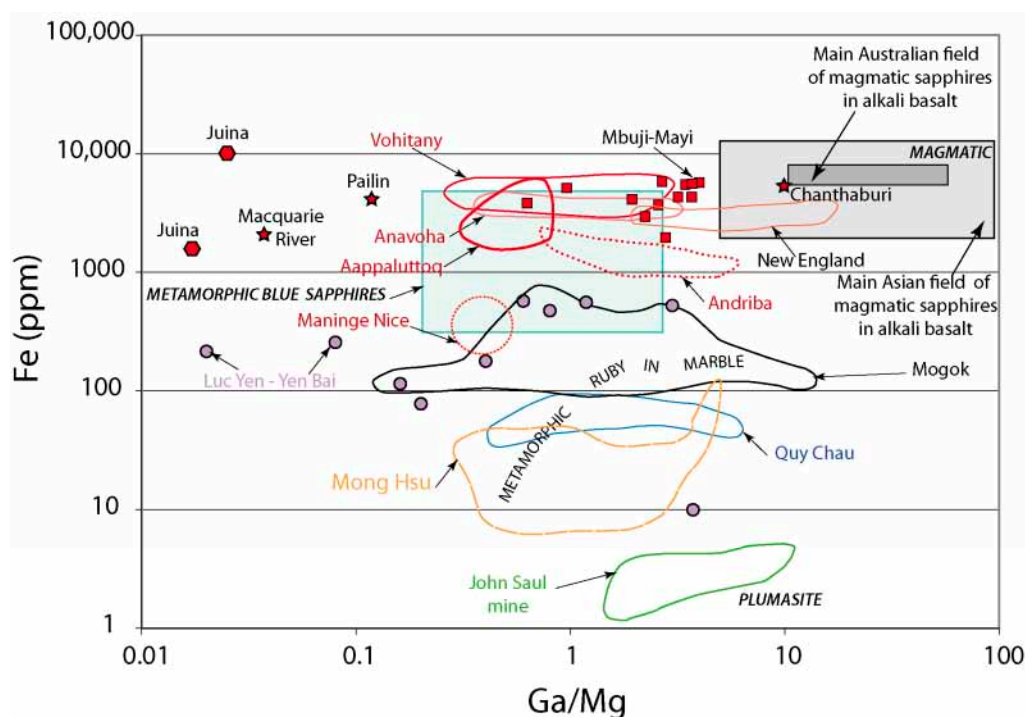


Figure 19. Fe (ppm) versus Ga/Mg discrimination diagram for ruby (this work; modified from [69]), showing the variation of Fe content for some rubies relative to their geological environments. The boxes for magmatic sapphire related to alkali basalts are reported for comparison with the plot of Pailin sapphire in Cambodia (data from [72,82]) as well as the box of metamorphic sapphires (drawn with the range of values defined in the tables of [70]). The following different types of ruby and/or their chemical fields are shown: (1) the chemical domain of rubies associated with M-UMR (red domains) from (i) Madagascar [72] with the occurrences of Vohitany (analysis, $n = 25$), Anavoaha ($n = 6$), and Andriba ($n = 6$); (ii) Greenland and the chemical domain of Aappaluttoq ruby deposit ($n = 24$, data from [83]); (iii) Mozambique (Montepuez mining district) with the colluvial deposit of Maninge Nice from (Pardieu, unpublished data); (2) inclusions of ruby in diamonds from Juina in Brazil (red hexagon) [43]; (3) xenocrysts of ruby from the Mbuji-Mayi kimberlite in the Democratic Republic of Congo (red square) [84]; (4) xenocrysts of rubies in alluvial of alkali basalts such as Pailin, Chanthaburi-Trat, and Macquarie River and New England in Australia (red star) [82,85,86]; (5) rubies in marble from Luc Yen-Yen Bai represented by single measurements (violet circle) and Quy Chau (blue domain) in Vietnam [57,66], Mogok (black domain) [87], and Mong Hsu (orange domain) [88]; and (6) rubies from the former John Saul (now Rockland) mine in Kenya (green domain) from desilicated pegmatites (Giuliani et al., unpublished data). These rubies show high variations in Fe, which permits discrimination of their geological type; this is characterized by a decrease of Fe from rubies in M-UMR to marble and metasomatic rocks (plumasite and shear-zones). The Ga/Mg ratio of rubies from M-UMR is different from magmatic sapphires but is within the range of values of metamorphic sapphires as defined by [69]. The domains represent the distribution of several spot analyses. The others analyses are the average values of punctual measurements.

The Ga/Mg ratio is highly variable, between 0.1 and 10, and some rubies such as those occurring as xenocrysts in alkali basalt (Chanthaburi-Trat and New England) and M-UMR (Madagascar) plot in the magmatic field of sapphire (right side of Figure 19). Such an overlap opens the question of the significance of such geochemical signatures and will be discussed elsewhere.

Geographic origin determination of ruby has become a great challenge during recent decades [72]. The sampling of rubies from reliable sources worldwide [20,36,89] has facilitated the assembly of reliable reference collections in the gem laboratories [90]. The mineral assemblages and inclusions combined with trace element chemistry sometimes make it possible to decipher the geographic origin of rubies. Trace elements are used by most of the laboratories and the data are collected with several analytical techniques [91] mainly LA-ICP-MS.

Representative analyses of rubies originating from deposits of different geological types are presented in Tables 1 and 2. The quantification of the various trace elements is done using commercially available calibration standards such as those provided by the National Institutes of Standards and Technology (NIST) or the United States Geological Survey (USGS). The difference in composition between the standards and the analyzed corundum has led to some uncertainties in the data generated by the different laboratories. The Gemmological Institute of America laboratory developed matrix-matched corundum standards of ruby and sapphire and the standard deviation of the analyzed ruby became negligible and therefore can be compared with a database of stones with known provenance [92]. The application of this analytical protocol to ruby made it possible to confirm the geological classification of gem corundum (ruby and pink corundum) for (1) Fe-poor ruby hosted in marble and (2) Fe-rich ruby in M-UMR (Figure 20). The geographic determination is not based on the Cr content of ruby because it appears by experience that it is not useful for origin certification [11]. The discrimination for Fe-rich rubies in M-UMR is based on the contents of V-Mg-Fe as shown in Figure 20 for deposits in Mozambique, Madagascar, and Thailand/Cambodia.

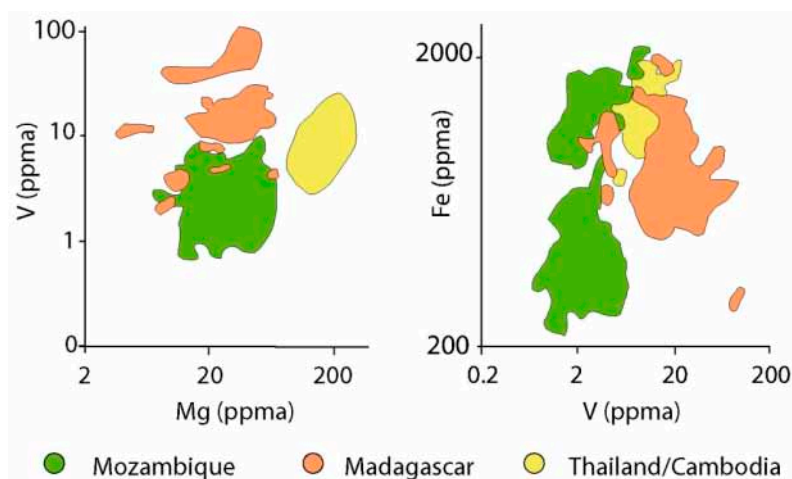


Figure 20. The geographic origin of rubies from Mozambique, Madagascar, and Thailand/Cambodia using V versus Mg and Fe versus V diagrams, modified from [11]. The limits of detection of the analyses by laser ablation-inductively coupled plasma-mass spectroscopy (LA-ICP-MS) are for Mg, V, and Fe respectively, 0.1–0.3, 0.03–0.2, and 5–20 ppm.

The geographic origin of ruby can usually be achieved based on inclusions in association with trace element chemistry despite some overlaps [11–14]. The oxygen isotopic compositions of these rubies overlap strongly and are not useful for geographic origin determination [93].

Table 1. Representative oxide (wt %) EMPA analyses of rubies originating from deposits of different geological types relative to the new enhanced geological classification for ruby.

Type of Deposit	Deposit	Color Corundum	Country	Al ₂ O ₃	MgO	TiO ₂	V ₂ O ₃ (in wt %)	Cr ₂ O ₃	FeO	Ga ₂ O ₃	Total	References
Type IA	Somiakatra	deep red	Madagascar	98.16	na	0.03	0.060	0.858	0.52	0.01	99.64	[94]
		pink		98.75	na	0.01	0.000	0.243	0.26	0.01	99.28	
Type IB	Mbuji Mayi	fuchsia	RDC	93.76	0.01	0.01	0.029	5.641	0.47	0.01	99.94	[84]
		red	Greece	97.58	bdl	0.01	0.010	2.650	0.39	0.07	100.71	[95]
Type IIA ₁	Montepuez	red	Mozambique	99.38	bdl	0.01	na	0.080	0.45	bdl	99.92	[96]
		red	Madagascar	99.06	0.01	0.01	0.000	0.219	0.59	0.01	99.90	[72]
Type IIA ₂	Ronda	red	Spain	99.33	0.02	0.01	na	0.120	0.19	na	99.67	[97]
		red to pink	Vietnam *	99.42	0.02	0.02	0.010	0.370	0.02	0.01	99.87	[98]
Type IIB ₁	Mogok	red	Myanmar	99.01	0.00	0.01	0.047	0.794	0.01	0.01	99.88	[72]
		red	Myanmar	99.20	0.01	0.08	0.041	0.521	0.00	0.00	99.85	
Type IIB ₂	Nangimali	pink	Pakistan	99.85	0.01	0.02	0.005	0.055	0.00	0.01	99.94	[72]
		pink	Madagascar	98.76	0.00	0.00	0.002	0.023	0.45	0.00	99.25	
Type IIB ₁	Naxos	pink	Greece	100.70	0.35	0.27	0.090	0.180	0.40	0.15	102.14	[95]
		red	Russia	95.16	bdl	bdl	na	3.860	0.44	na	99.46	[99]
Type IIB ₂	John Saul (Kimbo)	pink	Kenya	100.09	0.03	0.04	0.016	0.595	0.00	0.04	100.80	[72]
		red	Madagascar	98.63	0.01	0.03	0.005	0.188	0.30	0.01	99.17	[100]
Type IIB ₂	Hokitika	red	New Zealand	90.65	na	bdl	0.050	9.050	0.18	na	99.93	[42]
		red	New Zealand	98.43	0.02	0.04	0.040	0.761	0.52	0.02	99.83	
Type IIIA	Vatomandry	pink	Madagascar	99.29	0.03	0.04	0.005	0.161	0.44	0.02	99.99	[94]
		red brown		97.68	0.03	0.04	0.053	0.561	0.63	0.03	99.02	
Type IIIA	Antsabotraka	red brown	Madagascar	99.48	0.02	0.02	0.010	0.130	0.39	0.02	100.06	[94]
		red brown		99.50	0.03	0.02	0.012	0.127	0.21	0.01	99.91	
Type IIIA	Ambatomainty	red	Australia	99.07	0.09	bdl	na	0.450	0.22	na	99.83	[75]
		pink	Madagascar	99.28	0.01	0.01	0.001	0.178	0.29	bdl	99.77	[72]
Type IIIB	Quy Chau	red to pink	Vietnam [□]	99.28	0.00	0.03	0.020	0.580	0.06	0.01	99.98	[98]
		red to pink	Vietnam [□]	99.76	0.00	0.01	0.070	0.540	0.01	0.01	100.40	

na = not analyzed; *, [□] = number of analyses for calculating the presented average composition of ruby or pink corundum with respectively; * $n = 29$, [□] $n = 40$ and $n = 16$; bdl = below detection limit.

Table 2. Representative analyses (in ppm) obtained by LA-ICP-MS of rubies originating from deposits of different geological types relative to the new enhanced geological classification for ruby.

Type of Deposit	Deposit or Mining District	Country	Mg	Ti	V (in ppma)	Fe	Ga	Cr	Number of Analyses	References
<i>Type IIA₁</i> <i>in M-UMR</i>	Longido	Tanzania	(7–42)	np	(3–25)	(62–544)	(6–10)	(1604–5059)	16	[101]
	Winza		(0–118)	np	(0–1)	(405–1596)	(4–11)	(161–1094)	14	
<i>Type IIB₁</i> <i>Type IIA₂</i> <i>in marble</i>	Chimwadzulu	Malawi	(10–39)	np	(1–10)	(953–2760)	(5–15)	(269–1816)	18	
	Aappaluttoq	Greenland	(2–81)	(15–210)	(0.1–14)	(655–2516)	(0.7–25)	(50–2871)	17	[102]
	Mogok (Mo)	Myanmar	(5–75)	(7–80)	(48–1089)	(bdl-301)	(2–51)	np	65 = Mo + MH	[11]
	Dattaw (Mo)		(bdl)	(105–702)	(66–97)	(bdl-237) *	(32–42)	(105–702)	4	[103]
	Kadoke Tat (Mo)		(bdl-25)	(bdl-580)	(150–1472)	(bdl-644) *	(11–140)	(61–2963)	13	
	Baw-Padan (Mo)		(33–40)	(70–74)	(206–347)	(270–442)	(106–166)	(29–2339)	2	[87]
	Namya		(bdl-66)	(79–739)	(184–489)	(bdl-234) *	(23–107)	(479–6864)	12	[103]
	Mong Hsu (MH**) not precise	Vietnam	(48–115)	(778–1815)	(324–417)	(bdl-29)	(66–89)	(2026–7015)	65 = Mo + MH	[88]
Jegdalek	Afghanistan	(1–130)	(bdl-1214)	(2–214)	(bdl-28)	(1–122)	np	93	[11]	
<i>Type IIIA</i> <i>in alkali basalt</i>	Snezhnoe	Tajikistan	(7–380)	(9–486)	(4–135)	(bdl-1128)	(5–35)	np	74	
			(6–58)	(bdl-579)	(24–112)	(bdl-155)	(14–28)	np	48	
	Pailin	Cambodia	(4–72)	(6–75)	(51–122)	Bdl *	(61–83)	(1696–4204)	6	[104]
			(97–258)	(32–128)	(5–22)	(818–1935)	(5–11)	np	34	[11]
<i>Type IIIB</i> <i>in M-UMR</i>	Chantaburi-Trat	Thailand	(118–226)	(95–210)	(16–33)	(2454–3620)	(18–34)	(450–7761)	14	[105]
			(126–181)	(32–138)	(4–14)	(756–1442)	((5–10)	np	7	[11]
	New England	Australia	(102–163)	(81–219)	(9–30)	(2175–3794)	(16–32)	(955–2856)	10	[105]
<i>Type IIIB</i> <i>in MetamR</i>	Mugloto	Mozambique	(9–55)	(6–203)	(4–14)	(2560–3150)	(170–310)	(870–3370)	?	[81]
	Maninge Nice		(11–50)	np	(2–7)	(851–2034)	(5–12)	(506–1737)	14	[101]
	Montepuez		(19–47)	np	(1–6)	(261–402)	(6–9)	(1886–4941)	5	
<i>Type IIIB</i> <i>in MetamR</i>	Zahamena	Madagascar	(8–65)	(bdl-59)	(bdl-10)	(231–2154)	(5–14)	np	85	[11]
	Didy		(13–61)	np	(10–100)	(284–1994)	(10–30)	(135–3922)	14	[101]
	Andilamena		(0–67)	np	(2–17)	(533–1274)	(3–17)	(32–2698)	21	
			(19–53)	np	(4–29)	559–1559)	(7–21)	(53–1569)	14	

np = not precise because Cr is no longer used in the GIA laboratory as a discriminant for geographic origin determination; * = iron was measured by EMPA; MH** = range of averages composition of core and rim for two samples ($n = 33$ analyses) from Mong Hsu (MH); MetamR = metamorphic rocks environment; M-UMR = mafic-ultramafic rocks; Type IIA2 refers to the proposed new geological classification for ruby; bdl = below detection limit.

4. Geological Environment and Age of Primary Ruby Deposits

The global distribution of ruby deposits is closely linked to the Wilson cycle, i.e., collision, rift and subduction geodynamics [80,106,107]. Ruby forms in mafic, felsic, and metamorphosed carbonate platform geological environments, but it is always associated with rocks depleted in silica and enriched in alumina. In the presence of silica, Al is preferentially incorporated into Al-Si-bearing minerals such as feldspars and micas. The mineral association of corundum commonly consists of plagioclase, sapphirine, biotite, phlogopite, amphibole, pyroxene, and carbonates [108].

Two major geological environments are favorable for the presence of ruby, specifically amphibolite to medium-pressure granulite facies metamorphic belts, and alkaline basaltic volcanism in continental rifting environments. Three questions arise concerning ruby in metamorphic environments, which formed primarily via changes in temperature and pressure and fluid–rock interaction such as diffusion or percolation (metasomatism): (1) the origin and role of the parental fluids; (2) the nature and importance of the protolith; and (3) the characteristics of the paleogeography of the depositional sedimentary environment (in the case of carbonate platforms).

Gem ruby is rare because it requires the existence of several conditions: (1) an environment containing aluminum or the circulation of an Al-bearing metasomatic fluid; (2) a parental fluid issued either from the gem host-rock environment or exotic fluid circulations at medium to high temperatures ($T > 500\text{ }^{\circ}\text{C}$); (3) a seed surface and sufficient space for the growth of the crystal; (4) the incorporation of trace elements especially Cr, Fe, and V from the parental fluid in the unit cell of the mineral; and (5) the absence of internal crystalline deformation during and after growth.

In the amphibolite to medium-pressure granulite facies metamorphic belts, the gem corundum pressure-temperature field corresponds to a pressure domain above 2 kbar, and temperatures between 500 and 850 $^{\circ}\text{C}$ (Figure 21).

The host lithologies are alumina-rich and/or silica-poor rocks such as marble, aluminous gneiss, metamorphosed M-UMR, or juxtaposed meta-felsic and silica-poor rocks affected by the circulation of fluids at their contact and altered by metasomatism (metasomatites such as desilicated pegmatite called plumasite, skarn, etc.). Marble is a silica- and alumina-depleted rock, and under these conditions the transport of alumina by a fluid phase seems necessary for the crystallization of corundum; however, Al is usually considered to be an immobile element but investigations on different ruby deposits associated with fluid circulation and metasomatism have shown that Al was mobile [83].

Ruby-bearing skarns have not been clearly identified but the presence of silica enrichments in certain rubies from Mogok [87,103] led some authors to suspect the influence of thermal anomalies accompanying the different Si-rich intrusions affecting the mining district. This opens debate on the accuracy of determination of Si content in ruby, and the use of accurate ruby standards is necessary to decrease the detection limit of Si as done by [87,92]. Stone-Sundberg et al. [92] measured by LA-ICP-MS analysis Si ranging from 70 to 305 ppm in rubies from Mogok as well as other elements such as B (11–82 ppm), Ga (280–800 ppm), and Sn (2–35 ppm) that recorded potential skarn trace-element enrichments [88]. Emmett et al. [109] focused on the low mass resolution of quadrupole ICP-MS as the cause of that technique inability to measure accurately Si in corundum. Another problem is that ICP-MS occurs in a silica glass torch, which causes large variations in the Si background leading to high detection limits [109]. The results published up to now for different rubies [91,104] remain questionable. Measurements of Si by SIMS could be a more accurate method as explained by [109].

In alkali basalt volcanism, rubies are xenocrysts carried to the surface by the magmas. The corundum is found either as xenocrysts or crystal within xenoliths in lava flows and plugs of subalkaline olivine basalts, high alumina alkali basalt, and basanite. These magmas occur in crustal extensional environments impacted by the rise of upwelling mantle plumes. Ruby-bearing xenoliths are very rare because the mother rocks generally melt or disintegrate during storage in the magma chamber or during the magma transport. In Madagascar, xenoliths of ruby-bearing clinopyroxenite and metagabbro have been found in the Soamiakatra deposit. The metamorphic ruby formed in the lower crust at a temperature around 1100 $^{\circ}\text{C}$ and a pressure of about 20 kbar [77,94].

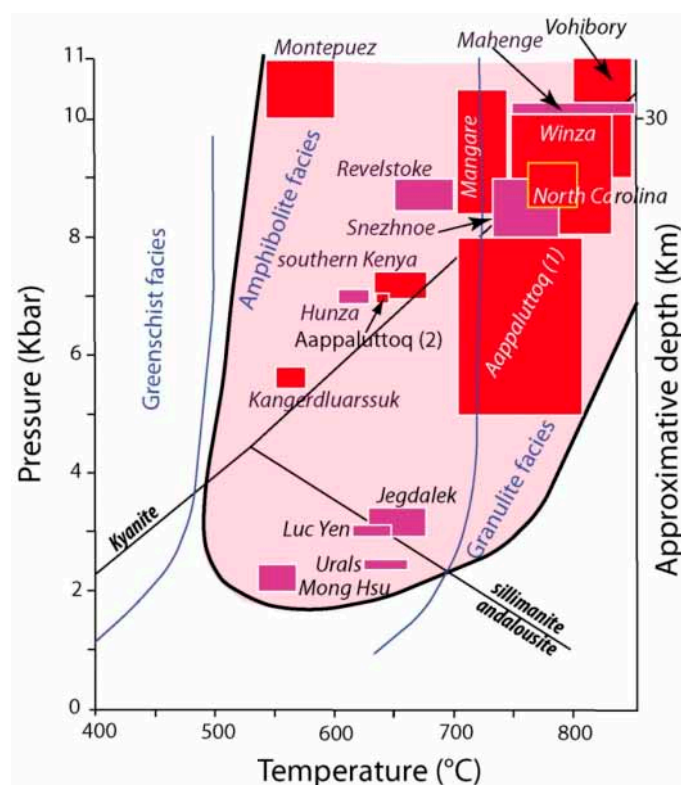


Figure 21. Pressure–temperature (P–T) formation conditions of metamorphic gem ruby (modified from [40,110]). The P–T fields of: (1) the marble type deposits from Mong Hsu [60], Urals [111], Luc Yen and Jegdalek [65], Hunza [112], Revelstoke [113], Mahenge [114], and Snezhnoe [115] are represented by violet rectangles and (2) the M-UMR deposits, metamorphic sensu stricto or associated with metasomatic metamorphism are represented by red rectangles: Greenland-Kangerdluarssuk [116], Aappaluttoq 1 [34] and 2 [83]; Southern Kenya [117,118]; Montepuez [96]; Mangare [119]; Winza [120]; North Carolina [121]; and Vohibory [122]. The P–T fields of ruby and pink corundum in clinopyroxenites and metagabbro xenoliths associated with alkali basalts are not shown. The schematic fields of Greenschist, Amphibolite, and Granulite facies are reported.

The ages of corundum formation are defined by indirect dating of a series of minerals (zircon, monazite, rutile, titanite, and micas) present either in the host rocks or as syngenetic inclusions in the corundum. These minerals have different blocking temperatures for closure to isotopic migration that make it possible to establish a cooling history for the corundum. Four main periods of gem corundum formation that include ruby and sapphire and encompass the main economic production worldwide, are presented in Figure 22 [80,106,107]. The others primary ruby occurrences known worldwide as in Australia, Norway, Finland, United-States, and other countries (see Figure 2) were not considered in the main periods of gem ruby formation. They are either uneconomical or without determination of ages.

The oldest deposits were formed in the Archean (2.97–2.6 Ga). An example is the Aappaluttoq ruby deposit in the 2.97 Ga Fiskensæset anorthosite complex, Greenland (Figure 2). The deposit occurs at the contact between two types of rocks, i.e., ultramafic rocks (meta-peridotite or dunite) and an anorthite-rich rock (anorthosite and leucogabbro) [34,83]. Ruby is hosted in phlogopite-calcic amphibole metasomatic rocks formed by fluid–rock interaction at the contact of the two lithologies. The metasomatic fluids were triggered by the intrusion of pegmatites dated between 2.72 and 2.70 Ga with U–Pb zircon geochronology by LA-ICP-MS [83]. U/Pb dating of monazite gave age at 2.64 Ga [34] and a direct Pb–Pb isochron age of 2.68 Ga was obtained on ruby by Thermal Ionisation Mass Spectrometry [103]. The age of ruby is correlated to the age of the pegmatites intrusion; consequently an average age at 2.71 Ga is considered for ruby formation [83].

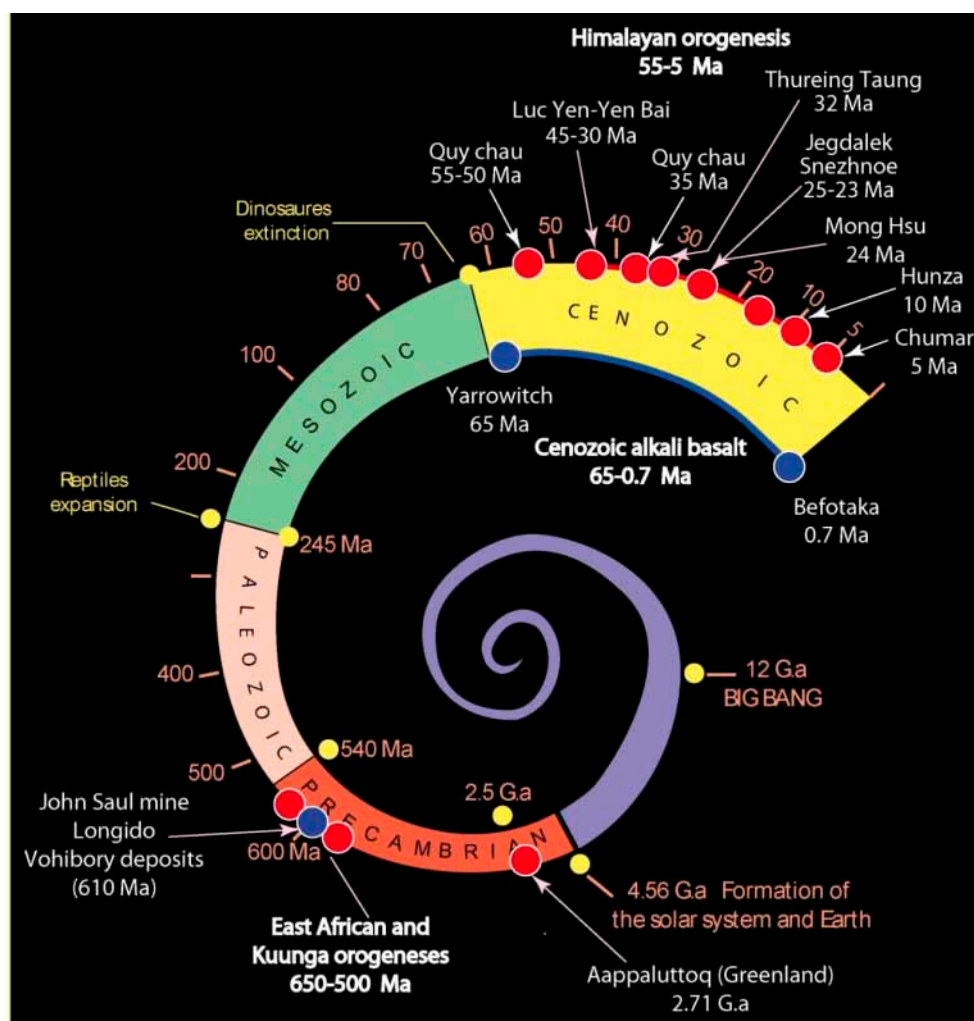


Figure 22. The spiral time diagram of corundum formation that includes economic ruby (and sapphire) deposits. Four main economic corundum periods have been defined worldwide by different methods of indirect dating of corundum. The oldest deposit is Aappaluttoq in Greenland where the ruby formed during the Archean at 2.71 Ga. The main period of gem rubies formation was the Pan-African orogeny (750–450 Ma). This includes primary ruby deposits in the Pan-African tectonic-metamorphic belt such as the John Saul mine in Kenya, Longido in Tanzania, and the deposits of Southern Madagascar, all formed at around 610 Ma. The third period corresponds to the Cenozoic Himalayan orogeny (55 Ma to the Quaternary) with the famous marble-hosted ruby deposits in Central and South-East Asia as in the deposits of Thureing Taung at Mogok and Mong Hsu in Myanmar [88]. The fourth period is dominated by the extrusion of alkali basalts in the Cenozoic (65 Ma to Quaternary) where ruby (and sapphire) were transported as xenocrysts or in xenoliths by the magmas. The age of the parental rocks of the ruby is unknown but a metamorphic origin is preferentially evidenced. Most of the ages are minimum cooling ages except those obtained on zircon by the U/Pb method.

The second period of corundum formation was the Pan-African orogeny (750–450 Ma). This includes primary ruby and sapphire deposits in the gemstone belt of eastern Africa, Madagascar, India, and Sri Lanka that are linked to collisional processes between Eastern and Western Gondwana during Pan-African tectonic-metamorphic events [123]. The metamorphic ruby and sapphire deposits in Southern Madagascar have numerous geological similarities with those in Eastern Africa, Sri Lanka, and Southern India (see [40]). U/Pb dating of zircon from the John Saul mine in Kenya (612 ± 6 Ma; [118]), Longido in Tanzania (610 ± 6 Ma; [124]), and the Vohibory deposits in Madagascar (612 ± 5 Ma; [125]) reveal similar periods of formation related to the East African orogeny. The precise

age of formation for the ruby deposit of Montepuez in Mozambique is unknown but a Pan-African age is probable [126]. Moreover, the U/Pb ages of zircon coeval with sapphire in the Andronandambo skarn deposit in Southern Madagascar range between 523 and 510 Ma [127], and the $^{40}\text{Ar}/^{39}\text{Ar}$ ages of biotite-phlogopite syngenetic with sapphire and ruby from the Ambatomena, Sahambano, and Zazafotsy deposits in Madagascar are between 494 and 487 Ma [128]. LA-ICP-MS dating of rutile inclusions in ruby from the John Saul and Aqua mines in the Mangare area gave ages of 533 and 526 Ma, respectively [129]. These cooling ages, lower than those obtained by the U/Pb method, must be considered as minimum ages but as confirming the existence of a metamorphic corundum episode during the late Pan-African orogenic cycle (Cambrian) and corresponding to the Kuunga orogeny [130].

The third period corresponds to the Cenozoic Alpine orogeny with tectonic events registered in the Alps; Rhodopes and Himalayas (55 Ma to the Quaternary). Examples include the marble-hosted ruby deposits in Campo Lungo (Switzerland) and Xanthi (Greece), and in Central and South-East Asia. In the Himalayas, the ruby deposits in marble occur in metamorphic blocks that were affected by major tectonic events during the collision of the Indian and Asian plates [131–134]. The ruby has been indirectly dated by $^{40}\text{Ar}/^{39}\text{Ar}$ stepwise heating experiments performed on single grains of coeval phlogopite, and by ion-probe U–Pb analyses of zircon included in the corundum [40,88,106,135]. Other indirect dating for the Snezhnoe deposits in Central Pamir was realized on bulk rock (ruby-bearing phlogopite-plagioclase rocks) by the Rb–Sr method [134]. The Rb–Sr errorchron age yielded 23 ± 1.6 Ma, which had to be considered as a minimum age for ruby formation. All of the Eocene to Pliocene ages (55–5 Ma) are consistent with extensional tectonic events that were active from Afghanistan to Vietnam in the ruby-bearing metamorphic belt.

The fourth main period of gem economic ruby is dominated by the extrusion of alkali basalts in the Cenozoic (65 Ma to Quaternary). Gem corundum occurs worldwide as xenocrysts or megacrysts in xenoliths or enclaves incorporated in basaltic magmas during their ascent. Such sapphire and ruby deposits occur from Tasmania through Eastern Australia, South-East Asia, and Eastern China to far Eastern Russia [68,85,88,106]. They are also found in Nigeria and Cameroon in the Air and Hoggar regions, the French Massif Central in the Limagne rift, and in Northern, Central, and Eastern Madagascar [39]. In the Australian West Pacific margins intraplate basaltic fields, the U/Pb ages on zircons are widespread between 60 and 1 Ma [69,73,85,86,106]. Nevertheless, U/Pb dating of zircons xenocrysts in the Barrington Tops deposits in New South Wales indicated multiple episodes of corundum formation and eruptive discharges between 60 and 3 Ma [136]. Few U/Pb data gave ages of 150 and 180 Ma for zircons from the deposit of Cudjegong [136], and 400 Ma for those from Tumbarumba [137]. These oldest ages signify that the Australian West Pacific margins has been essentially a passive margin in a couple hundred million years until the Cenozoic basalts related to continental rifting brought corundum to the surface.

5. Classification of Ruby Deposits

5.1. Genetic Classifications

Gem corundum deposits are classified as either primary or secondary deposits. The primary deposits contain corundum either in the rock where it crystallized or as xenocrysts and in xenoliths in the rock that carried it from the zone of crystallization in the crust or mantle to the Earth's surface [39]. The secondary deposits, i.e., present-day placers, are of three types [138]: (1) eluvial concentrations derived by in situ weathering, or weathering plus gravitational movement, or accumulation; (2) colluvial deposits corresponding to decomposed primary deposits which have moved vertically and laterally down-slope as the hillside eroded; and (3) alluvial deposits resulting from erosion of the host rock and transport of corundum by streams and rivers. Concentration occurs where water velocity drops at a slope change in the hydrographical profile of the river, e.g., at the base of a waterfall, broad gullies, debris cones, meanders, and inflowing streams. Sometimes the corundum placers are mined in beach sands [139,140].

Classification systems for corundum deposits have evolved over time and are based on different mineralogical and geological features including: (1) the morphology of the corundum [141]; (2) the geological context of the deposits [5]; (3) the lithology of the host rocks [142]; (4) the genetic processes responsible for corundum formation [110]; (5) the genetic type of the deposit [143], (6) the geological environment and nature of the corundum host-rock [40,80,108,140]; (7) the oxygen isotopic composition of the corundum [144], and (8) discriminant factors developed using oxide concentrations in 900 corundum samples from the main primary deposits [72]. Classification systems for ruby deposits have not been previously proposed.

5.2. An Enhanced Classification for Ruby Deposits

In this work we proposed classifying ruby from primary and secondary deposits into three main types (Table 3).

Primary ruby deposits were subdivided into two types based on their geological environment of formation: (Type I) magmatic and (Type II) metamorphic.

(Type I) Magmatic-related with two sub-types:

(1) Sub-Type IA: Rubies either as xenocrysts or in xenoliths hosted by magmatic rocks such as alkali basalts (Madagascar, and others; see Figure 2);

(2) Sub-Type IB: Xenocrysts of ruby in kimberlite (Democratic Republic of Congo).

(Type II) Metamorphic-related with two sub-types:

(1) Sub-Type IIA: Metamorphic deposits *sensu stricto* in metamorphosed mafic and ultramafic rocks (M-UMR; Sub-Type IIA₁) and marble (Sub-Type IIA₂). Examples of Sub-Type IIA₁ include the ruby deposits in M-UMR from Montepuez (Mozambique), Bekily-Vohibory region (Madagascar), and others, examples of Sub-Type IIA₂ concern the ruby deposits in marble from the Mogok Stone Track, and others.

(2) Sub-Type IIB: Metamorphic-metasomatic deposits characterized by high fluid–rock interaction and metasomatism (Sub-Type IIB₁), i.e., plumasite or desilicated pegmatites as at the former John Saul mine in Kenya, and metasomatites in M-UMR as at Aappaluttoq (Greenland), and marble, and shear zone-related or fold-controlled metasomatic-metamorphic deposits in different substrata, corundum-bearing Mg-Cr-biotite schist and gneiss or marble (Sub-Type IIB₂). Examples are respectively the ruby occurrences at Sahambano, Zazafotsy, and Ambatomena in Madagascar, and Mahenge and the Uluguru Mountains in Tanzania.

Secondary ruby deposits are defined as Type III, i.e., sedimentary-related. They are divided into three sub-types hosted in sedimentary rocks:

(1) Sub-Type IIIA: Gem placers in alkali basalt environments (Eastern Australia, Central Madagascar, South-East Asia, and others).

(2) Sub-Type IIIB: Gem placers in metamorphic environments (Montepuez in Mozambique and the Mogok Stone Track in Myanmar, and others).

(3) Sub-Type IIIC: Gem placers with ruby originating from multiple and unknown sources, such as Ilakaka in Madagascar, Tunduru and Songea in Tanzania, and others.

Table 3. Typological classification of ruby occurrences and deposits worldwide.

Type of Deposit	Magmatic-Related					Metamorphic-Related					Sedimentary-Related *	
Geological Environment	Magmatic					Metamorphic					Sedimentary	
Metamorphic Conditions	Amphibolite to Granulite or Eclogite Facies					Greenschist–Amphibolite–Granulite Facies					No Metamorphism	
Host-Rocks	Magmatic and Metamorphic Rocks					Metamorphic Rocks					Detritic Rocks	
Types of Deposit	TYPE I Magmatic-Metamorphic			Type IIA Metamorphic <i>sensu-stricto</i>			Type IIB Metamorphic-Metasomatism (Fluid-Rock Interaction)				TYPE III (Placers)	
Sub-Types Host-rock of Ruby	TYPE IA Alkali Basalt	TYPE IB Kimberlite *	TYPE IIA ₁ Mafic-Ultramafic Rocks (M-UMR) *			TYPE IIA ₂ Marble	Type IIB ₁ Plumasite * or Metasomatite		Type IIB ₂ Shear-Fault-fold in Gneiss, Schist, M-UMR	Type IIIA Rudites–Arenites–Lutites		Type IIIB Metamorphic Environment
	Xenocryst-Xenolith	Xenocryst	"Verdite"	"Anyolite"	Metamorphosed M-UMR	Mafic Gneiss	Calc-Silicate Rocks	M-UMR	Marble	Alkali Basalt-Kimberlite Fields		
Corundum	Metamorphic (and magmatic?) ruby	Metamorphicruby	Ruby**	Ruby	Ruby	Ruby	Ruby*	Ruby**	Ruby	Ruby	Ruby**	
Deposits Worldwide	All in alkali basalt environment with the presence of either disseminated <i>ruby xenocrysts</i> in volcanoclastics, epiclastics, diatremes, or in <i>ruby-bearing xenoliths</i> of pyroxenite and metagabbro (Antanifotsy, Soamiakatra*, Madagascar)	DRC (Mbuji-Mayi)	Zimbabwe (O'Briens)	Tanzania (Longido)	Tanzania (Winza).	India (Mysore).	Afghanistan (Jegdalek).	South Africa (Transvaal).	Tanzania (Mahenge ^{oo}),	Madagascar (Sahambano *; Zazafotsy *; Ionaivo ,	Australia (Lava Plains;	Sri Lanka (Ratnapura;
		xenocrysts			Madagascar (Andriba;		Nepal (Chumar; Ruyil).	Zimbabwe (O'Briens).	Kitwalo and	Anakie fields;		Elahera,
			South Africa (Barberton)		Bekily-Vohibory (Ejeda;		Pakistan (Hunza valley;	Kenya (Mangare area,	Greyson mines).	Ambatomena **).	New England fields;	Polonnaruwa).
					Ianapera; Fotadrevoo;		Batakundi; Nangimali).	Aqua; Penny lane;		India (Kerala).	Macquarie-Cudjegang;	Myanmar (Mogok;
					Anavoha, Gogogogo,		Tajikistan (Turakuloma**;	Rockland-John Saul mine;		Kenya (Mangare area).	Barrington Tops;	Mong Hsu).
					Maniry; Vohitany;		Badakhshan).	Hard Rock).		Tanzania (Morogoro,	Tumbarumba;	Madagascar (Ilakaka****;
					Ethiopia (Kibre mengist).		Myanmar (Mogok;	Umba-Kalalani).		Mahenge;	Western Melbourne fields).	Andilamena; Didi;
					Kenya (Kitui; Mangare).		Mong Hsu).	Madagascar (Vohibory area - Bekily, Vohitany);		Uluguru Mountains ***).		Zahamena).
					Malawi (Chimwadzulu).		China (Qinghai;	Anavoha***;			China (Muling).	Vietnam (Luc Yen;
					Mozambique (Montepuez;		Yuan Jiang).	Andilamena).			Thailand (Chantaburi- Trat);	Yen Bai; Quy Chau).
					M'sawize; Ruambeze).		Vietnam (Luc Yen;	Russia (Polar Urals, Hit Island;				Tanzania (Tunduru;
					France (Brittany; Lozère;		Yen Bai; Quy Chau).	Karelia).			Cambodia (Pailin).	Songea; Winza;
					French Massif Central,		Tanzania (Morogoro;	Australia (Poona ****; Harts Range ^o).			Madagascar	Umba valley,
					Haut-Allier, Peygerolles).		Mahenge).	United-States (Corundum Hill).			(Ankaratra massif;	Morogoro; Mahenge).
					Italy (Piemont).		Kenya (West Pokot).	France (Haut Allier, Chantel)			Vatomandry).	Mozambique (Montepuez;
					Norway (Froland).		Canada (Revelstoke ***).	Greenland (Aappaluttoq;			Kenya (Baringo).	M'sawize; Ruambeze).
					Finland (Kittilä).		Macedonia (Prilep).	Nuuk-Stovø;			Democratic Republic of	Malawi (Chimwadzulu).
					Greece (Paranesti).		Switzerland (Kangerdluarssuk).				Congo (Mbuji-Mayi).	United-States (North Carolina-Cowee Creek)
					Pakistan (Dir).		(Campo Lungo).	India (Kerala)			Brazil (São Luis).***	
					India (Orissa; Kerala).		France (Pyrenees).	United-States (North Carolina).				
			New Zealand (Hokitika)		Russia (Urals).							
			Spain (Alboran Sea)		Greece (Xanthi).							
			New Zealand (Hokitika).									

Table 3. Cont.

Type of Deposit	Magmatic-Related		Metamorphic-Related					Sedimentary-Related *			
Geological Environment	Magmatic		Metamorphic					Sedimentary			
Metamorphic Conditions	Amphibolite to Granulite or Eclogite Facies		Greenschist–Amphibolite–Granulite Facies					No Metamorphism			
Host-Rocks	Magmatic and Metamorphic Rocks		Metamorphic Rocks					Detritic Rocks			
Types of Deposit	TYPE I Magmatic-Metamorphic		Type IIA Metamorphic <i>sensu-stricto</i>			Type IIB Metamorphic-Metasomatism (Fluid-Rock Interaction)			TYPE III (Placers)		
Sub-Types	TYPE IA	TYPE IB	TYPE IIA ₁			TYPE IIA ₂	Type IIB ₁	Type IIB ₂	Type IIIA	Type IIIB	
Host-rock of Ruby	Alkali Basalt	Kimberlite *	Mafic-Ultramafic Rocks (M-UMR) *			Marble	Plumasite * or Metasomatite	Shear-Fault-fold in Gneiss, Schist, M-UMR	Rudites–Arenites–Lutites		
	Xenocryst-Xenolith	Xenocryst	"Verdite"	"Anyolite"	Metamorphosed Mafic M-UMR	Calc-Silicate Rocks	M-UMR	Marble	Alkali Basalt-Kimberlite Fields	Metamorphic Environment	
Remarks	*very rare economic deposit	*very rare occurrence	*including metamorphosed mafic-ultramafic rocks, mafic gneisses, and special cases of retromorphosed UMR as verdites and anyolite. ** most of the time "corundum".			* include pink corundum. ** Al-rich metapelite or metabauxite intercalated in marble *** metapelite intercalated in marble	* desilicated -pegmatite or -gneiss and other -felsic metamorphic rocks. ** sometimes corundumite. *** rocks called sakenites by Lacroix (1922).	**** ruby associated with emerald. □ in amphibolite. □□ metasomatism of mafic dyke in marble.	* in biotites with sapphires ** circulation of fluids in MR **** circulation of fluids in folds hinge.	* netotectonics and basins. ** include pink sapphire. *** inclusion of ruby in diamond.	**** placers are hosted by detritic rocks of the Triassic Isalo sedimentary serie, unknown origin for ruby.
Economy	non-economic		carving, and gems	economic for some deposits	non-economic	economic for some deposits	economic for some deposits	±economic	economic for some deposits	economic for most of the deposits	

6. The Different Types of Ruby Deposits

We will now examine the main ruby deposits worldwide using the above classification.

6.1. Magmatic-Related (Type I)

6.1.1. Sub-Type IA: Metamorphic Rubies either as Xenocrysts or Xenoliths in Magmatic Rocks such as Alkali Basalts (See Table 3)

During recent decades, studies of sapphire and ruby xenocrysts in alkali basalts focused on the nature of solid and fluid inclusions [11,75,85,145–150], trace element chemistry [70,72–74,81,150], oxygen isotopes [40,144,151–153], and the nature of their parental xenoliths [75,77,81,145,154] to show that gem corundum may have different magmatic and metamorphic origins. Whatever their origin, these rubies are classified in the Type I category because the classification is based on their geological environment and not on their genetic origin.

The origin of ruby has long been debated but its metamorphic origin was accepted based on the work done by Australian researchers on different deposits from eastern Australia [68,106], work that focused on trace element diagrams, mineral inclusions, and oxygen isotopes [155]. A metamorphic origin has been questioned once more by recent studies showing melt inclusions in ruby from the Chanthaburi-Trat region of Thailand and Pailin in Cambodia [105].

The metamorphic origin of xenocrystic rubies as in Eastern Australia, the Kanchanaburi-Bo Rai and Nam Yuen deposits in Thailand, and Pailin in Cambodia, and Central and Eastern Madagascar is characterized by their trace element distributions and inclusions. The classical Fe/Ti versus Cr/Ga chemical variation diagram proposed by [74] permits characterization of “metamorphic” ruby and pink corundum, which are rich in Cr and poor in Ga ($\text{Cr}_2\text{O}_3/\text{Ga}_2\text{O}_3$ ratio > 3), and contain inclusions of chromiferous spinel, pleonaste, Al-rich diopside, and sapphirine. Recently, [81] characterized rubies (up to 3370 ppm Cr) and pink corundum (up to 1520 ppm Cr) from New England placers, which have distinctive trace element features compared to those found elsewhere in Eastern Australia. In particular they exhibit very high contents of Ga (up to 310 ppm) and Si (up to 1820 ppm). High Ga and Ga/Mg values are unusual in ruby, and the trace elements suggest a magmatic–metasomatic influence for the genesis of New England rubies. The oxygen isotopes ($\delta^{18}\text{O} = 4.4 \pm 0.4\text{‰}$, $n = 22$) fit within the range of $\delta^{18}\text{O}$ values defined for ruby hosted in M-UMR. Zoned ruby and pink corundum (Figure 23A) have high Mg, Ga, and Cr and the Fe versus Ga/Mg diagram suggests magmatic affinity (Figure 23B).

The geological origin of New England rubies before their transport by alkali basalts remains a great mystery. Sutherland et al. [81] proposed for their formation either the interaction of intrusive fractionated I-type granitoid magmas, during the New England orogeny, with Cr-bearing ophiolites, or ruby-bearing eclogites and -cliopyroxenites in metamorphosed M-UMR. It is important to note that the different chemical parameters (such as Ga/Mg, Fe/Ti, Fe/Mg, and Cr/Ga) proposed by [70] were designed only for origin determination of blue sapphires. In some cases, the use of these chemical diagrams is not useful for discriminating geologic or geographic origin of corundum. In the case of Australian rubies, the majority of the data are scattered in the field of metamorphic sapphires, but those of New England overlap the field of magmatic ones. The New England case, and other as for Chanthaburi-Trat and Pailin rubies illustrate the complexity and ambiguity of the use of trace element chemistry [11].

These chemical domains have no genetic significance for some cases and they illustrate only the variation of metals in the parental fluids before their incorporation in the structure during crystal growth, i.e., a kind of chemical color signature. On the contrary, the Fe (ppm) versus Ga/Mg discrimination diagram applied to ruby (see Figure 19) shows that the high variation of Fe in ruby correlates with the geological classification of ruby deposits characterized by decreasing Fe in ruby from M-UMR to marble and plumasite. The overlap is not extensive, as it is for sapphires and the diagram can apparently be used for deciphering the geological origins of ruby.

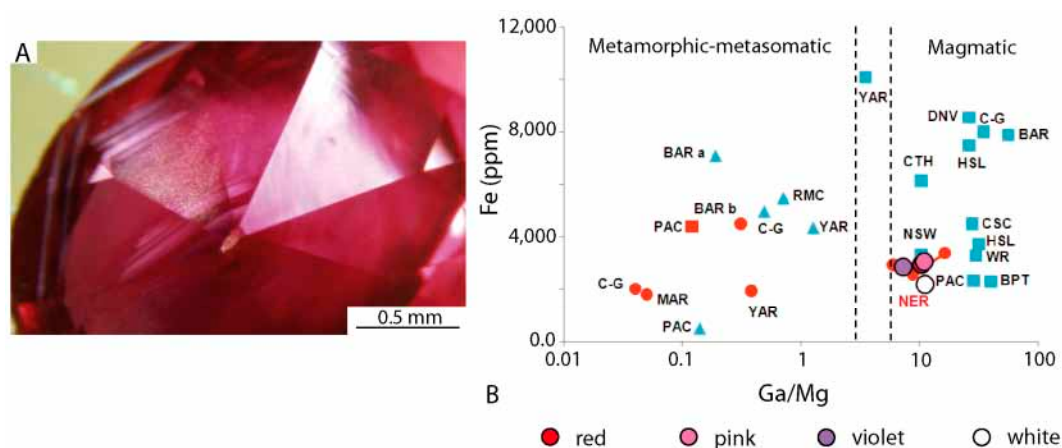


Figure 23. Rubies from the New England locality of Eastern Australia. (A) Apex culet view of an oval-cut 2.31 carats zoned ruby showing alternating growth zones passing through violet to white and pink bands and to ruby on the extreme margin of the top table, Collection Australian Museum. Photo: Gayle Webb; (B) Fe (ppm) versus Ga/Mg diagram for ruby and pink, violet, and white corundum from New England ruby (NER) and other Eastern Australian localities; chemical data from [86]. The red symbols indicate ruby, the blue triangles metamorphic sapphire suites, and the blue squares magmatic-transitional sapphire suites. The different localities are: NSW = New South Wales; BAR = Barrington Tops; YAR = Yarrowitch; C-G = Cudgegong-Gulgong; MAR = Macquarie River; WR = Weld River, NE Tasmania; PAC = Pailin, Cambodia; BPT = Bo Phloi, Thailand; HSL = Huai Sai, Laos; CSC = Changle, Shandong, China; DNV = Dak Nong, Vietnam; CTH = Chanthaburi-Trat, Thailand; RMC = Rio Mayo, Colombia.

Mineral inclusions are also key features in the debate about metamorphic versus magmatic origin of rubies. The most common solids are clinopyroxene (Al-rich diopside), plagioclase (bytownite to andesine), K-feldspar-spinel association [148,149], garnet (pyrope, \pm almandine), sapphirine, scapolite, Cr-spinel, meionite, phlogopite, anatase, apatite, sillimanite, and sulphides [5,68,77,105,145,146,154,156]. All of these minerals are described in rubies found in metamorphic environment, although some of them are also found in magmatic assemblages. The discovery of melt inclusions in ruby reopened the debate about their possible magmatic origin [105,148,149]. Glassy melt inclusions are described frequently for sapphires in alkali basalts [157] and lamprophyres [147,158] but not commonly in rubies. Melt inclusions in rubies from Thailand and Cambodia were reported by [16], recognized by [156], and confirmed by [148,149]. Two types of melt inclusions were observed in the Thai and Cambodian rubies [106]: (1) glassy melt inclusions with negative crystal morphology, generally 25–100 μm in size, and with a contraction bubble; (2) polycrystalline aggregates, 200–500 μm across, considered to be recrystallized melt inclusions. The EMPA analyses of two melt inclusions in ruby from Thailand and Cambodia gave similar chemical compositions in wt % oxides: 53.4. < SiO_2 < 55; 23.6 < Al_2O_3 < 24; 4.9 < CaO < 6.2; 4.4 < Na_2O < 5.2; 0.1 < K_2O < 3.1; 1.2 < FeO < 1.6; 1.4 < MgO < 1.9; 0.1 < TiO_2 < 0.2, and 6.3 < volatiles < 7.5. These chemical data are comparable to those found for melt inclusions in Yogo Gulch sapphires from Montana. Palke et al. [105] suggested that corundum formed during partial melting of hydrated and carbonated lower crustal anorthosites or troctolites by local intrusion of the lamprophyres or alkali basalts (for the Thai and Cambodian deposits) that eventually carried the corundum to the surface. The genetic model proposed by [105] for the Thai and Cambodian rubies is an anorthosite that was converted at higher pressure to a garnet-clinopyroxenite. In this scenario, Palke et al. [105] argued that ruby is not an “accidental xenocryst” transported by the alkali basalt but rather an “in situ” xenocryst enclave in the alkali basalt itself before its transport to the surface. To the contrary and despite the presence of melt inclusions in ruby from Bo Rai, Promwongan et al. [148,149] and Sutthirat et al. [154] considered that the assemblage Al-rich pyroxene, plagioclase, pyrope, and spinel closely resembles the mineralogy of mafic granulite xenoliths in alkali basalt associated with the Bo Rai gem field.

The main discussion that arises from this genetic scenario is that the proposed anorthosite protolith for ruby formation has been affected by deformation and consequent metamorphism at high temperature. Under these conditions, how can we define the exact nomenclature and the genesis of ruby, i.e., magmatic origin (anorthosite) or metamorphic (clinopyroxenite or metagabbro in the eclogite facies), or both? The following studies are examples of the ongoing debate:

(1) Sutthirat et al. [145] reported ruby (0.27 wt % Cr_2O_3) included in a clinopyroxene (0.22 wt % Cr_2O_3 ; 16.7 wt % Al_2O_3 ; and 1.8 wt % Na_2O) xenocryst in the Nong Bon alkali basalt, one of the Cenozoic Chantaburi-Trat basalts of Eastern Thailand. Ruby from the alluvial deposits contains inclusions of garnet (pyrope), sapphirine, and Al-Na-clinopyroxene. Thermodynamic calculation constrained the temperatures of ruby + clinopyroxene crystallization to between 800 and 1150 ± 100 °C and pressures of between 10 and 25 kbar, corresponding to depths of 35–90 km. The pyrope + ruby assemblages formed at depths greater than 60 km and the source rock proposed was a mafic ruby-pyrope-pyroclastic or ruby-pyrope-clinopyroxenite. Sutthirat et al. [145] rejected a magmatic crystallization for the ruby and this was confirmed by later studies of Thai ruby [148,149,154].

(2) Sutherland et al. [75] studied a suite of alluvial-sourced pink corundum and ruby (up to 0.6 wt % Cr_2O_3) from the paleodrainage deposits along the Cudgong-Macquarie River in New South Wales, Australia. The ruby contained inclusions of clinopyroxene (0.1 wt % Cr_2O_3 ; 20.3 wt % Al_2O_3 ; and 1.0 wt % Na_2O), meionite, and anatase. Primary fluid inclusions are either two-phase (liquid + gas) or three-phase (liquid + gas + daughter phases), but melt inclusions were not reported. The comparison of clinopyroxene-ruby thermometry at Cudgong-Macquarie suggested ruby formation at temperatures between 1000 and 1300 °C. The P–T diagram showing thermometric paths for Al-rich diopside-ruby pairs from different ruby deposits in Thailand and Australia represented in Figure 24 [75,81]. Saminpanya et al. [146] confirmed the presence of inclusions of garnet (pyrope), Al-rich diopside, and sapphirine in Thai rubies. They proposed that the rubies crystallized in high-pressure metamorphic rocks of UMR composition in the upper mantle.

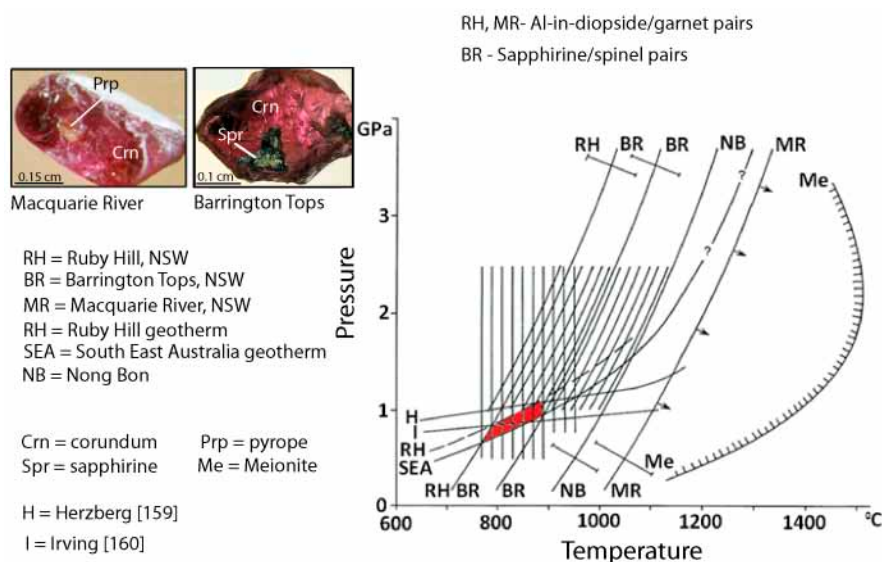


Figure 24. Thermometric traces for mineral inclusion pairs for rubies from Australia (Ruby Hill, Barrington Tops, and Macquarie River) and Thailand (Nong Bon), modified from [81]. The P (GPa)–T (°C) diagram is based on Al- in diopside/garnet and sapphirine/spinel pairs, after [75,136]. The traces intersect the T range for Barrington Tops rubies (vertical lines), the East Australian ruby-bearing xenolith-derived Mesozoic garnet granulite (RH) and late Cenozoic (SEA) geotherms, the garnet to spinel pyroxenite transition of [159] (H), and the garnet-clinopyroxene-plagioclase transition of [160] (I). The red area represents P 6–8 kbar for the Barrington Tops ruby suite. The extreme Al-rich diopside and meionite-bearing Macquarie River ruby suggests a P–T crystallization between thermometric trace (MR) and the meionite stability boundary (Me).

(3) Sutthirat et al. [154] studied different types of xenoliths contained in basalts from Bo Rai viz. (1) peridotites; (2) clinopyroxenites; and (3) ruby-bearing mafic granulites with plagioclase-clinopyroxene-spinel-garnet. Peridotitic xenoliths have characteristics of depleted mantle (lherzolite to harzburgite and dunite) and the P–T estimates yielded approximately 1000–1300 °C at 1.6–1.9 GPa. Clinopyroxenite and mafic granulites xenoliths are mantelic cumulates formed at P–T, respectively, between 950 and 1200 °C and 1.6 and 2.2 GPa, and 700 and 1000 °C and 0.95 and 1.3 GPa. The xenoliths suffered a few metamorphic events and the authors argued that ruby formation is clearly related to mafic granulite xenoliths (which appear to have formed at about 30–50 km depths before transport by basaltic eruption).

(4) The Soamiakatra ruby deposit in the Antsirabe area, Antananarivo province, was an economic in situ mining site such as at Pailin, Cambodia, where ruby was found either as xenocrysts in alkali basalt or in xenoliths brought to the surface by the Cenozoic Ankaratra volcanism [77]. The deposit at Morarano known as Soamiakatra [95,161–163] was discovered in 1997. Ruby has been extracted by panning from alluvial and soils, but prospecting and mechanization of operations exposed the weathered primary deposit at the top of the basaltic plug (Figure 25A). The ruby-bearing clay and phyllitic material of whitish color (20 m thick) was exploited for two years before bedrock was reached (Figure 25B). The secondary deposit assured an easy and effective ruby production of high quality.

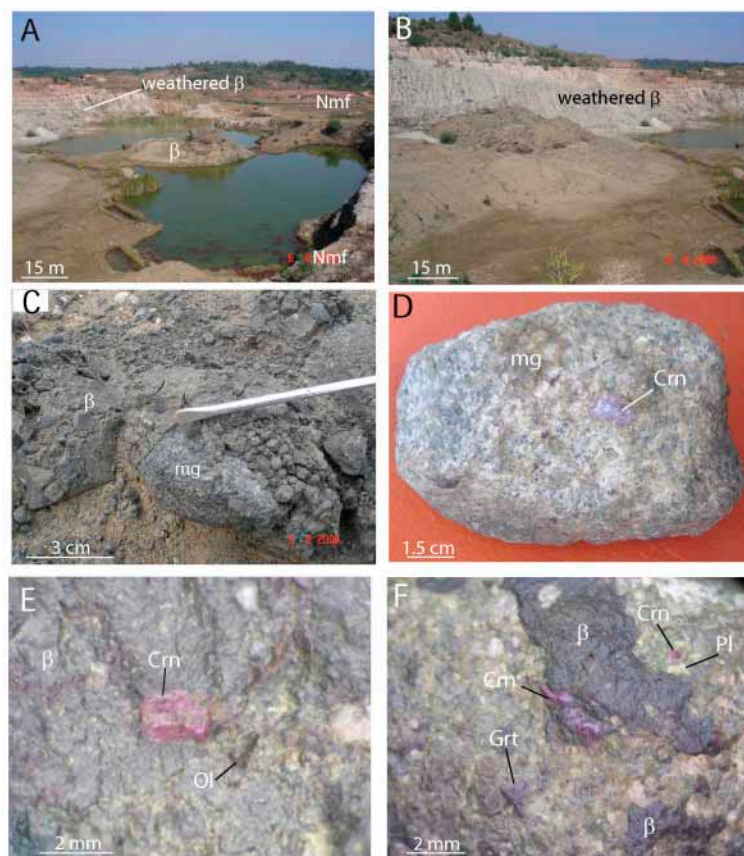


Figure 25. The Soamiakatra ruby deposit (Madagascar). (A) View of the quarry showing the contact of the alkali basalt (β) plug with the Neoproterozoic metamorphic formations (Nmf). The economic weathered upper zone of the alkali basalt (β) was mined in the past up to the non-weathered basalt; (B) aspect of the ruby-bearing weathered basaltic zone, around 20 m thick, mined in benches; (C) ruby-bearing metagabbro xenolith (mg) carried by the alkali basalt (β); (D) macroscopic aspect of a ruby (Crn)-bearing metagabbro xenolith (mg); (E) xenocryst of ruby with an olivine (Ol) crystal in the alkali basalt (β); and (F) ruby-garnet (Grt)-plagioclase (Pl)-bearing metagabbro crosscut by the alkali basalt (β) flow. Photos: Gaston Giuliani and Saholy Rakotosamizanany.

The alkali basalt dyke intruded graphitic gneisses, khondalites, and migmatites of the Neoproterozoic Ambatolampy and Tolongoina series. The alkali basalt hosts numerous enclaves and xenoliths (Figure 25C), 2–20 cm across, of crustal (gneiss, migmatite, and granitoid) and mafic (peridotite, clinopyroxenite, gabbro, and garnetite) origin. Ruby was found: (1) as xenocrysts up to 2 cm across in the alkali basalt (Figure 25E); (2) in clinopyroxenite xenoliths composed of plagioclase (labradorite and bytownite), scapolite (meionite), garnet (pyrope), clinopyroxene (Al-diopside), orthopyroxene (85 mol % En), and pargasite; and (3) in banded metagabbro (Figure 25D,F) composed of alternating dark and greyish ruby-bearing bands. The dark bands contain pyrope (Figure 26A,C), plagioclase (labradorite-bytownite), Mg (\pm Cr)-spinel, scapolite (meionite), Al-diopside, and orthopyroxene (85 mol % En). The greyish band is made up of labradorite-bytownite, diopside, magnesian spinel, sapphirine (Figure 26D), some calcite, and pyrope. Diopside formed as a clean and clearly visible corona around both corundum and Mg (\pm Cr)-spinel (Figure 26D). Two generations of clinopyroxene are discriminated (Figure 26A,B): (1) early Al-rich crystals (13–17.5 wt % Al_2O_3), 1–2 mm across, associated with plagioclase, garnet, and scapolite (Cpx1), and (2) late and less Al-rich crystals (5–8.8 wt % Al_2O_3 , Cpx2), 10–40 μm across, formed around Cpx1 (Figure 26B) or as inclusions in ruby.

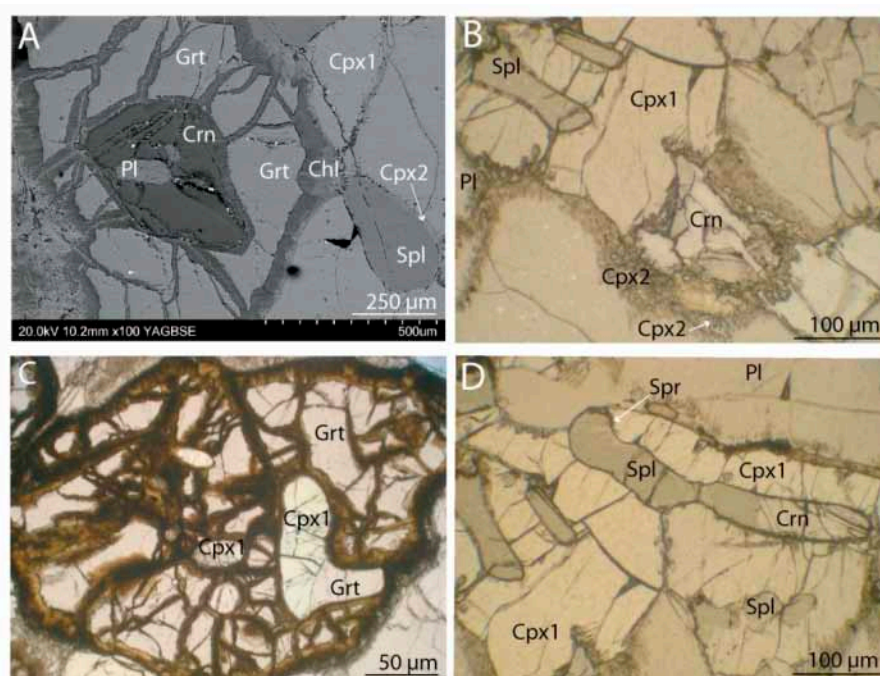


Figure 26. Petrographic aspects of the metagabbroic xenoliths in the Soamiakatra ruby deposit. (A) Plagioclase (Pl)-bearing ruby (Crn) within garnet (Grt). Garnet (pyrope) associated with an Al-rich clinopyroxene (Cpx1) and showing a keliphitic texture. The keliphitic halo is composed of small grains of chlorite (Chl). The spinel (Spl) and Cpx1 are bordered by a second generation of clinopyroxene (Cpx2); (B) association ruby-Cpx1-plagioclase (Pl)-spinel. The ruby formed upon Cpx1 while small crystals of Cpx2 formed later; (C) inclusions of Cpx1 in pyrope (Grt); and (D) association spinel-ruby with Cpx1 with plagioclase. Spinel is bordered by sapphirine (Spr). Photos: Saholy Rakotosamizany.

Mineral inclusions in the ruby consist of phlogopite, rutile with some lamellar exolutions of ilmenite, zircon, albite, Al-pyroxene, garnet (pyrope), and Mg-spinel. The trace element chemistry of the ruby is characterized by low Ga_2O_3 (between 70 and 110 ppm) and high $\text{Cr}_2\text{O}_3/\text{Ga}_2\text{O}_3$ ratios (see Figure 16). Vanadium varies from less than 22 to 860 ppm. Titanium ranges between 60 and 940 ppm, and Cr between 350 and 3830 ppm. The Soamiakatra rubies fall into the metamorphic domain defined by [68] when plotted on the $\text{Fe}_2\text{O}_3/\text{TiO}_2$ versus $\text{Cr}_2\text{O}_3/\text{Ga}_2\text{O}_3$ diagram (see Figure 16).

Petrographic examinations showed two main stages for the mineral assemblages: (1) the first stage is typified by the association Cpx + garnet + scapolite + ruby, and spinel + ruby + garnet. The spinel

is always surrounded by a ring of ruby, clinopyroxene, and sapphirine, and the mineral association is in turn haloed by coronitic garnet. Thermodynamic calculations constrained the P–T estimates of the assemblages to around 1100 °C and 2 GPa; (2) the second stage results in the destabilization of scapolite to anorthite + calcite with the destabilization of some Al-diopside in pargasite, and also the reaction spinel + ruby to sapphirine (T 1100 °C and P 15 GPa).

The P–T conditions of around 1100 °C and 2 GPa clearly show that the xenoliths originated from the upper mantle and that the metagabbros experienced the eclogite facies. During decompression the mineral assemblage was marked by the destabilization of Cpx1 and the formation of Cpx2 (in the granulite facies). Rakotosamizany et al. [77] hypothesized that the ruby formed in M-UMR at the base of the lower crust-upper mantle and was later transported to the surface by the alkali basalt. The oxygen isotopic composition of the rubies ($1.25\text{‰} < \delta^{18}\text{O} < 5\text{‰}$, $n = 5$) is within the range of values defined for ruby in basaltic environments ($1.25\text{‰} < \delta^{18}\text{O} < 5.9\text{‰}$, $n = 4$; mean $\delta^{18}\text{O} = 3.1 \pm 1.1\text{‰}$, $n = 80$) and in metamorphosed M-UMR ($0.25\text{‰} < \delta^{18}\text{O} < 6.8\text{‰}$, $n = 19$; [163]. Rubies from Chantaburi-Trat volcanics have similar O-isotopic ranges ($1.3\text{‰} < \delta^{18}\text{O} < 4.2\text{‰}$; [152]) and the P–T conditions are identical to those proposed for the Soamiakatra rubies.

(5) Occurrences of ruby in the Neoproterozoic Vohibory formation from Southern Madagascar (see Figure 1E) are found in M-UMR complexes of meta-peridotite, -gabbro, and -troctolite transformed into amphibolites and serpentinites with anorthositic dykes [116]. The ruby occurrences include Anavoaha, Gogogogo, Maniri, Vohitany, Ianapera, and Marolinta [164]. The ruby frequently occurs in sapphirine or gedrite and locally garnet (pyrope-almandine)-bearing amphibolites and locally anorthosite [122]. These rocks are associated with garnet-bearing granulites (salite + almandine + hornblende + andesine). At Anavoaha, ruby occurs with (1) sapphirine or gedrite + garnet, and (2) anorthosite with ruby + garnet + anorthite. These ruby-bearing rocks are associated with a coronitic metatroctolite.

The transition is sharp between the metatroctolite and the sapphirine or gedrite amphibolites and gradual between the garnet (50% almandine-35% pyrope)-ruby-bearing anorthosite and amphibolites. The ruby is surrounded by a corona of green spinel and anorthite and the mineralogical association is gedrite + anorthite + garnet (60% pyrope) + ruby ± spinel. Sometimes the ruby is totally replaced by spinel. The P–T conditions of ruby formation during the Neoproterozoic metamorphism was estimated at $P = 0.9\text{--}1.15$ GPa and $750\text{--}800$ °C [116], similar to those reported by [75] for the ruby-bearing xenolith of Ruby Hill in Australia.

At Vohitany and Anavoaha, ruby is also found in desilicated pegmatites at the contact of amphibolites.

We previously examined the origin of ruby transported to the surface by basaltic volcanism by studying examples from Thailand, Australia [81], and Madagascar. Mafic cumulate xenoliths are rare worldwide and [154] showed that mantle and deep crustal xenoliths from the Bo Rai ruby deposit were the probable source of “basaltic rubies” mined in placers from Thailand and Cambodia. The Cpx-Spl-Grt ± (Ol) ± (Opx) and Pl-Cpx-Spl ± (Grt) ± (Crn) assemblages were considered to be two different types of mafic cumulates with high Al₂O₃ contents that suffered metamorphic overprints [154]. P–T constraints based on textural observations gave estimated depths of formation between 30 and 80 km. These xenoliths are similar to those reported for ruby-related alkali basalts from Madagascar [77]. At Soamiakatra, the estimated temperature 1100 °C and pressure 2 GPa of ruby formation are comparable to those proposed for mafic cumulates from Bo Rai. Al-rich clinopyroxene-pyrope-anorthite is the main assemblage of these ruby-bearing metagabbros and clinopyroxenites. Spinel and ruby are associated but ruby also formed at the expense of clinopyroxene.

The probable original source of the ruby in the mafic cumulates carried by Cenozoic alkali basalt plugs in the Ankaratra massif is visible in the Neoproterozoic metamorphic rocks of the Vohibory formation in Southern Madagascar. The ruby-bearing amphibolites and anorthosites are the fruit of the metamorphic transformation of a magmatic cumulate complex.

The presence of melt inclusions as described by [105,148,149] opened the debate about the possibility of “magmatic” ruby. The genetic model proposed by [105], i.e., an anorthosite

converted at higher pressure to a garnet-clinopyroxenite, is debatable but not applicable for ruby in Madagascar. The melt inclusions can result either from an incongruent melting of plagioclase during metamorphism [165] or directly through a peritectic melting reaction involving plagioclase or other al-rich minerals. In consequence, most rubies in alkali basalts can be considered actually as metamorphic in origin but the presence of primary melt inclusions in ruby [105] indicates that a free magma phase existed during ruby growth. Additional studies characterizing carefully the inclusions in more basalt-related rubies would be helpful to shed more light on the two possible origins, i.e., metamorphic versus magmatic. The ruby-bearing mineral assemblages described in M-UMR, metamorphosed and recrystallized at depth within the mantle, at Beni Bousera, Morocco [166,167] and Ronda, Spain [97], and considered of metamorphic origin, can be described as a potential restitic component of a partially melted mafic M-UMR protolith?

The $\delta^{18}\text{O}$ values of ruby from the Soamiakatra, Bo Rai, Pailin, Barrington, Anavoha, and Beni Bousera occurrences fit within the worldwide range defined for ruby in basaltic environments ($1.25\text{‰} < \delta^{18}\text{O} < 5.9\text{‰}$, mean $\delta^{18}\text{O} = 3.5 \pm 1.3\text{‰}$, $n = 57$) and ruby associated with M-UMR ($1.25\text{‰} < \delta^{18}\text{O} < 7.0\text{‰}$, mean $\delta^{18}\text{O} = 5.0 \pm 1.2\text{‰}$, $n = 32$; [84], Figure 27). Both ranges of $\delta^{18}\text{O}$ values overlap and are closed to the $\delta^{18}\text{O}$ mantle value of $5.5 \pm 0.4\text{‰}$ [168]. Nevertheless, the genetic source of ruby, i.e., strictly metamorphic or magmatic cannot be specified as the oxygen isotopic composition of ruby is largely buffered by that of its protolith, whether metamorphic or magmatic [92].

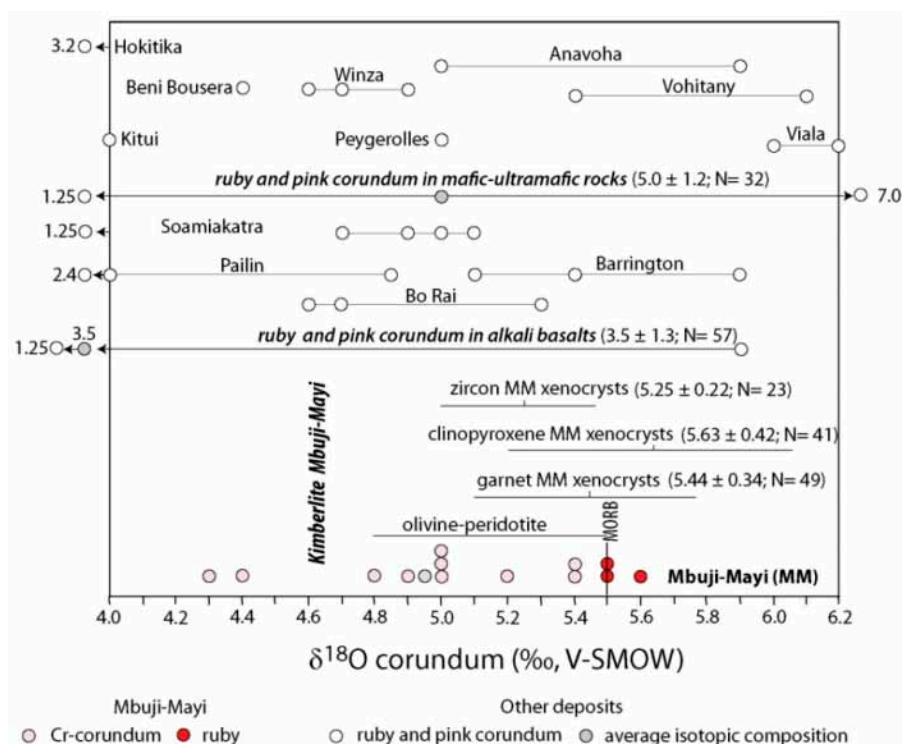


Figure 27. Oxygen isotope ranges defined for different ruby and pink corundum deposits and occurrences related to metamorphosed mafic-ultramafics and alkali basalts worldwide as well as the kimberlite at Mbuji-Mayi, modified from [84]. The data are reported in the conventional delta notation relative to V-SMOW (Vienna Standard Mean Ocean Water). The $\delta^{18}\text{O}$ values for zircon, clinopyroxene, and garnet megacrysts from the Mbuji-Mayi kimberlites are from [163]. The deposits that occur in amphibolites are Anavoha and Vohitany (Madagascar), Viala and Peygerolles (France), Kitui (Kenya), and Winza (Tanzania). The Hokitika (New Zealand) and Beni Bousera (Morocco) occurrences are linked to metamorphosed M-UMR.

6.1.2. Sub-Type IB: Metamorphic Rubies as Xenocrysts in the Mbuji-Mayi Kimberlite (Democratic Republic of Congo; See Figure 2, Table 3)

Ruby has been described as micrometric crystal inclusions in diamond at Juina in Brazil [43,169–171]. Crystals of ruby and Cr-bearing corundum (up to 2 cm) xenocrysts have been found in the Mbuji-Mayi kimberlite in the Democratic Republic of Congo [84]. The kimberlite contains megacrysts of garnet and diopside [172], zircon and baddeleyite, and also Mg-rich ilmenite, Nb- or Cr-rich rutile, corundum, kyanite, Mg-rich chlorite, and rutile-silicate intergrowths [173]. The 0.5–2 cm-sized corundum megacrysts are:

(1) Gem rubies from red to fuchsia and flashy-pink deep pink rubies ($n = 3$) that contain Cr-bearing spinel (with Cr_2O_3 up to 1.5 wt %), chromite, and rutile. The rubies have very high contents of Cr_2O_3 (0.71–4.59 wt %) and FeO (0.22–0.66 wt %). Vanadium is between 986 and 1867 ppm, and Ti less than 68 ppm. The contents of MgO (31–100 ppm) and Ga_2O_3 (50–193 ppm) range to moderate levels with a low Ga/Mg ratio (0.6–2.6, see Figure 19).

In the diagram $\text{FeO}-\text{Cr}_2\text{O}_3-\text{MgO}-\text{V}_2\text{O}_3$ versus $\text{FeO} + \text{TiO}_2 + \text{Ga}_2\text{O}_3$ [84], the three rubies plot in the domain R3 of M-UMR (Figure 28):

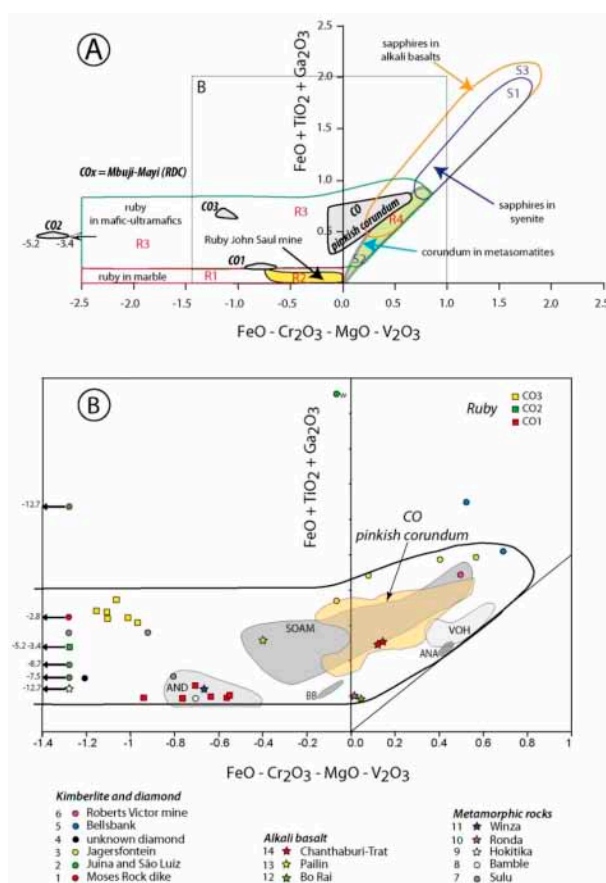


Figure 28. Chemical variation of ruby and pinkish corundum from the Mbuji-Mayi kimberlite in the Democratic Republic of Congo. (A) The $\text{FeO}-\text{Cr}_2\text{O}_3-\text{MgO}-\text{V}_2\text{O}_3$ versus $\text{FeO} + \text{TiO}_2 + \text{Ga}_2\text{O}_3$ (analysis in wt %) classification diagram, modified from [84]. The different chemical fields of the studied corundum are reported with respect to those for ruby (samples CO1, CO2, and CO3) and pinkish corundum (CO, yellowish field); (B) Field of chemical compositions of the ruby and pink sapphires from Mbuji-Mayi. Different chemical fields are reported for ruby from Beni Bousera in Morocco (BB), Soamiakatra (SOAM), Anavoha (ANA), Vohitany (VOH), and Andriba (AND) from Madagascar. Other representative compositions of ruby from occurrences in kimberlite and diamond, alkali basalt, and metamorphic rocks are also shown; modified from [84,164].

- (a) The field of sample CO1 overlaps the plots of rubies from Andriba in Madagascar hosted in ultramafics [174], the Winza deposit in Tanzania located in amphibolite and metagabbro [120], high-grade Proterozoic orthoamphibolites of the Bamble area in Norway [43], and ultrahigh pressure ruby-rich garnetite layers in garnet lherzolite in the Sulu terrane of China [175].
- (b) The field of sample CO2 is defined by the very high Cr₂O₃ content of ruby up to 4.6 wt %. Chromium-rich ruby is rare and found in the Brazilian São Luiz alluvial deposit and in the Juina kimberlite [43,170], the Moses Rock Dyke kimberlite in Utah [176], the metagabbros at Karelia in Russia [41], and in the serpentinite at Hokitika in New Zealand [42].
- (c) The field of sample CO3 is comparable to the chemical composition of ruby-bearing garnetite xenolith in garnet peridotite from the Sulu terrane in China [175].

The rubies have a restricted range of $\delta^{18}\text{O}$ values from 5.5‰ to 5.6‰ ($n = 3$; Figure 27). They fit within the worldwide O-isotopic range of rubies associated with metamorphosed M-UMR.

(2) Cloudy pinkish to greyish corundum ($n = 10$), which are host to inclusions of Mn-rich ilmenite, margarite, and rutile. They are richer in FeO (0.38–0.75 wt %) than rubies and they always contain some Cr₂O₃ (0.08–0.58 wt %) and V (318–1128 ppm). The Ga/Mg ratio (1.95–3.95) is in the range of, or above, the Ga/Mg ratio of ruby. They have $\delta^{18}\text{O}$ values in the range 4.3–5.4‰ with a mean $\delta^{18}\text{O}$ value of $4.9 \pm 0.4\text{‰}$ ($n = 10$; Figure 27), within the accepted range of mantle values [168]. These oxygen isotope values are within the range of values defined for ruby xenocrysts or megacrysts carried to the surface by alkali basalts [84]. They are also similar to those found for ruby in eclogites derived from oceanic crust [166] and hosted by clinopyroxene xenocrysts from Bo Rai alkali basalt alluvials as well as those from the Soamiakatra metagabbros.

Kimberlites, like alkali basalts, are conveyors of gems (respectively diamond and corundum) from the asthenosphere and/or lithosphere to the upper crust [86,177]. Ruby and sapphire inclusions in diamond are rare and corundum xenocrysts or megacrysts in kimberlites are exceptional. On the contrary, diamond has never been found as inclusions in corundum or within xenocrysts in alkali basalts. The chemistry and oxygen isotope composition of ruby from Mbuji Mayi allow for different possible origins:

(1) An upper mantle-derived material (garnet lherzolite, garnetite and pyroxenite) that could have been infiltrated and metasomatized by the kimberlite melt, or a high-pressure orogenic peridotite; or (2) eclogite-type xenoliths (omphacitic clinopyroxene-bearing metagabbro and/or clinopyroxenite) affected by a retrograde metamorphic stage in the granulite facies at the base of the continental crust (Figure 29).

The pinkish to greyish corundum could also have different probable origins: either as subducted oceanic crust transformed into eclogite, or as clinopyroxenite layers/horizons in peridotite.

6.2. Metamorphic-Related (Type II)

6.2.1. Sub-Type IIA: Metamorphic Deposits *Sensu Stricto* with Two Different Types Formed in Amphibolite to Granulite Facies (See Table 3)

Sub-Type IIA₁ includes ruby in metamorphosed mafic and ultramafic rocks (M-UMR) as found at Montepuez in Mozambique (see Table 3).

Ruby and pink corundum in metamorphosed M-UMR called “ruby in amphibolite” by some gemmologists originate from the metamorphism of gabbroic and dunitic rocks from ophiolites or volcano-sedimentary sequences. These deposits are the main sources of pink and red corundum but generally not of gem quality material.

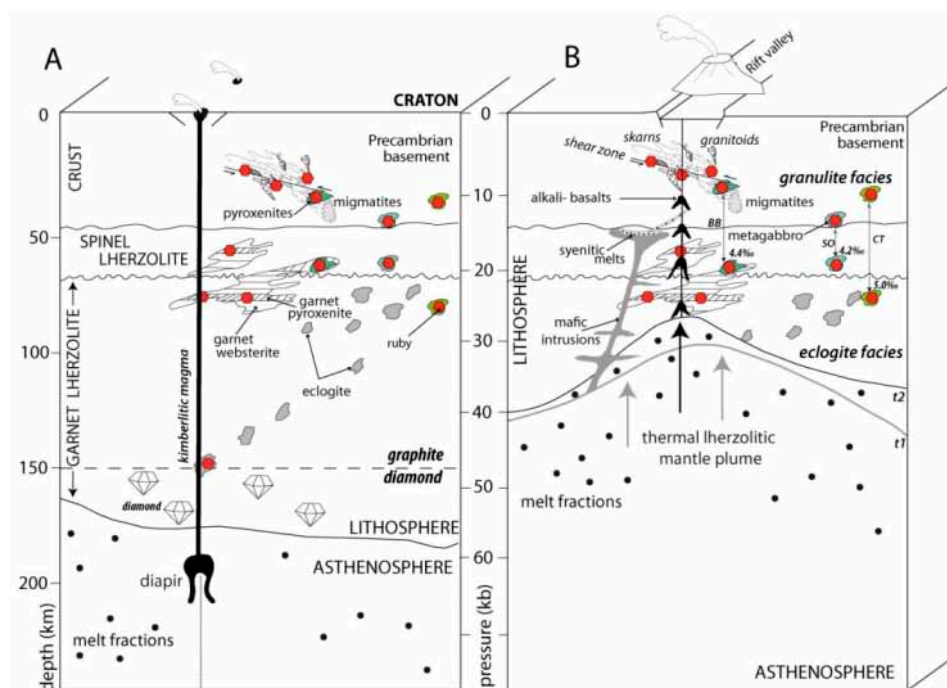


Figure 29. Schematic genetic models for gem corundum related to kimberlite (A) and alkali basalt (B) environments, modified from [178–180]. The drawings show the different types of corundum occurrences hosted in Precambrian basements in the crust, and lherzolites in the lithosphere. Selected ruby occurrences are indicated (with their corresponding $\delta^{18}\text{O}$ composition, in ‰) including the Beni Bousera (BB) garnet clinopyroxenite, the Soamiakatra (SO) garnet metagabbro and -clinopyroxenite, and the Chanthaburi-Trat (CT) pyroxene inclusion in ruby, with their retrograde metamorphic location in the granulite facies. Panel (B) shows ruby deposits associated with alkali basalt in continental extension domains characterized by thermal anomalies linked to mantle plumes and rift valley fracturing and volcanism in the upper part of the crust. t1 and t2 are two successive ascent stages of the alkali basalt magmatism.

The crystals are used for cabochon cut and ornamental artifacts such as the famous ‘anyolite’ from Longido in Tanzania [181–183] (see Figure 4B). Such ruby deposits in amphibolite and gabbro are known (see Figure 2) from Kittilä in Finland [184], Sittampundi in India [185], Chantel in France [186], Paranesti in Greece [95,187], Lossogonoi in Tanzania [181], Kitui in Kenya [188], Chimwadzulu in Mozambique [189,190], the Vohibory formations in Madagascar [119,122,164] (see Figure 1E), the Harts Range in Australia [191,192], Dir in Pakistan [193], Hokkaido in Japan [194], and some of the deposits in North Carolina in the USA [5,121,195]. In Africa, the ruby deposits discovered in the last decade are highly economic for their color, clarity, and quantity; these are Winza in Tanzania [120,196,197] (see Figure 4C), and at Montepuez, Ruambeze, and M’sawize in Mozambique [21–23,25,26,96,198] (see Figure 1C).

The common mineral assemblage of the ruby-bearing amphibolite includes corundum, anorthite, amphibole (gedrite, pargasite), and margarite [21,22,121,122]. Others minerals including sapphirine, pyrope-almandine garnet, spinel, kornepurine, plagioclase, phlogopite, and zoisite may be present. The initial basic composition of the protolith includes gabbro, dunite, and troctolite [121,122,194,199].

(1) The ruby deposits at Longido and Lossogonoi in Northeastern Tanzania are hosted in amphibolite dykes that crosscut metamorphosed M-UMR (Figure 30). At Longido, the ruby is located in amphibolite dykes up to 1 m thick that are oriented parallel to the metamorphic foliation [118]. The dykes crosscut a serpentinite with relics of olivine and orthopyroxene. They are retroformed to a rock composed of zoisite and ruby called “anyolite” (green stone in Massai language). The contact of the dyke with the serpentinite is outlined by the presence of phlogopite and Mg-amphibole schist.

The mineral assemblage in the amphibolite is anorthite + corundum + amphibole + green spinel while the anyolite contains zoisite + corundum ± tschermakite. The age of formation of the ruby obtained on zircon by the U/Pb method is 610 Ma [124].

(2) At the Winza deposit in central Tanzania, high-quality ruby and sapphires have been recovered from an eluvial deposit. Mining revealed that the gem corundum crystals are embedded in dark amphibolite [120,196,197]. The corundum is locally associated with areas of brown to orangey garnet ± feldspar, with accessory Cr-spinel, mica, kyanite, and allanite. The ruby and sapphire crystals are closely associated with dykes of a garnet- and pargasite-bearing rock crosscutting amphibolite (Figure 31A). The central part of the dyke is composed of garnet (pyrope-almandine) + pargasite ± plagioclase ± corundum ± spinel ± apatite. Metamorphic conditions estimated from the garnet-amphibole-corundum equilibrium assemblage are $T 800 \pm 50 \text{ }^\circ\text{C}$ and $P 8\text{--}10 \text{ kbar}$ [120]. The rubies and pink corundum are zoned with rhombohedral twin planes. The rubies exhibit a suite of inclusions with amphibole, garnet, apatite, and opaque minerals (chalcocite). Medium and vivid red rubies have orange-brown hair-like inclusions of unknown composition [120]. The chemical compositions of the Winza ruby and pink sapphires (Figure 31B) include moderate contents of Cr (0.1–0.8 wt % Cr_2O_3) and Fe (0.2–0.8 wt % Fe_2O_3), very low to low amounts of Ti (55–192 ppm TiO_2) and V (up to 164 ppm V_2O_5), and low to moderate Ga (64–146 ppm Ga_2O_3).



Figure 30. The ruby-bearing amphibolite from Longido, Northern Tanzania. (A) The amphibolite dyke, which is up to 1 m thick and parallel to the metamorphic foliation, crosscuts a serpentinite. The contact zone between the two rocks is marked by the presence of a phlogopite and amphibole-bearing schist. Photo: Elisabeth Le Goff; (B) anyolite with patches of ruby (Crn) and retrograde zoisite (Zo). Remnants of the amphibolite (Amph) highlight the metamorphic foliation. Photo: Elisabeth Le Goff; (C) representative samples of anyolite with ruby and black amphibole (tschermakite). Photo: Vincent Pardieu; (D) ruby crystals extracted from new veins that are very different to the classical massive ruby of Longido. Photo: Vincent Pardieu.

(3) The majority of gem-quality rubies from Africa are from deposits located in metamorphosed M-UMR from the Neoproterozoic Metamorphic Mozambique Belt (NMMB). The Rockland mine was the main producer of cabochon-grade ruby until the discovery of the Winza deposit in 2007. Then,

the confirmed presence of ruby in the Niassa National Reserve in Mozambique in 2008 opened the economic reign of Mozambique over the production of very high quality rubies worldwide as in the Montepuez mining district (Figure 32) [21,22,198,200,201]. A review and summary of the history, geology, and gemmological properties of ruby from Mozambique was recently published by [26].

The NMMB is subdivided into several complexes grouped in four geological entities, which are from west to east [202–204]: (1) the Ponta Messula complex; (2) the Unango and Maruppa complexes; (3) the Nampula complex; and (4) the east–west Pan-African overthrusts (e.g., Nairoto, Meluco, Muaquia, M’sawize, Xixano, Lalamo, and Montepuez), which form the Cabo Delgado complex overlying the Marrupa complex (see Figures 2–42 from [40]). The ruby deposits are within the Cabo Delgado complex:

(a) The Ruambeze (or Luambeze) deposit, in Niassa province, is located between Marrupa and Meculo along the Luambeze River. It was apparently discovered in 1992 [21] and it has produced dark red to brown cabochon grade material.

(b) The M’sawize deposit, in Niassa province, is located in the Niassa National Reserve, about 43 km southeast of M’sawize village [21]. The M’sawize complex is composed of orthogneiss and paragneiss. The M’sawize ruby deposit is hosted by metagabbro and gabbroic gneiss [22]. The ruby is associated with actinolite, anorthite, scapolite, epidote, and diopside, as well as with eluvial ruby-rich soil [22]. Ruby has Fe and Cr oxide contents between 0.28 and 0.33 and 0.12 and 0.48 wt %, respectively, which fall in the range of the Winza ruby from Tanzania [23].

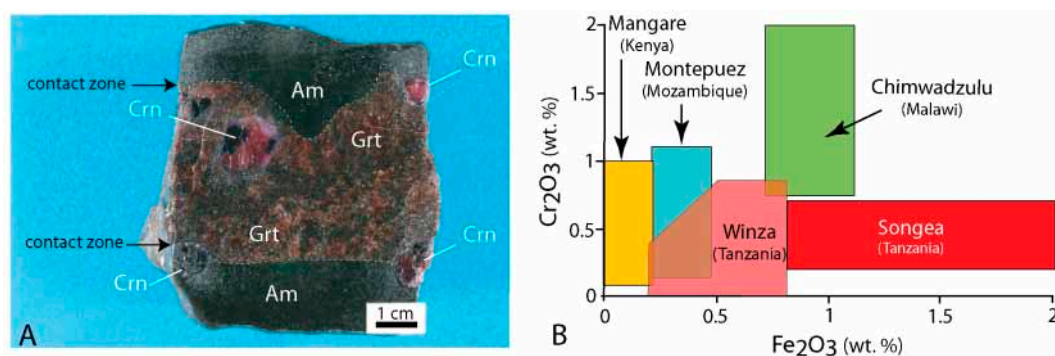


Figure 31. The Winza ruby deposit in Tanzania. (A) The primary ruby and sapphire (Crn) mineralization is hosted by an orangey brown garnet-rich rock (Grt) intercalated in a fine-grained amphibolite (Am). Photo: Patrick Lagrange; (B) the Cr₂O₃ versus Fe₂O₃ diagram showing the chemical composition of the Winza rubies compared with those from other ruby deposits hosted in metamorphosed M-UMR in the Neoproterozoic Metamorphic Mozambique Belt: Chimwadzulu (Malawi), Mangare (Kenya), Montepuez (Mozambique), and the placers at Songea (Tanzania).

(c) The Namahumbire and Namahaca deposits in Delgado province are together called the Montepuez deposits. The Cabo Delgado nappe complex represents the remnant of Neoproterozoic volcanic arcs and a microcontinent after 596 ± 11 Ma [205]. The lithological succession is very complex due to intense deformation but structural trends can be drawn from satellite images (Figure 32; [25]). The ruby area includes high-grade metamorphic rocks such as gneisses, migmatites, marbles, and amphibolites [96]. At the end of 2018, mining was being done by companies such as Fura Gems, Beleza Ruby, Gemfields, Mustang, and Redstone [25], and by numerous small-scale miners working either in community areas such as at Nacaca or illegally inside other company concessions.

Two types of deposits are known: (1) extensive secondary deposits, i.e., colluvials, which are the main source of faceted-grade material [25] (also see Chapter 6.3.2. Sub-Type IIIB) and (2) primary deposits in amphibolite [96,198,200].

The primary deposit is made up of ruby- and pink corundum-bearing lenses of amphibolites in migmatitic gneiss. They contain amphibole (pargasite), anorthite, and mica [22,96,200] (Figure 33).

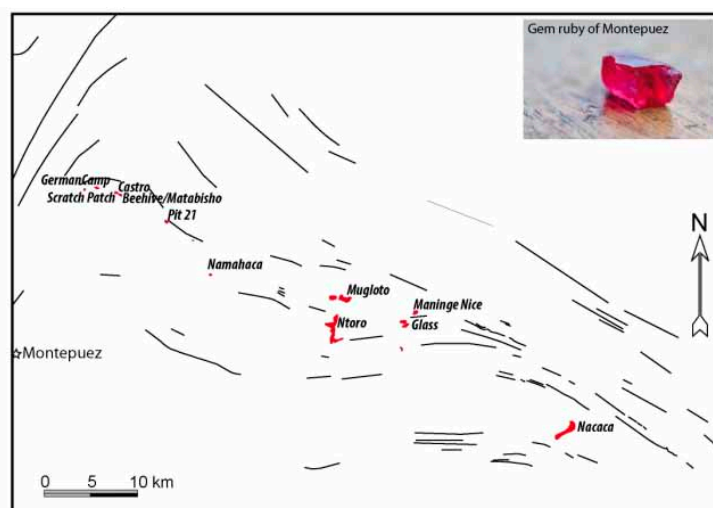


Figure 32. The Montepuez mining district with the different ruby mines of primary and mostly secondary deposits (drawn as red spots). The structural trends observed from both satellite imagery and field works are shown. The ruby mineralization defines a N110°E trending zone that extends for 40 km; modified from [25]. Crystal of ruby (size 1 cm long). Photo: Vincent Pardieu © GIA.



Figure 33. The Mozambican ruby deposits. (A) Ruby-bearing amphibolite (Am) at the M’sawize deposit, Niassa Province, 2009. The weathered amphibolite (wAm) is crosscut by whitish plagioclase veins (Plv); (B) the Maninge Nice deposit, Concession Gemfields, Montepuez, 2012. The ruby (Crn) is surrounded by a plagioclase corona (Pl, anorthite) in a weathered amphibolite (wAm); (C) euhedral pargasite (Prg) in ruby. Field of view 1.5 mm; (D) inclusions of actinolite (Act) in ruby. Field of view 2.5 mm; (E) crystal of pargasite associated with mica (Mca) in ruby. Field of view 1.1 mm; (F) a melted mica (Mca) surrounded by a halo of fluid inclusions (Flincl) arranged in a “butterfly wing” indicative of decrepitation and recrystallization phenomena. The pargasite is euhedral and devoid of deformation. Field of view 1.7 mm. Photos A and B: Vincent Pardieu © GIA. Photos C to F: Jonathan Muyal © GIA.

The texture is granoblastic with 120° triple junctions between amphibole and anorthite. The mineral assemblage formed during prograde metamorphism. The ruby often shows a corona

of spinel + anorthite formed during the retrograde stage [96]. The ruby porphyroblasts have sizes between 1 mm and 1 cm. The P–T conditions of ruby formation ($P = 10\text{--}11.5$ kbar and $T = 450\text{--}600$ °C), calculated from P–T pseudosections, show the lowest temperature of formation compared to similar ruby-bearing amphibolites (see Figure 21) such as at Mangare [119], Winza [120], North Carolina [121], and Vohibory [122]. These calculated P–T conditions obtained by pseudo-sections [97] for the formation of ruby of Montepuez is somewhat questionable because clinocllore (and quartz) is a retrograde mineral in M-UMR and not in equilibrium with ruby. Geochemical analyses of amphibolites indicated that the protolith was basaltic and associated with subduction-related arc magmatism [96], following the model proposed by [206] for the arc assembly and continental collision in the Neoproterozoic East African Orogen.

Sub-Type IIA₂ includes rubies in marble such as those of the Mogok Stone Track (Myanmar), and others from central and eastern Asia, Canada, and Tanzania, (see Table 3).

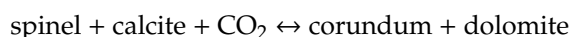
Ruby and pink corundum deposits hosted in marbles are known from Asia [5,30,65,103,112,115,134,207–210], North America [113,211], Europe [95,110], and Africa [48,110,114,182] (see Figure 2). These ruby deposits are hosted by meta-pure or impure limestone of carbonate platforms and are of two types: (1) in marble where the gem corundum crystallized as a result of prograde and retrograde isochemical metamorphic reactions, mainly in a closed system, and where the ruby occurs as disseminated crystals in marble, in Central and Southeast Asia and other places worldwide [65]; and (2) in impure marble containing gneiss and silicate layers where the ruby crystallized at the peak of prograde metamorphism, such as at Revelstoke in Canada [113,212], Snezhnoe in Tadjikistan [115,134], and Morogoro in Tanzania [114,163].

(1) Ruby mines in marble in Central and South-East Asia.

These are one of the main worldwide sources of high-quality ruby with intense color and high transparency [5]. There is extensive literature on the geology and gemmology of these deposits; see [5,29,40,65,80,87,88,110,133,143,156]. Below we will present a short overview of the geology of these ruby deposits and focus on the significance of the mineral associations and geochemistry of the paleofluids in order to discuss the genesis of the corundum.

These deposits occur from Afghanistan to Southern China (see Figure 2) in marbles that are intercalated with garnet biotite-sillimanite- or biotite-kyanite-bearing gneisses, amphibolites, and quartzites (Figure 34A), which are sometimes intruded by granitoids, as in the Mogok district [87,88,213]. The marble units consist of discontinuous horizons up to 300 m in thickness, oriented parallel to the main regional foliations, thrusts, or shear zones related to the Cenozoic Himalayan orogenesis between 45 and 5 Ma [88,133]. The ruby mineralization is restricted to impure marble horizons. The protolith of the ruby-bearing metamorphic rocks comprises of carbonates enriched in detrital clays and organic matter, and intercalated evaporitic layers (Figure 34B). Ruby crystals occur: (1) disseminated within marbles and associated with phlogopite, muscovite, scapolite, margarite, spinel, titanite, pyrite, and graphite, as at Jegdalek, Afghanistan; Chumar and Ruyil, Nepal; Hunza and Nangimali, Pakistan; Mogok and Mong Hsu, Myanmar; Luc Yen, Vietnam; and Yuan Jiang in China; (2) in veinlets or gash veins, as in some occurrences in Northern Vietnam, and associated with phlogopite, margarite, titanite, graphite, and pyrite, and sometimes related to micro-shear zones, as at Nangimali in Pakistan (Figure 34C); and (3) in pockets associated with K-feldspar, phlogopite, margarite, graphite, and pyrite in some occurrences in Northern Vietnam.

The thermobarometric conditions of mineral equilibrium have shown that ruby could have grown during both prograde and retrograde metamorphic events. The most common reaction is the formation of ruby by the destabilization of spinel (Figure 35A):



Ruby formed during the retrograde metamorphism stage at T 620–670 °C and P 2.6–3.3 kbar [65]. The aluminum and the chromophorous elements in the ruby originated from marbles (Al up to 1000 ppm, V and Cr between 5 and 30 ppm for the Nangimali deposit).

The variations of local chemistry of the marbles along several decimeters are due to lateral facies variations of the protoliths which resulted in a succession of different F-Na-SO₄²⁻-rich mineral associations: (1) F-aspidolite (Na₂O-rich phlogopite; Figure 34D) associated with F-phlogopite and F-paragonite in the different mineralized zones, as seen in the Nangimali deposit in Pakistan [214]; (2) anhydrite either associated with F-tremolite, F-edenite, F-pargasite, and carbonates in samples from the Hunza Valley, Pakistan and Luc Yen, Vietnam, or included in ruby with relics of spinel (Figure 35A,B); (3) anhydrite and salt crystals (CaCl₂, NaCl, and KCl) as solids in the Nangimali, Luc Yen, and Mogok deposits; and (4) F-bearing dravite-uvite tourmaline and apatite, indicating a low activity of water in the fluid.

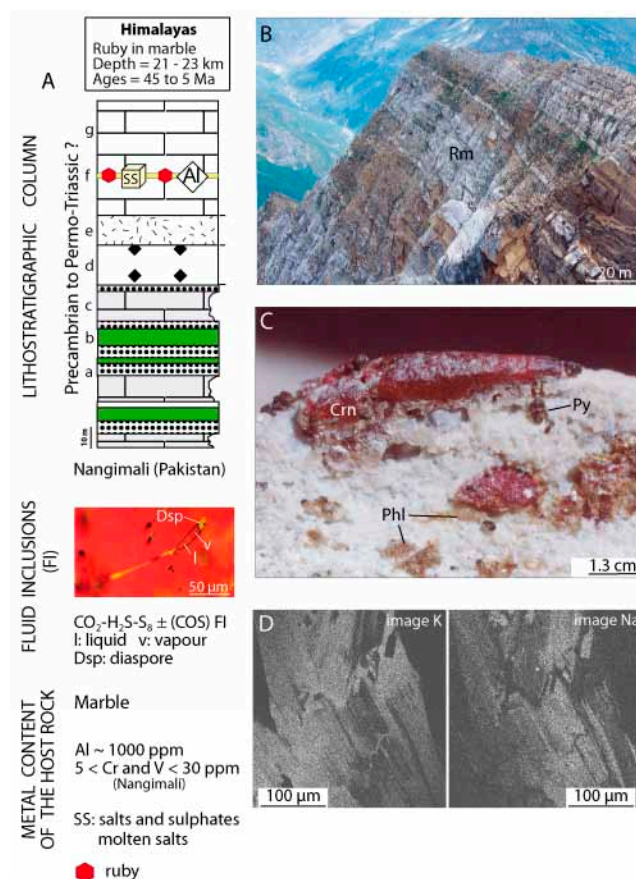


Figure 34. Ruby in metamorphosed carbonate platforms from Central and South-East Asia. (A) The Nangimali formation, Pakistan, showing the location of the ruby deposit in the metamorphic pile. Abbreviations: a: quartzite; b: amphibolite; c: mica-bearing marble; d: pyrite-bearing marble; e: calc-schist and garnet-biotite micaschist; f: ruby-anhydrite-bearing yellow Mg-marble; g: white dolomite and/or calcite marble; (B) the succession of marble (white) and garnet-sillimanite-bearing calc-schist and micaschist (brown); the unique ruby-bearing marble is reported as Rm; (C) gem ruby-bearing gash vein: (Crn), phlogopite (Phl) and pyrite (Py) in marble; and (D) back-scattered electron images of coexisting phlogopite and aspidolite with their X-ray images for potassium (K) and sodium (Na) [214]. Photos: Gaston Giuliani.

Paleo-fluids trapped as primary fluid inclusions in the minerals during their growth allow access to the composition of the mineralizing fluids. The combination of these data with those obtained for the stable isotope ratios of elements such as oxygen, hydrogen, sulphur, and boron on minerals coeval with the gems allows for characterization of the origin and source of the different chemical elements. Microthermometry studies combined with Raman spectroscopy of primary fluid inclusions in ruby revealed the coeval trapping of two types of carbonic fluid inclusions [62,63]: mono- to two-phase fluid inclusions (Figure 35D) in the system CO₂-H₂S ± COS ± S₈ ± (1 < H₂O < 10 mol %), and polycrystalline

fluid inclusions (Figure 35C) in the system $\text{Na-K-Ca-CO}_3\text{-SO}_4\text{-NO}_3\text{-Cl-F} \pm \text{CO}_2\text{-H}_2\text{S} \pm \text{H}_2\text{O}$. The different solids in the polycrystalline fluid inclusions are mixtures of carbonates with Ca-Na-Al cations, such as shortite and dawsonite, sulphates (mainly anhydrite and barite), phosphates (F-apatite), nitrates, fluorides (fluorite), and chlorides (halite, Ca and K chlorides). These solids are daughter minerals of ionic liquids formed during the metamorphism of evaporites and limestones [65]. In ruby, these polycrystalline fluid inclusions are rare because if the salts are not immediately trapped by the crystals, and they dissolve because of their high solubility in water-rich fluids.

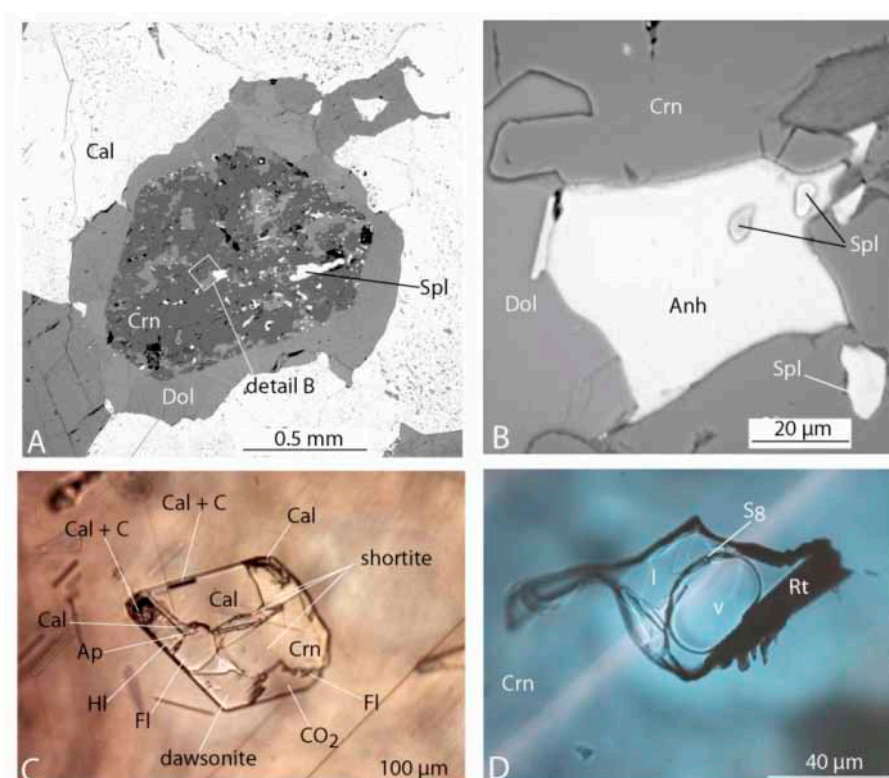


Figure 35. Mineral assemblage and fluid inclusions in ruby-bearing marble deposits from Central and South-East Asia. (A) Association ruby (Crn), dolomite (Dol), calcite (Cal), and spinel (Spl) illustrating the formation of ruby by the chemical reaction: $\text{spinel} + \text{calcite} + \text{CO}_2 \leftrightarrow \text{corundum} + \text{dolomite}$, Hunza valley (Pakistan); (B) inset of Figure 35A (detail B) showing the presence of anhydrite (Anh) with spinel inclusions (Spl). Spinel is a pre-ruby phase that has high Cr (up to 19 wt % Cr_2O_3) and Zn (up to 10 wt % ZnO) contents; (C) primary polycrystalline fluid inclusion cavity in ruby containing different solids (molten salts), which are mixtures of carbonates, with Ca-Na-Al cations such as calcite (Cal), dawsonite (Dw), shortite, and apatite (Ap), fluorite (Fl), halite (Hl), graphite (C), and a $\text{CO}_2\text{-H}_2\text{S}$ -bearing fluid phase (CO_2), Mogok, Myanmar; and (D) three phase fluid inclusions with CO_2 and H_2S liquid (l) + vapor (V) phases and native sulphur (S_8) trapped by ruby in a rutile (Rt)-bearing cavity, Mong Hsu deposit Myanmar. Photos A and B: Virginie Garnier, [65]; Photos C and D: Gaston Giuliani, [62,63].

Crushing and leaching of rubies [62] showed that chloride is the dominant anion (25 to 53 mol %) with sulphate (2 to 36 mol %), nitrate (2 to 17 mol %), and fluoride (0 to 25 mol %). Sodium is the dominant cation (16 to 42 mol %). The presence of nitrate is a strong argument for a continental input to the original sediment as, generally, nitrate salts precipitate in closed basin playas or salars. In addition, the isotopic variation of sulphur in anhydrite included in ruby and marble defines two sets of $\delta^{34}\text{S}$ (V-CDT) values: the first, between 27‰ and 23‰, for a marine anhydrite; the second, between 4.8‰ and 1.6‰, for a continental source [65].

The presence of sulphate-carbonate-fluorine mixtures decreased the melting temperature of halite and other salts, and allowed the formation of chlorine- and fluorine-bearing ionic liquids. Fluorine of

continental origin probably played an important role in the extraction of the Al present in impurities (clays) from the impure limestone. The existence of an ionic liquid trapped in the form of polycrystalline solids in ruby explains the color and clarity of the ruby by (1) the mobilization of Al, Cr, and V contained in the meta-limestone, and (2) their incorporation in an isotropic environment allowing crystalline growth with a minimum of defects.

The presence of evaporites of either continental or marine origin in the Ca-Mg protoliths is the key feature in the metamorphic model for ruby in marble. Ruby formed during the metamorphism, in the amphibolite facies, of carbonates interbedded with mudstones and containing intercalations of sulphates-chlorides-nitrates-borates of impure evaporites. The lithological control of the mineralization is a function of the paleogeography of the carbonate platform environment. The original sedimentary landscape converges to an epeiric carbonate platform succession with a combination of salt and evaporite mudflats of gypsum and anhydrite [62].

(2) Ruby and pink corundum in marble with intercalated silicate and gneiss layers.

(i) The Revelstoke occurrence is in the Monashee Complex of the Omineca belt of the Canadian Cordillera, British Columbia [113,212]. Ruby ($\text{Cr}_2\text{O}_3 \leq 0.21$ wt %) occurs in folded and stretched layers associated with green Cr-V-Ti-Ba-rich muscovite + Ba-bearing K-feldspar + anorthite \pm phlogopite \pm Na-poor scapolite. Other silicate layers within the marble are: (1) diopside + tremolite \pm quartz and (2) almandine-rich garnet + Na-rich scapolite + diopside + tremolite + (Na,K)-amphiboles. Corundum formed at the peak of metamorphism (T 650–700 °C and at P 8.5–9 kbar) and the sources of the Cr are the silicate layers and gneiss.

(ii) The Snezhnoe deposit in Tadjikistan [115,134] is localized in the Muzkol-Rangkul anticlinorium within the Cimmerian zone of the Central Pamir. The Muzkol metamorphic series consists of calcitic marbles present as layers intercalated with amphibole-pyroxene and scapolite calciphyres, gneisses, Ti-Ba-rich muscovite schists, and quartzites. These calcitic marbles host the Snezhnoe deposit, formed by micaceous ruby-bearing lenses arranged as discrete en echelon lenses along the marble foliation. Ruby is found in four mineral assemblages as (i) scapolite + phlogopite + muscovite + margarite; (ii) plagioclase + muscovite + margarite; (iii) muscovite + phlogopite + margarite; and (iv) calcite. The main economic paragenesis is associated with ruby + calcite. The temperature of the metamorphic processes was estimated at 760 ± 30 °C using Zr-in-rutile geothermometry [134]. Ancient Al-enriched sediments such as metapelite or meta-bauxite intercalated in the marbles are suggested to be the possible protolith for the ruby-parent rocks.

(iii) At the Ngong'Oro mine, Morogoro district in Tanzania [182], ruby is located in metasomatic zones concordant to the metamorphic foliation, and formed at the contact between marble and biotite gneiss layers. The ruby is associated with spinel and sapphirine.

6.2.2. Sub-Type IIB: Metamorphic-Metasomatic Deposits Formed by Fluid–Rock Interaction and Metasomatism (See Table 3)

1. **Sub-Type IIB₁** corresponds to desilicated pegmatites (plumasite) and associated metasomatites in M-UMR such as at the Rockland mine (Kenya) or Polar Urals and Karelia (Russia), and others (see Table 3). This sub-type also concerns deposits associated with M-UMR intercalated with Si-Al rocks (gneiss, leuco-gabbro, or anorthosite), which have suffered fluid percolation and consequent metasomatism such as at the Aappaluttoq ruby deposit in Greenland.

These deposits formed at medium to high temperatures during hydrothermal–metamorphic fluid circulation and bi-metasomatism that developed at the contact of two contrasting lithologies, i.e., either granitoid or pegmatite or gneiss adjoining different rocks, such as metamorphosed M-UMR or marble [83,110]. The metasomatic reactions are related to the infiltration of post- or magmatic or metamorphic solutions, which originated from the same granite or from other magmatic or metamorphic events. The geochemical mechanism of dissolution of quartz (desilication) by a loss of a SiO₂-bearing rock, involves diffusion of Si from a pegmatite vein to a M-UMR for example (which plays the role of SiO₂ sink) at a rate more rapid than the diffusion of Al. The Al:Si ratio increases in the

pegmatite vein, and a metasomatic plagioclase-corundum association in which the mass of alumina per unit volume is much greater than in the initial rock may develop if the volume of rock decreases at the same time and is underlain by a zone of quartz dissolution. These desilicated pegmatite or granitoidic veins are called plumasite following the definition of [215] that were formerly described as an oligoclase-corundum rock [216] forming a dyke in a serpentized peridotite at Plumas, California. Gordon [215] noted that they were described from several countries (United-States, South Africa, and Russia) as “an abnormal group of granitic pegmatites, composed either of plagioclase, usually albite, alone (albitite), of plagioclase and corundum or largely corundum, all of which occurring exclusively in peridotites or their altered equivalents”. Gordon [215] indicated that the desilication occurred by fluid–rock interaction along the contact between the pegmatite and the intruded M-UMR. The mineralogical composition of the desilicated pegmatite and contact rocks depends of the degree of desilication. Some desilicated pegmatites present metasomatic zoning characterized by different mineral assemblages from the centre to the periphery of the dyke as described by [195] at the ruby Corundum Hill mine, in Macon County (United-States).

World-class gem corundum samples, including tabular ruby in desilicated pegmatites, have been described from the Umba and Kalalani deposits, which are located in serpentinite bodies [217] in Tanzania. World-class rubies were mined in the Mangare area in southern Kenya, including from the well-known (and formerly) John Saul mine [118,119]; and the Polar Urals in Russia [218] and Karelia [41]. Another unusual case of bi-metasomatism that is not a desilicated pegmatite, is related to the intrusion of ultramafic dykes in marble as observed at the Kitwalo ruby occurrence in the Mahenge district (Tanzania). At Kitwalo the ruby is hosted by phlogopite schists and formed via fluid–rock interaction at the contact between marble and an ultramafic dyke (Figure 36) [182].



Figure 36. The ruby occurrence at Kitwalo, Mahenge district, Tanzania. (A) Amphibolite vein (Amph) crosscutting a dolomitic marble (Mb) and (B) detail of the contact between the two rocks showing a phlogopitite (Phl), a result of fluid–rock interaction. The amphibolite exhibits a high degree of phlogopitization (PhlAmph) associated with the ruby deposition (Crn). Photos: Elisabeth Le Goff.

We proposed to examine different deposit cases in order to characterize the infiltrational fluid metasomatism of M-UMR during medium to high grade metamorphism:

(1) In the United-States, these deposits are associated with M-UMR intercalated with Si-Al rocks metamorphosed in the amphibolite to granulite facies. The contact between meta-dunite and amphibolite with gneisses at different scales is underlined by metamorphic-metasomatic zones. The Corundum Hill mine at Macon County in North Carolina presents different types of contacts and distributions of ruby [195]:

(a) A gradual transition between ruby accumulations and meta-dunite with some remnants of M-UMR in the ruby zone (Figure 37A).

(b) The contact zone is characterized by a metasomatic column, of 6–7.5 m width, symmetrical from the periphery to the centre (Figure 37B) with dunite, talc schist, fibrous enstatite, green chloritite, chloritite-bearing ruby, and spinel (1.8–2.4 m wide). At Hunters mine, the amphibolite presents a plagioclase vein with symmetrical metasomatic zoning, 0.9–1.2 m wide, from the outer to inner zones the following mineral assemblage: amphibolite, actinolite, ruby-bearing margarite-vermiculite, and ruby-bearing feldspar vein altered into kaolin (Figure 37C). These different types of contact indicate the circulation of metamorphic-metasomatic fluids between two rocks of different competency and chemistry. The considerable width of some metasomatic columns, up to 7.5 m, indicates a clear infiltrational metasomatic process as described for the Polar Urals [99].

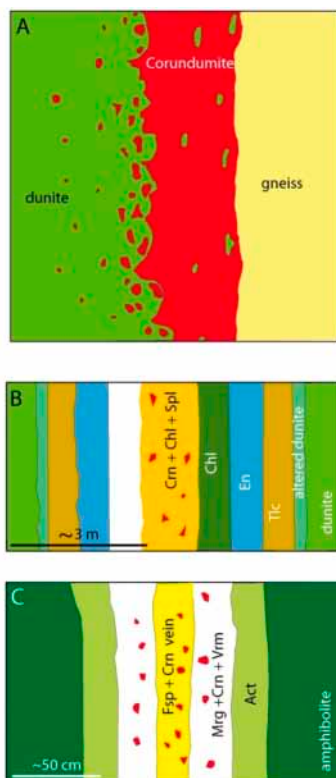


Figure 37. Metasomatic zoning in ruby-bearing metamorphosed dunites and amphibolites in the deposits of North Carolina, USA, modified from [195]. (A) The contact between dunite and gneiss is outlined by corundumite, Corundum Hill mine, Macon County. The scale is not qualitative; (B) ruby-bearing metasomatic zones in dunite at the Corundum Hill mine. The central part contains green chlorite (Chl) + ruby (Crn) + spinel (Spl) and the other zones are symmetrically disposed from this centre part. En = enstatite; Tlc = talcose rock; (C) ruby-bearing feldspar vein in amphibolite at Hunters, Iredell County. A metasomatic-metamorphic symmetrical zoning is developed around the vein. From the centre to the periphery: (1) a zone composed of vermiculite (Vrm)-bearing ruby with some margarite (Mrg) and (2) an actinolite (Act) zone at the contact with the amphibolite.

(2) In Kenya, rubies were discovered in the Mangare area, Voi mining district, in 1973 by John Saul [183]. Mining in the John Saul mine (recently renamed the Rockland mine) provided a regular supply of either facet grade or cabochon rubies from 1993 to 2012. The John Saul, Penny Lane, and Hard Rock deposits occur in lenses of serpentinized ultramafic rock (UMR) bound by shear zones in a metasedimentary series composed of graphitic gneiss and felsic gneiss (Figure 38) [118]. Fe-poor ruby ($\text{FeO} < 0.06 \text{ wt } \%$) and pink corundum is located in (i) micaceous lenses and pockets along the contact of a shear zone with the metasomatized UMR. The ruby is associated with \pm spinel \pm sapphirine + mica or in some cases with phlogopite + Mg-chlorite; (ii) in plumasitic veins that crosscut the serpentinites

where the ruby is associated with zoisite and anorthite \pm muscovite [119]. The P–T conditions for ruby formation are between 700 and 750 °C and 8 and 10 kbar in the metamorphic granulite facies.

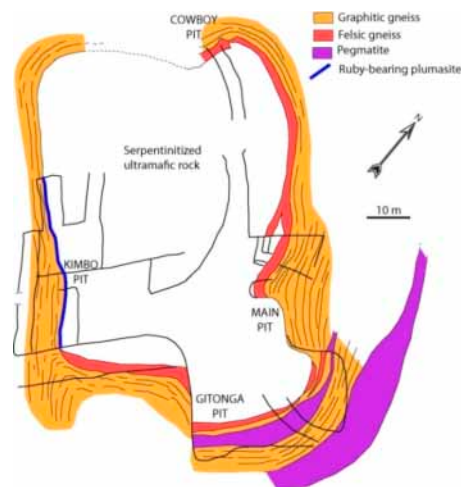


Figure 38. Geological map of the John Saul (now Rockland) mine and its serpentinized ultramafic rock body located in the metamorphic formations of Mgama-Taita, modified after [118]. The Kimbo Pit extension follows the structural direction of the desilicated pegmatite vein, i.e., a ruby-bearing plumasite, which formed at the contact between the graphitic gneisses and the ultramafic body.

As seen in the Kimbo Pit at the John Saul mine (Figure 38), the ruby-bearing-plagioclase vein is always present at a depth of 40 m and has a longitudinal extent of 100 m. The contact of the vein with the UMR is outlined by a phlogopite schist with apatite and Mg-chlorite [118]. The plagioclase is coarse-grained and is composed of oligoclase-andesine (Figure 39A). Locally, a huge concentration of ruby (around 70% in volume), green tourmaline (uvite-dravite), and blue apatite with some phlogopite is observed (Figure 39B). In other places, the ruby exhibited zoned scalenohedron crystals (Figure 39C) or “mushroom” (so-called by John Saul) habits up to 3 cm across (Figure 39D). The production of ruby from July 1995 to April 1997 was estimated to have been 36 kg/m³ [219]. The U/Pb age obtained on zircons from the plumasite was 612 \pm 0.6 Ma and the P–T conditions for ruby formation were estimated to have been 500 °C and 5 kbar [118].

(3) The ruby occurrences in Northwestern Karelia in Russia, located between the Kola and Karelia Archean blocks, is another case of desilication of pegmatite and gneisses due to the fluid–rock interaction [143,220]. The deposits, which are located in a 3.0–2.5 Ga polymetamorphic Archean complex, are in ruby-bearing paragneisses, amphibolites, and amphibole schists. Several collisional episodes occurred but at 1.9–1.8 Ga metamorphism and regional intrusions with pegmatites were responsible for the ruby formation through metasomatic processes. The ruby-bearing plumasite veins crosscut biotite-hornblende gneiss and amphibolite. The veins range from several cm to 10 m thick and up to 60 m long, and are parallel to the metamorphic foliation. The plumasite is composed of plagioclase (oligoclase-andesine), phlogopite, tourmaline, zoisite, epidote, and chlorite. The corundum crystals have prismatic and bladed shapes, 5 cm long and up to 3 cm in diameter. The ruby contains up to 9.4 wt % Cr₂O₃. Ruby and pink corundum from the Proterozoic gneisses have the lowest-known $\delta^{18}\text{O}$ compositions (–1.5‰ to –27‰) for terrestrial corundum [221], while the corundum in the amphibolite has $\delta^{18}\text{O}$ contents between –2.3‰ and 7‰ [1] (Figure 40). The plagioclase and amphibole have similar O-isotope values as the ruby. The highly depleted $\delta^{18}\text{O}$ values are due to the circulation of meteoric glacial subwaters in a rift zone at around 2.4 Ga, which affected the initial isotopic composition of the protolith prior to ruby formation [41,222].

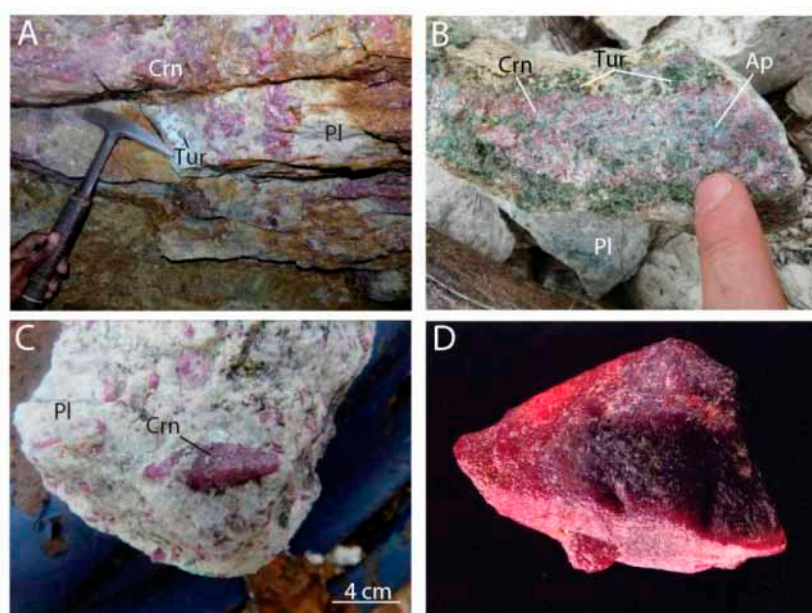


Figure 39. The ruby-bearing rocks of the John Saul mine, Voi area, Kenya [118,163]. (A) The Kimbo Pit and its ruby-bearing plumasite showing the mineral assemblage ruby (Crn), plagioclase (Pl), and some tourmaline (Tur); (B) concentration of ruby, green tourmaline, and blue apatite (Ap) in the plagioclase vein of the Kimbo Pit; (C) ruby showing the scalenohedron habit in the plagioclase matrix of the plumasite, Kimbo Pit; and (D) mushroom habit of a ruby, 3 cm across, from the John Saul mine. Photos A–C: Gaston Giuliani; Photo D: Courtesy John Saul.

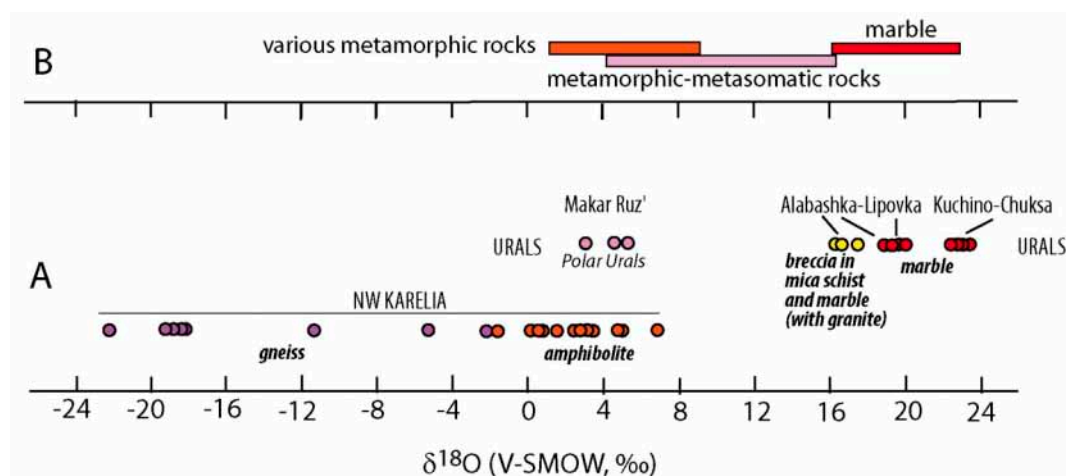


Figure 40. Oxygen isotopic composition of ruby from various Russian occurrences. (A) Oxygen isotopic composition of ruby in marble, breccia in mica schist and marble, and plagioclase-dominated metasomatic rocks from the Urals, and gneisses and amphibolites from northwest Karelia, Russia, modified from [153] and (B) the oxygen isotopic range of values for ruby worldwide associated with primary deposits [40,41,93,163].

(4) Ruby-bearing plagioclase vein at Makar Ruz' in the Ray-Iz ophiolitic belt of Polar Urals, Russia (see Figure 2) [143,223]. The Paleozoic ophiolitic massif consists mainly of dunite and harzburgite that underwent polyphase metamorphism with a high degree of serpentinization. Chromitite in dunite yielded an Ordovician Re-Os age of 470 Ma [224] while zircon from the ruby-bearing plagioclase vein gave a Silurian U/Pb between 380 [218] and 398 Ma [225]. The vein was completely mined out and is no longer visible. Scherbakova (1975, in [99]) recognized two types of plagioclase: (i) plagioclase-rich and phlogopite-rich. The plagioclase vein, 10–12 m thick, presented a clear symmetric metasomatic

zoning as also observed in emerald-bearing plagioclase hosted in metamorphosed M-UMR [226]. From the centre to the outer metasomatic zones (Figure 41) this is: (i) plagioclase (andesine to oligoclase), 1.5–2.5 m wide, with amphibole (actinolite-tremolite, pargasite) and without ruby; (ii) a ruby ($0.3 < \text{Cr}_2\text{O}_3 < 7.5$ wt %)-bearing phlogopite-rich zone (with Na-rich phlogopite, i.e., aspidolite in Cr-spinel; [99]), 0.3–1 m thick, with plagioclase, Cr-spinel ($0.46 < \text{Cr}\# < 0.86$). The phlogopite is Ba-rich ($0.8 < \text{BaO} < 2.7$ wt %, [218]). Paragonite ($0.8 < \text{Sr} < 2.3$ wt %), margarite, and zoisite always occur between the ruby and plagioclase, and are probably retromorphic phases. The mean modal composition is plagioclase (32–67 vol %), paragonite (7–31 vol %), phlogopite (10–22 vol %), and Cr-spinel (5–7 vol %); (iii) plagioclase, amphibole (pargasite), clinocllore, Cr-spinel, talc, and augite in a 7–8 m thick zone; (iv) finally the dunite, which exhibited three sub-zones, from the inner to the outer, respectively: (a) chlorite + talc + Cr-spinel; (b) chlorite + talc + carbonate + serpentine + olivine; and (c) amphibole (actinolite-tremolite) + chlorite + Cr-spinel + talc + serpentine + olivine.

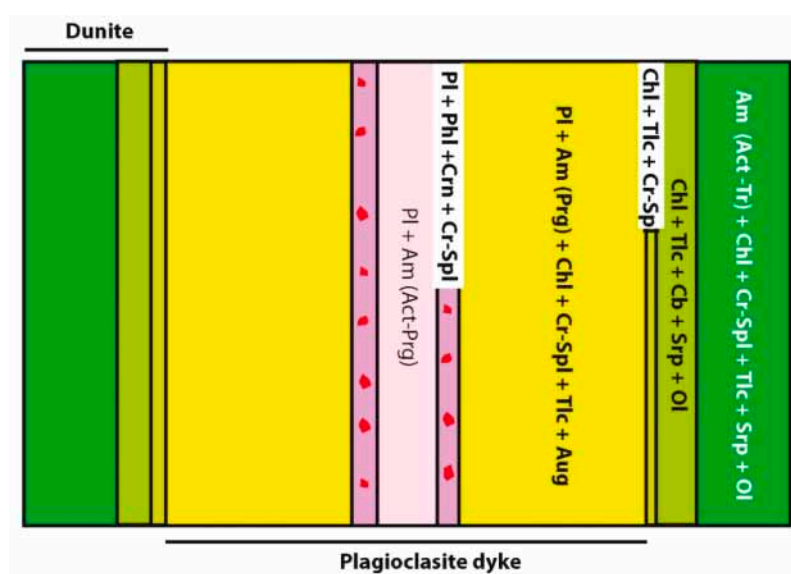


Figure 41. The ruby-bearing plagioclase dyke in a serpentinized dunite from the Makar Ruz' deposit in the Ray-Iz ophiolitic belt of Polar Urals, Russia, modified from [99]. The plagioclase shows a symmetrical metasomatic zoning with sharp contact zones characteristic of metasomatic zoning and percolation of fluids. Ruby (Crn) is hosted in the plagioclase (anorthite)-phlogopite (Phl)-Cr-spinel (Cr-Spl) inner zone of the metasomatic column. Abbreviations: Am = amphibole, Act = actinolite, Tr = tremolite, Prg = pargasite, Tlc = talc, Srp = serpentine, Ol = olivine, Pl = plagioclase, Chl = chlorite, Aug = augite, and Cb = carbonate.

Aqueous fluid inclusions in the plagioclase are rich in HCO_3^- , SO_4^{2-} , and Cl^- . Zircon ϵ_{Hf} values are between -11 and $+13$; the calculated ϵ_{Nd} (380 Ma) value is $+3.3$ for the whole-rock plagioclase [227] and the ϵ_{Nd} (400 Ma) values are $+6.4$ and $+6.6$, respectively for dunite and harzburgite (Ronkin, 2000 in [99]).

Based on these considerations, different authors agree that (i) the vein minerals resulted from the fluid–rock interaction with the dunite and not from the fractional crystallization of ultramafic magma as proposed by [228]; (ii) the source of Cr is the chromitite in the dunite; and (iii) the metasomatic columns are due to fluid circulation, which is considered subduction-zone-derived and from metasomatism in the mantle wedge. The association plagioclase-corundum gave P–T estimates at 1.0–1.1 GPa and between 600 and 700 °C [99]. The formation of ruby and pink corundum is attributed to desilication of the dunite by the Na–Al–Si fluid circulation [218] rather than derivation from precursor pegmatite [100]. Such metasomatic zones that display clear zonation with very sharp metasomatic fronts, i.e., metasomatic columns (see Figure 37C), formed by infiltrational processes following the

rules of [229], are also seen in the Haut-Allier, France [40,186], at Corundum Hill mine in North Carolina [195], and in the Vohibory unit in Southern Madagascar [164].

(5) In Southern Madagascar, desilicated rocks called “sakenites” by [230] occur at Sakeny, northwest of Ihosy. Sakenite is a whitish to greenish rock composed of anorthite \pm corundum (mostly sapphire and sometimes ruby) \pm spinel \pm sapphirine \pm phlogopite \pm amphibole (edenite) \pm clinopyroxene \pm zircon, and is found in boudinaged bands or benches in the Precambrian high-grade granulitic domain of Southern Madagascar. The “sakenites” are intercalated with Al-rich paragneisses, amphibolites, and clinopyroxenites. The benches can attain 10 m width and display petrographic variations within a single bench, with local predominance of one mineral species. [230] distinguished sapphirine, spinel, spinel + sapphirine-bearing “sakenites”, and sometimes “anorthitic corundumite” (anorthite + corundum or \pm spinel) and “corundumite” occurring as pebbles and rounded blocks in rivers [231] (Figure 42A). Raith et al. [232] revisited the occurrence and described sakenites associated with phlogopitites, calc-silicate rocks, and marbles. The P–T conditions of formation of the intercalated Al-rich paragneisses were estimated at 800 °C and 6–7 kbar [232].

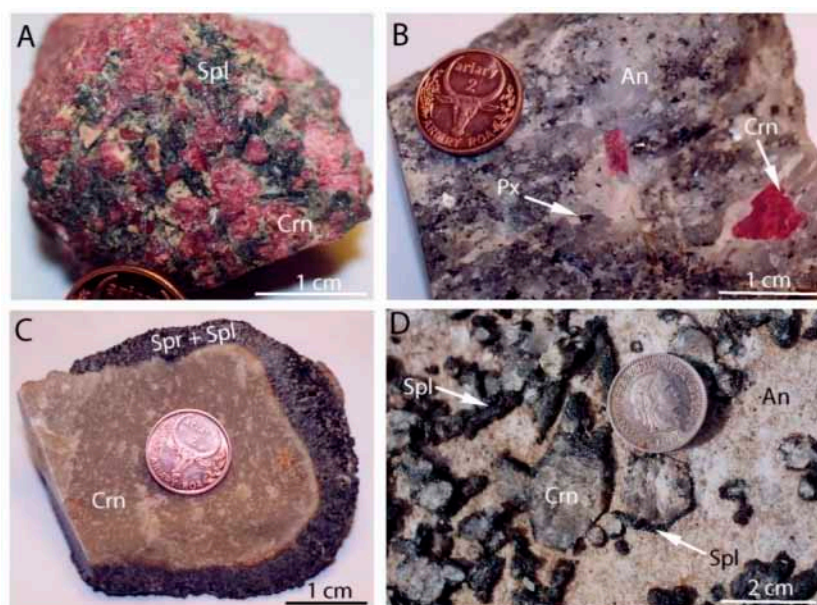


Figure 42. The sakenites from Sakeny and other sites in Southern Madagascar. (A) Corundumite composed of ruby (Crn) and spinel (Spl). Collection Lacroix, MNHN, Muséum National d’Histoire Naturelle de Paris; (B) sakenite, i.e., plumasite from the Anavoha occurrence. The ruby crystals are disseminated in a matrix of anorthite (An) and pyroxene (Px). Collection Lacroix, MNHN Paris; (C) the corundumite from Sakeny. A corona of sapphirine (Spr) and spinel is present around the whitish sapphire (Crn). Collection Lacroix, MNHN Paris; (D) sakenite vein with anorthite, corundum + spinel at Bekinana (Tranomaro area). The corundum generally shows a corona of black spinel. Photos: Gaston Giuliani.

At lower P–T conditions (750–700 °C and 6 Kbar) the sakenite was affected by the circulation of potassic fluids. The corundum + anorthite assemblage was transformed into phlogopite and Mg–Al minerals producing corundum-spinel-sapphirine-bearing phlogopitites. Subsequently the corundum was replaced by spinel, spinel-sapphirine, or sapphirine at lower temperatures and pressures [232].

Other occurrences in southern Madagascar include Vohidava, Anavoha (Figure 42B), and Bekinana [164]. These rocks are anorthitites showing corona textures due to the partial or complete replacement of corundum porphyroblasts by spinel and sapphirine (Figure 42C,D), or spinel + hibonite, spinel + sapphirine, K-feldspar + spinel, and anorthite + sapphirine. Lacroix considered “sakenites” to be a product of high-grade metamorphism of clay-rich marls. [233] favored metamorphism/metasomatism of clay-rich limestones. Raith et al. [232] suggested kaolinite-rich sediments or calcareous bauxites as a

protolith. The chemical composition of the “anorthitic corundumite” [230], i.e., 12.3 wt % SiO_2 and 73.6 wt % Al_2O_3 , implies a loss of silica with drastic enrichment of alumina, with mafic rocks (amphibolites and clinopyroxenites) or marble and calc-silicate rocks playing the role of SiO_2 sink at a rate more rapid than the diffusion of Al.

(6) In Southwest Greenland, numerous ruby occurrences have been discovered and mapped in the Fiskenæsset Anorthosite Complex [33,34,83,234,235]. Fagan [34] stated that there are at least 534 individual corundum occurrences in the area and an open-pit ruby mine recently opened at the Aappaluttoq locality (Figure 43A). The deposit has defined minable reserves of 59.2 million grams of pink corundum and ruby [35].



Figure 43. (A) The ruby mine at Aappaluttoq. Photo: Vincent Pardieu; (B) gem corundum in outcrop. Photo: Vincent Pardieu; (C) ruby rough. Photo: Vincent Pardieu; (D) a selection of cut gems (0.5–0.75 ct) from the Greenland deposits [34], courtesy of True North Gem Inc.

The 2.97 Ma Fiskenæsset Complex is one of the best preserved layered Archean intrusions in the world ([236] and references therein). It consists of a ca. 550-m-thick association of anorthosite, leucogabbro, gabbro, and metamorphosed UMR (dunite, peridotite, pyroxenite, and hornblendite), which are found in the mining area at Aappaluttoq (Figure 44). Despite amphibolite to granulite facies metamorphism (that peaked at 2.80 Ga ([235] and references therein)) and polyphase deformation, primary cumulate textures and igneous layering are well-preserved [236].

The rubies occur in a reaction metasomatic zone (Figure 43B) formed at the contact between an anorthite-rich rock, such as anorthosite or leucogabbro, and an UMR, such as a metamorphosed dunite or peridotite. The metasomatic zones resulting from fluid percolation are typically 0.5–5 m wide and contain ruby, phlogopite, cordierite, spinel, sapphirine, calcic amphibole, sillimanite, and kornepurine [83]. The ruby reaction zone consists of three main groups: (i) phlogopite with 80% mica (eastonite-phlogopite) and up to 20% corundum; (ii) sapphirine-gedrite rocks, and (iii) anthophyllite-cumingtonite (-pargasite) rocks. The rubies formed at approximately 640 °C and 7 kbar, when pegmatites intruded, at 2.71 Ga, the anorthite-rich rock and juxtaposed UMR [83,235]. This caused the anorthite to alter to calcic amphibole, releasing Al, and Cr from the UMR to be mobilized by the pegmatitic fluids. The ruby-forming reaction occurred at upper amphibolite facies conditions and under high fluid flux interaction between two rocks of contrasting chemistry.

Keulen et al. [83] proposed to name this kind of deposit as ruby-bearing ultramafic complexes. The description of the deposit confirms that it formed through an intense fluid–rock interaction

that resulted in large amounts of K-metasomatism (ruby-phlogopite zone). In consequence, the Aappaluttoq deposit might be classified in the Sub-type IIB₁ proposed by the enhanced classification for ruby deposits (see Table 3). The nature of the protoliths can vary worldwide from mafic to ultramafic rocks for low Si and Cr-bearing rocks, and from gneiss, granitoid to anorthosite rocks for Si-Al-K-rich rocks.

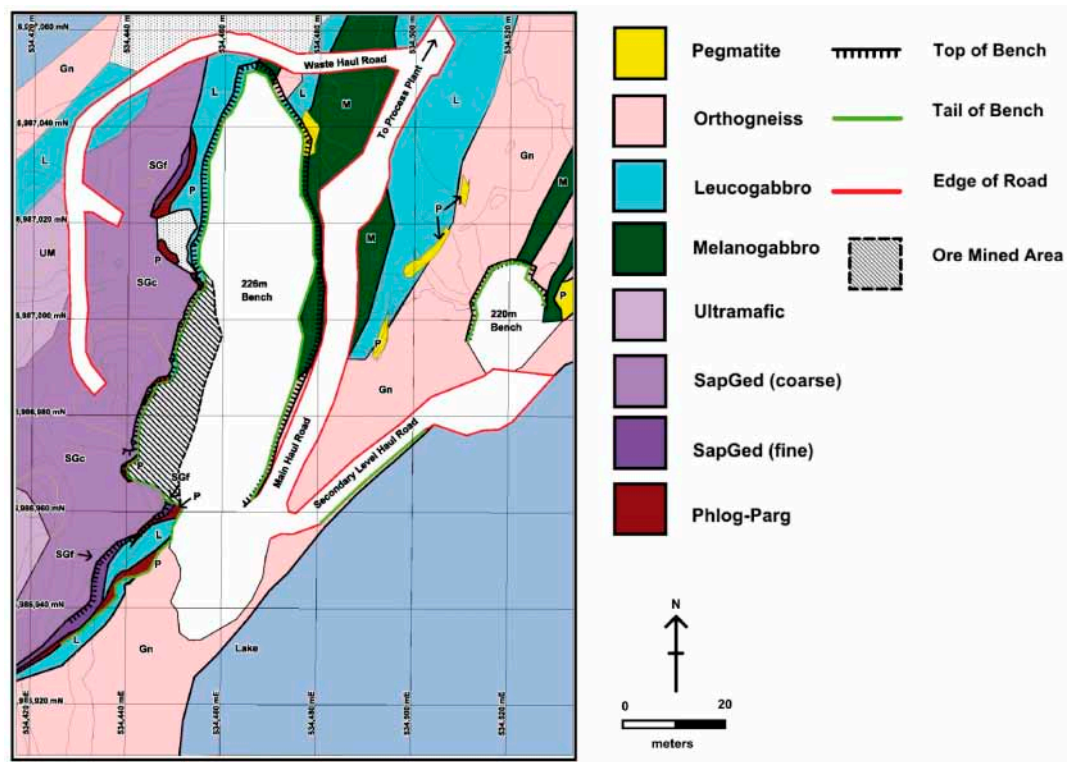


Figure 44. Geological map of the Aappaluttoq ruby mine [34]. SapGed: sapphirine-gedrite; Phlog-Parg: phlogopite-pargasite; Gn: orthogneiss; SGc and SGf: coarse (c) and fine (f) sapphirine-gedrite; L: leucogabbro; M: melanogabbro; UM: ultramafic rock; and P: pegmatite (yellow) or phlogopite (maroon).

According to [83] rubies from the Fiskenæsset Complex (Figure 43C) are distinguished by their high Cr, intermediate Fe, low V, Ga, and Ti, low O isotope values (1.6–4.2‰), and rare mineral inclusions (e.g., anthophyllite + biotite) and growth features. Numerous faceted pink corundum to ruby more than 1 carat have been cut (Figure 43D) and the largest piece of Cr-corundum recovered to date is the carved opaque 440 ct Kitaa Ruby [35].

There are also a number of occurrences in Greenland north of the Fiskenæsset Complex. Keulen et al. [83] listed (approximately from north to south): Ujarassuit Nunaat, Maniitsoq NW, Kangerluarsuk, several occurrences on the island of Storø, and Kapisillit.

At Kangerluarsuk, ruby occurs in schist with plagioclase, both surrounded by biotite, with minor orthopyroxene, amphibole, and olivine ([237] and references therein). The ruby formed by a metamorphic reaction between a metaperidotite and a kyanite-quartz-garnet schist (with minor plagioclase, spinel, and mica) at amphibolite-facies conditions.

At Ujarassuit Nunaat, an ultramafic enclave experienced amphibolite-grade metamorphism resulting in gabbro anorthosite with amphibole-calcite plagioclase and a small amount of red corundum overgrowing the latter [238].

On Storø Island, similar to Kangerluarsuk, the ruby occurs in a mica schist layer up to 3 m thick and formed by a metamorphic reaction between a metaperidotite and a sillimanite-biotite-garnet schist (with minor plagioclase) at amphibolite-facies conditions [237].

At both Kangerluarsuk and Storø Island, the ruby is thought to have resulted from the breakdown of kyanite and sillimanite at elevated temperatures due to the removal of SiO₂. The reaction was facilitated by a chemical potential gradient between the relatively Si- and Al-rich metasedimentary rocks and the low-Si ultramafic rocks. According to [237], the additional required Al₂O₃ was supplied via metasomatism, with the Al mobilized by complexation with hydroxide at alkaline conditions or transported as K-Al-Si-O polymers at deep crustal levels.

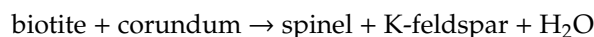
Poulsen et al. [239] described several occurrences of pink corundum near Nattivit in Southeast Greenland. The corundum occurs where late-stage felsic pegmatites crosscut and interact with metamorphosed ultramafic rocks. The source of Al is the plagioclase in the pegmatite with removal of Si by interaction with the UMR [239].

2. **Sub-Type IIB₂** is characterized by ruby and pink corundum in shear zone-related or fold-controlled deposits in different substrata (M-UMR, gneiss, schist, and marble) with fluid circulation and metasomatism.

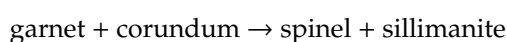
These deposits formed at medium to high temperatures during metasomatic-metamorphic fluid circulation. They include ruby or pink corundum-bearing metamorphosed and metasomatized M-UMR and marble (see Table 3) such as those from the Neoproterozoic occurrences of Zazafotsy, Sahambano, and Ambatomena (Southern Madagascar), Kerala (southern India), and Mahenge and the Uluguru Mountains (Tanzania).

(1) For Madagascar, the geology and genesis of these types of deposits was described by [40,164]. These studies focused on the Sahambano and Zazafotsy deposits that produced sapphires (rather than rubies) from feldspar-rich mafic gneisses. Fractures and tension gashes associated with shear zones favored fluid circulation and biotitization of the host rocks. At Sahambano, sapphires and pink to reddish corundum (1000 < Cr₂O₃ < 2000 ppm) occur in biotitites with sillimanite and spinel, and also in gneisses with sapphirine, K-feldspar, biotite, sillimanite, spinel, garnet, and albite. The corundum formed at T 650 °C and P 5 kbar [240,241]. At Zazafotsy, the corundum deposit lies in the Zazafotsy shear zone system [242]. The corundum occurs in lenses with different mineral assemblages:

(i) Almandine garnet, biotite, plagioclase, and sillimanite, with a corona of spinel and K-feldspar formed around corundum (Figure 45A). The resulting mineral assemblage can be described by the following reaction:



The association of corundum, garnet, spinel, and sillimanite in some samples results from the reaction:



(ii) In biotite schist with biotite, corundum, spinel, and minor grandidierite (Figure 45B).

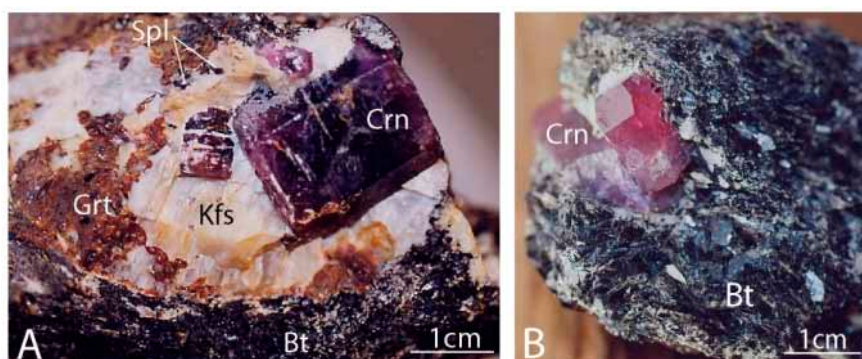


Figure 45. The Zazafotsy ruby and sapphire deposit, northeast of Ihosy, Southern Madagascar. (A) Purple sapphires (Crn) in a garnet (Grt)-bearing biotite schist (Bt). The crystals are embedded in a corona of K-feldspar (Kfs) and spinel (Spl) and (B) pink corundum hosted by a biotite (Bt). Photo: Gaston Giuliani.

The Ambatomena ruby deposit was exploited by a private mining company between 2000 and 2001. The production was of very good quality with euhedral crystals up to 2 cm across and 3 cm long. The ruby deposit is located in the Androyan granulitic metamorphic series, which is composed of para- and orthogneisses, marble, granite, clinopyroxenite, and quartzite. The four ruby deposits (called D1 to D4) formed lenses of clinopyroxenite (D1 and D2), sapphirinite (D3), and plagioclase (D4) intercalated with garnet-bearing granofels [243] (Figure 46). The formation of ruby is linked to the percolation of fluids at the contact between the lenses and the granofels. The ruby ($2180 < \text{Cr}_2\text{O}_3 < 6670$ ppm) is found in phlogopitized clinopyroxenites (G2), sapphirinites (G3 and G4; Figure 47A), and plagioclases (G4; Figure 47B). The mineral assemblage of the ruby is spinel, K-feldspar, plagioclase, clinopyroxene, sapphirine, phlogopite, sillimanite, cordierite, titanite, rutile, and hibonite (Figure 47C,D). The retrograde metamorphic stage is characterized by the destabilization of ruby into spinel in the plagioclases and sapphirine in the clinopyroxenites, each mineral forming a corona around ruby crystals.

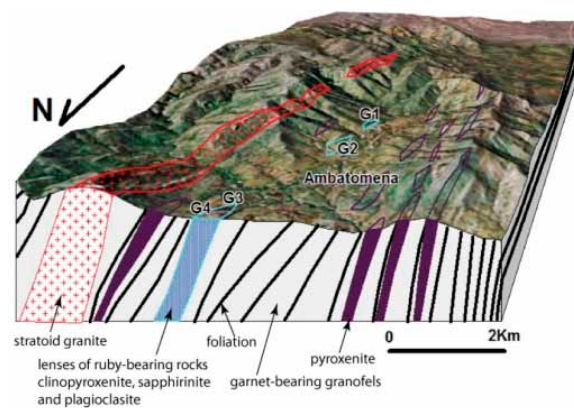


Figure 46. Panoramic view and geological cross-section of the Ambatomena ruby deposit, Betroka region, Southern Madagascar, modified from [243]. The correlation between the ruby-bearing occurrences (G1–G4) and the garnet-bearing hornfels and pyroxenites can be seen in the cross-section.

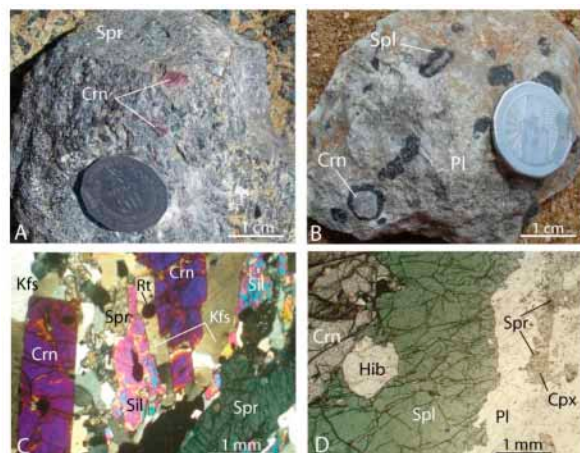
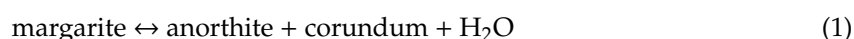


Figure 47. The Ambatomena ruby deposit, south of Betroka, Southern Madagascar. (A) Ruby (Crn)-bearing sapphirinite (Spr); (B) plagioclase (Pl) with whitish corundum (Crn) showing a corona of spinel (Spl); (C) microscopic image of ruby-bearing sapphirinite with a granoblastic texture of K-feldspar (Kfs), sapphirine (Spr), sillimanite (Sil), and rutile (Rt). The ruby sometimes has a corona of sapphirine and K-feldspar; (D) microscopic image of the corundum-bearing plagioclase. The texture is granoblastic decussate with plagioclase (Pl) and corundum. The plagioclase is associated with some sapphirine and clinopyroxene (Cpx). The corundum is embedded in a corona of green spinel with some hibonite (Hib). Photos: Alfred Andriamamonjy.

(2) For Tanzania, the ruby deposits in the Uluguru and Mahenge Mountains are located, respectively, in dolomite- and calcite-dominated marbles but deformation controlled the mineralization, which is located in saddle reef structures within fold hinges [114] (Figure 48A). The ruby is metamorphic and formed between 620 and 580 Ma. At Mahenge the deposits are Kitwalo, Ipango, Matote, and Lukande. The Morogoro mining district consists of the Kibuko, Mwalazi, Nyama Nyama, Visaki, and Msonge deposits. The marbles belong to the Neoproterozoic cover sequence that was thrust onto the gneissic basement of the Eastern Granulites. At Uluguru, the mineral assemblage is dolomite, phlogopite ± spinel, pargasite, scapolite, plagioclase, margarite, chlorite, and tourmaline.

At Mahenge, the paragenesis is calcite, plagioclase, phlogopite ± dolomite, pargasite, sapphirine, titanite, and tourmaline. Two episodes of ruby formation were defined by [114]:

(i) Ruby formed during the prograde metamorphic stage at T 750 °C and P 1.0 GPa by the breakdown of either diaspore or via the chemical reaction:



The metamorphic mineralizing fluids circulated along the zones of higher permeability at granulite facies conditions.

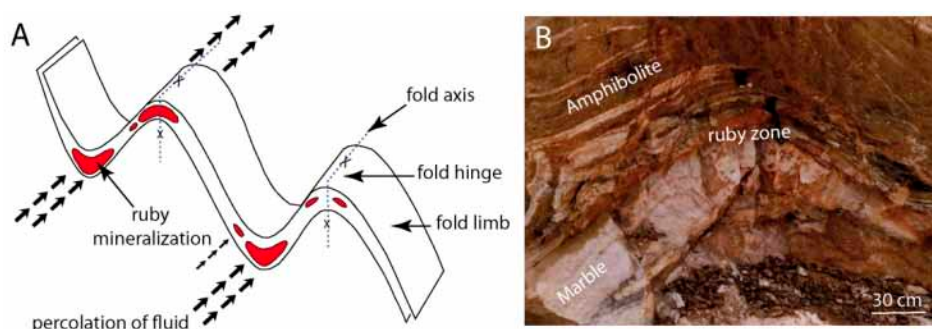
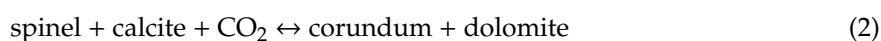


Figure 48. (A) The schematic structural control of ruby mineralization in the Uluguru and Mahenge mountains, Southern Tanzania, modified from [114]. Ruby formed in zones of higher permeability near fold hinges; (B) the structural control of ruby formation by folding and opening of fractures is also observed at the Lukande ruby deposit in the Mahenge Mountains. The ruby mineralization is located in the hinge of a fold that affected both marble and amphibolite. The contact between the two contrasting rocks hosts a metasomatic zone composed of carbonates, phlogopite, and Mg-amphibole. Photo: Gaston Giuliani.

(ii) Changes in the T-XCO₂ conditions of the metamorphic fluid triggered the ruby deposition through two main reactions:



The sources of Cr (and V) were not discussed by [114] but two possibilities can be proposed: (i) a sedimentary source, i.e., limestone or Mg-limestone (muds or clays interbedded with impure carbonates) from the carbonate platform of the Neoproterozoic Mozambican ocean. Such a source was also proposed for the tsavorite mineralization in Northern Tanzania [244]. Both tsavorite at Merelani and ruby in the Mahenge and Uluguru Mountains formed in a similar geological setting and during the East African orogeny; (ii) a mafic source such as amphibolite that was infiltrated by the fluids circulating along zones of higher permeability during folding and the formation of saddle reef structures.

At the Lukande deposit, the marbles are intercalated with Cr-bearing amphibolites that were folded and fractured (Figure 48B). Both types of rocks have suffered fluid percolation and

ruby-bearing metasomatic zones formed at the marble-amphibolite contact. The mineral assemblage is ruby-carbonate-phlogopite-magnesian amphibole. The style of deformation and the nature of the protoliths are similar to those proposed for the formation of tsavorite vein deposits from the Merelani area [244]. The metamorphic formations were affected by tight ductile isoclinal folding and shearing, and the tsavorite occurs at the hinges of sheared isoclinal folds within saddle-reef structures.

6.3. Sedimentary-Related (Type III): Placer Deposits

Placers are hosted in sedimentary rocks (soil, rudite, arenite, and silt) that formed via erosion, gravity effect, mechanical transport, and sedimentation along slopes or basins related to neotectonics. Climate is a major factor in the formation of secondary deposits. In tropical areas, rocks are exposed to meteoric alteration, resulting in an assemblage of clay minerals, Fe and Mn oxides, and other supergene phases. Corundum and zircon are resistant minerals found in soils, laterites, and gravelly levels overlying bedrock. In high-altitude areas such as in Nepal, Pakistan, and Azad-Kashmir the alteration is mechanical and ruby is found in boulders accumulated on the lower part of the slopes as for the Nangimali deposit [245]. Present-day placers are illustrated in Figure 49, which follows the classification proposed by [138]:

(i) Eluvial concentrations derived by in situ weathering or weathering plus gravitational movement or accumulation. Eluvial-deluvial deposits are on slopes and in karst cavities (marble type). Colluvial deposits correspond to decomposed primary deposits, which have moved vertically and laterally down-slope as the hillside eroded.

(ii) Alluvial deposits resulting from the erosion of the corundum-bearing host rock and transport by streams and rivers. Concentration occurs where water velocity drops at a slope change in the hydrographical profile of the river, e.g., at the base of a waterfall, broad gullies, debris cones, meanders, and inflowing streams. Terminal placers [138] formed by deltaic, aeolian, and marine accumulations are unknown for ruby deposits.

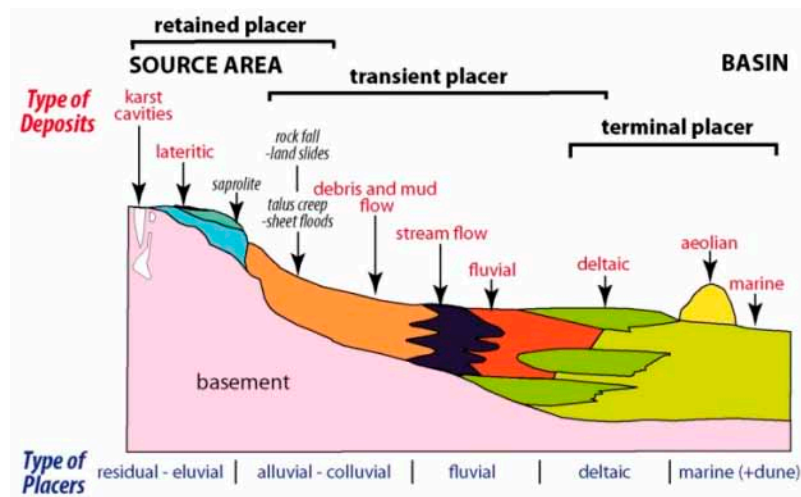


Figure 49. The different types of placer deposits formed on the continental surface and deltaic or marine basins, modified from [138]. The majority of these types of placer, except for aeolian and marine placers, occur for gem corundum deposits worldwide.

The placer deposits are divided in three main sub-types (Table 3).

6.3.1. Sub-Type IIIA: Gem Placers in an Alkali Basalt Environment (Eastern Australia, Pailin-Chanthaburi-Trat, Eastern and Central Madagascar, and Others)

Ruby-bearing placers linked to volcanic rocks are found in continental alkali basalt extrusions [68] (Figure 2). These deposits are sporadic and economically quite rare when compared to sapphire deposits of the same type, except for the ruby deposits at Pailin and Chanthaburi-Trat [145]. In Australia, Ray et al. [246]

showed that within the New South Wales deposits, in 420 listed gem corundum occurrences, 10% had ruby. However, the production realized on the short-term depended on worldwide demand.

Ruby placers in alkali basalt environments include the deposits in eastern Australia [81,106,247–250]; Asia, with deposits at Pailin, Cambodia [5,74,82,248] and the provinces of Chanthaburi-Trat and Kanchanaburi [145,146,148,149,154,251]; China with the Muling deposit in Shandong province [252]; Eastern Africa, in Kenya with the Baringo deposit, which is linked to the volcanism of the East African rift [118]; and in Madagascar at Antsirabe in Antananarivo province [95,161,231] and Vatoman-dry in Toamasina province [77,78].

(1) In Eastern Australia, ruby placers linked to volcanic rocks are found in continental alkali basalt extrusions [68] (Figure 2). They occur as scattered deposits that are subordinate to sapphires [81,85] (Figure 50). Rubies are found in alluvial placers shed from Cenozoic lava fields within an eruptive zone extending from Northeast Queensland to Southeast Tasmania. The main deposits are located in New South Wales, i.e., Barrington Tops, Macquarie-Cudgegong Rivers, and New England (Figure 50A). Occurrences are also found in South Australia at Adelaide, Victoria around Melbourne, and Tasmania.

In New South Wales the deposits are found [81,85,86]:

(i) At Barrington Tops, erosion and transport by drainages of the eroded Barrington Tops volcano gave rise to the formation of mineable placers in the river. Ruby was found in 1851 and alluvial prospecting was done over a long period between the 1960s and 1990s. The geology of the Barrington Tops Plateau was described in the early 2000s [253] and mining at Upper Manning River took place from early 2005 until 2008 (Figure 50B). The ruby is associated with other pink, purple, and pastel blue corundum used for jewelry (Figure 50C).

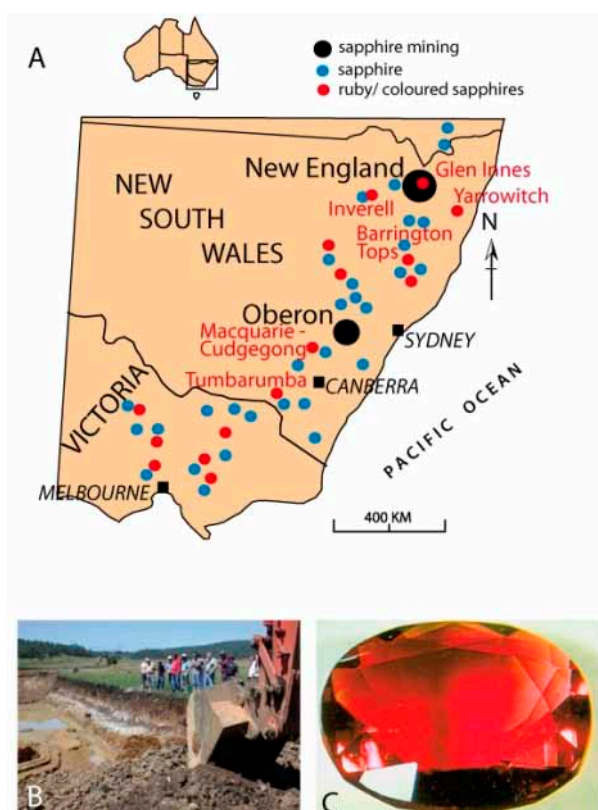


Figure 50. (A) Location of ruby deposits in New South Wales, modified after [81,86]; (B) opening of the Barrington Tops mine, March 2005, upper Manning flats. Photo: Cluff Resources Pacific M/L, Courtesy Lin Sutherland; (C) faceted 1 carat ruby, 6 mm × 4 mm across, Gloucester Tops, SE Barrington Tops plateau. Photo: Gayle Webb.

(ii) At Yarrowitch, the alluvial gem field is more restricted than at Barrington Tops and the ruby is associated with sapphires, red zircon, and spinel. The alluvial occurrences have not been mined.

(iii) At Macquarie-Cudgegong Rivers, extensive alluvial exploitation took place in the rivers from 1851 to 1941. The placers contain ruby, sapphires, zircon, gold, and diamond; their original source is unknown, despite the presence of numerous basaltic vents in the area.

(iv) At Tumberumba, ruby is minor and the placers contain blue to green sapphires, which are corroded and worn.

(v) At New England, the Inverell-Glen Innes area is known for its sapphire placers. Ruby is scarce but is recovered from all the rivers. The crystals grade from red into pink and purple corundum [86]. Sometimes, the crystals are zoned with red to pink cores, a white peripheral zone, and a violet rim. Several large gem crystals have been cut, such as the 48 carat “Aurora” zoned stone found near Glen Innes in 1988, which was cut into a 17 carats red, a 9 carats blue, and a 2 carats pink stones [249]. Other stones have been faceted, such as a 2.13 carats purple red oval cut, a 0.31 carats light red baguette cut, and a 0.22 carats red marquise cut [81].

In Queensland, rubies are very rare and the deposits are mainly composed of sapphires. In Victoria and Tasmania, pink to red corundum are rare and the high content of Fe turns the color to brown [254].

(2) The presence of corundum in alluvial placers from Madagascar has been known since the beginning of the 20th century [231]. The deposits formed by the erosion of corundum-bearing Cenozoic lava fields within eruptive zones extending from the centre of the island, in the Ankaratra massif, Antananarivo province, to the north in the Montagne d’Ambre, Antsiranana province (Figure 51). The production of ruby in Madagascar became significant after the discovery in 2000 of two ruby deposits in the province of Toamasina named Andilamena [164] and Vatomandry [255].

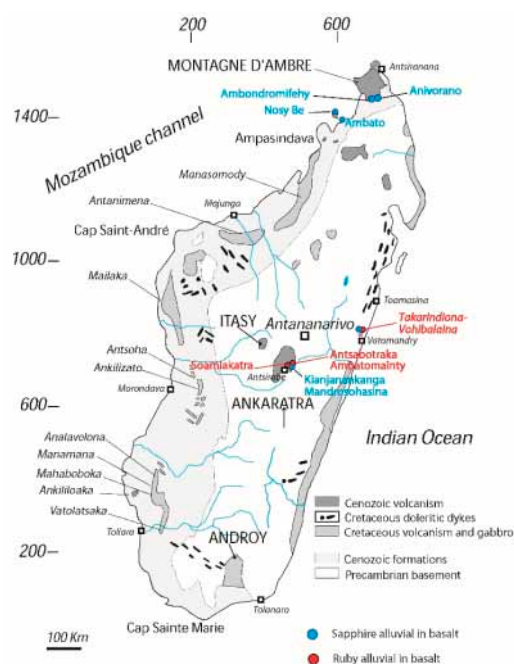


Figure 51. The volcanic provinces of Madagascar, modified from [256] with the localities of the basaltic corundum deposits related to the Cenozoic basalts in the provinces of Antsiranana, Antananarivo, and Toamasina [161,162]. The deposits of gem corundum: north in Antsiranana Province, the mining districts of Ambondromifehy and Anivorano in the Montagne d’Ambre, Ambato peninsula and Befotaka in Nosy Be island; Central Madagascar in Antananarivo Province, the mines of Soamiakatra, Mandrosohasina–Kianjanakanga (Antsirabe area) in the volcanic Ankaratra massif; and east in Toamasina Province, with the deposits of Vatomandry in the Takarindiona and Vohibalaina basaltic areas. The geographic coordinates are related to the Laborde projection.

In 2005 Madagascar was the third largest ruby-exporting country after Kenya and Tanzania (see Figure 3). The secondary deposits, i.e., alluvial placers and paleoplacers are located (i) to the north and east of Antsirabe city in Antananarivo province (Ambatomainty, Antsaboetra, and Soamiakatra deposits) and (ii) to the north of Vatomaniry in Toamasina province. In this last province the alluvial and paleoplacer deposits border the Takarindiona and Vohibalaina basaltic massifs (Figure 51). The mining sites are Amfao, Sahanonoka, and Antsidikana near the commune of Amboditavolo. They are located in a number of watersheds and major river systems downstream of the Vohibalaina volcanic massif, and those of Antanambao, Mahatsara, and Ankazombanga on the southern and eastern borders of the Takarindiona massif [94].

At Vatomaniry, the ruby is associated with crystals of sapphire and red zircon in some paleoplacers but mostly in alluvials. Generally, the gem gravels consist of 0.5–2 m thick sediments overlying bedrock in the riverbeds. The ruby crystals are 5 mm to 3 cm across, rounded and with different colors (red, red purple, red brown, and pink), but a red-purple color is dominant [77].

The most common inclusions in ruby from the Sahanonoka deposit are rutile and zircon (Figure 52A), which are cogenetic and arranged in clusters [161,162,255]. Ilmenite, rutile, and Al-silicates also occur as inclusions (Figure 52B). The other solids are talc (Figure 52C), phlogopite (Figure 52D), pentlandite, plagioclase, titanite, ilmenorutile, hematite, and Al-silicates. Apatite was observed by [78]. Rutile crystals were identified as a daughter phase in the cavities of fluid inclusions trapped by the ruby. The fractures in the rubies are filled by limonite and kaolinite [78].

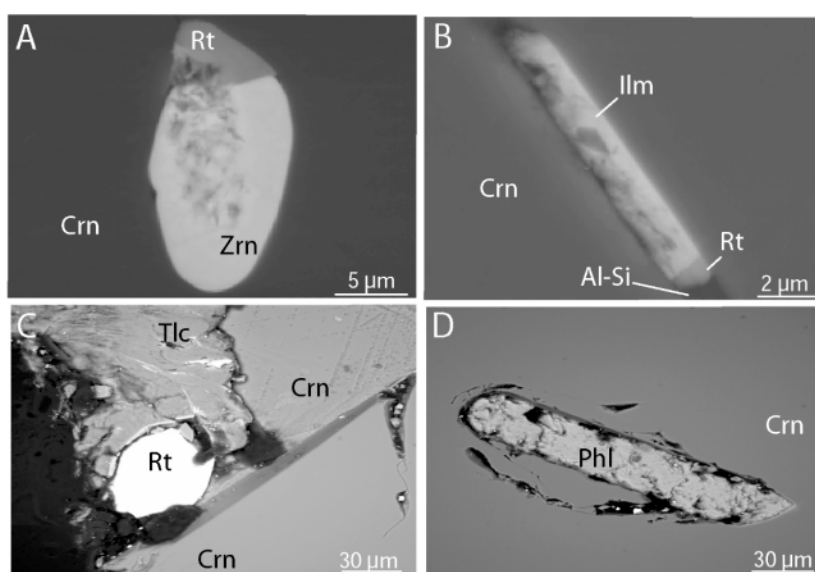


Figure 52. Inclusions in ruby from the Sahanonoka deposit in the Vatomaniry area [94]. (A) Zircon (Zrn) associated with rutile (Rt); (B) rutile, ilmenite (Ilm), and Al-silicate (Al-Si); in ruby (Crn); (C) association of rutile and talc (Tlc) in ruby; and (D) phlogopite (Phl) crystal included in a ruby.

The original source of these rubies is unknown neither xenocrysts nor corundum xenoliths have ever been observed in the basalts. The placers that are proximal and downstream of the different basaltic volcanics, ruby crystals associated with fragments of basalt, and red to orangey zircon and sapphires leave a high probability that the rubies were connected to the different basaltic flows of the Takarindiona and Vohibalaina basaltic massifs.

The Fe contents of the rubies (1500–8460 ppm) are always higher than Cr and V. The Cr₂O₃ contents differ with color: (i) red brown (4760–6670 ppm), (ii) red (3500–3800 ppm), (iii) pink (1390–11,670 ppm), and (iv) red to purple (720–2000 ppm). The chemical diagram for classification of corundum deposits (Figure 53) shows a distinctive bimodal chemical distribution for the rubies from Vatomaniry, which plot in the metamorphosed M-UMR (R3) and metasomatic (R4) domains. The first field in the R3

domain (M-UMR signature) contains red and red brownish rubies; the second field in the R4 domain (metasomatic such as plumasite or metasomatite in M-UMR) contains red to purple and pink stones. The bimodal distribution is also present for the rubies from Soamiakatra in Ankaratra and Andimalena, while the rubies from Antsabotraka and Ambatomainty plot in the metasomatic domain.

The $\delta^{18}\text{O}$ values for rubies from the Vatomandry mining district span the range 2.7–6.7‰ ($n = 8$) with a mean value of $\delta^{18}\text{O} = 5.1 \pm 1.4\text{‰}$. They fit within the worldwide range defined for ruby in basaltic environments ($1.3\text{‰} < \delta^{18}\text{O} < 5.9\text{‰}$, mean $\delta^{18}\text{O} = 3.1 \pm 1.1\text{‰}$, $n = 57$; [80]) and ruby associated with M-UMR ($0.25\text{‰} < \delta^{18}\text{O} < 6.8\text{‰}$, $n = 19$). Solid inclusions, chemical composition, and oxygen isotopes are compatible with a metamorphic origin for the Vatomandry rubies.

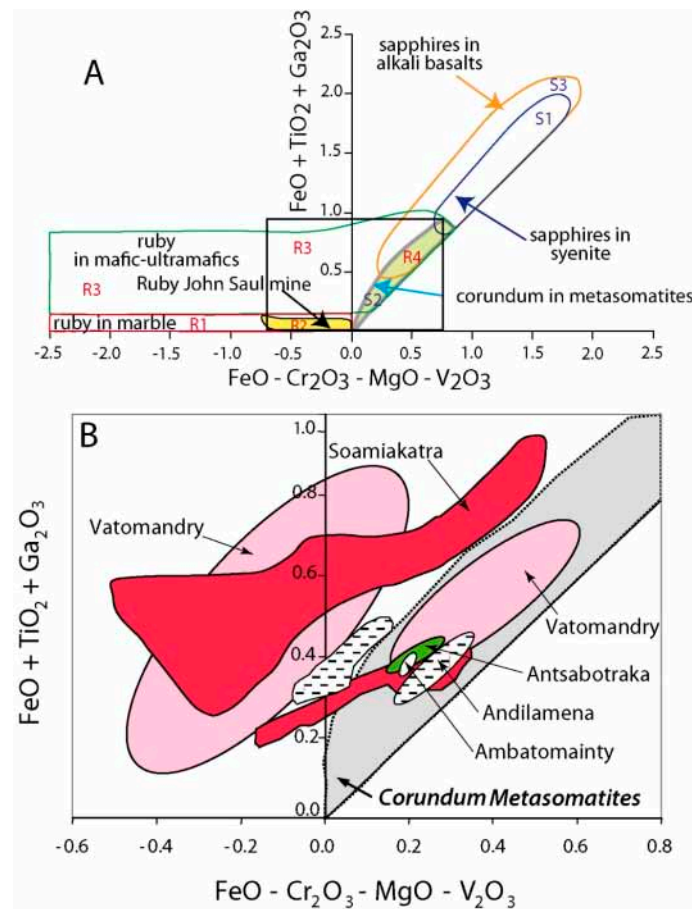


Figure 53. (A) Chemical diagram $\text{FeO}-\text{Cr}_2\text{O}_3-\text{MgO}-\text{V}_2\text{O}_3$ versus $\text{FeO} + \text{TiO}_2 + \text{Ga}_2\text{O}_3$ showing the main chemical fields defined for different types of corundum deposits worldwide [72,77]; (B) field of chemical compositions of ruby from the Vatomandry deposits (Toamasina Province) compared with the primary deposit at Soamiakatra, and the placer deposits of Antsabotraka and Ambatomainty (Antananarivo Province). The Vatomandry and Soamiakatra deposits show a distinct bimodal chemical distribution in the M-UMR (R3) and metasomatite (R4) domains, respectively. The deposit at Andilamena in Toamasina Province is apparently not related to alkali basalts but is likely derived from plumasite in M-UMR because field work has shown the presence of in situ highly altered mafic rocks, biotite schists, and kaolinite-bearing rocks.

6.3.2. Sub-Type IIIB: Gem Placers in Metamorphic Environment in M-UMR (Montepuez, Mozambique) and Marble (Mogok Stone Track, Myanmar, and Others)

(1) At Montepuez in Mozambique, the main source of facet-grade material in the Gemfields Group Ltd. properties is secondary deposits in M-UMR environments [25,26] (see Figures 32 and 54). The placer deposits were previously interpreted as alluvial and related to a flood event in the river

systems [27,200,257,258]. However, Simonet [25] concluded that the deposits were not alluvial since there was no evidence of systematic rounded pebbles, variations in the grain sizes and graded bedding in the sediments.



Figure 54. The placer deposits in the Montepuez mining district in Mozambique. (A) Aerial view of the Mugloto Pit operated by the Gemfields Group Ltd. The miners are using a back-filling technique (top) and using tree plantations for rehabilitation (bottom); (B) the ruby-rich gravel layer at Mugloto in the Montepuez mining district. The detritic levels contain sub-angular quartz and clay pebbles located between 4 and 10 m under the surface. Gemfields removes the overburden and uses an excavator to collect this gravel layer, that is then sent to the wash plant to extract rubies; (C) small scale miners near Nacaca village, an area reserved for locals outside the southeast border of the Gemfields concession, where a few thousand people have worked since 2012. At this location small rubies are found in gravels under to 2–5 m of overburden. The Nacaca stones are usually smaller and contain more inclusions than those from Mugloto and their iron content is similar to that of the material from Maninge Nice; (D) parcel of rough rubies from Mugloto Pit near Montepuez (about 0.5 g per stone) at a Gemfields rough ruby auction in Singapore. The rubies coming from a gravel layer range from bright to dark red (depending on their iron contents), and present some abrasion features. The area was discovered in early 2014 and probably more than 90% of Gemfields income since then has been extracted from this deposit. Photo: Vincent Pardieu © GIA.

The secondary deposits are mainly colluvial with limited horizontal transport (more sub-angular fragments) and a few alluvial pebbles (smooth and round appearance). Most of the mineralized horizons are stone lines, i.e., weathering-resistant rock fragments formed over millions of years of erosion [25]. The stone lines, which are composed of angular fragments of quartz and pegmatite, are excellent traps for smaller grains of high-density minerals such as ruby. The colluvial deposits (Figure 54) are either associated with the proximal primary deposits (as at the Maninge Nice/glass mines) or disconnected (as at the Mugloto mine). Simonet [25] proposed an exploration scheme for the colluvial deposits in the Montepuez area based on detailed mapping of the primary deposits (stressing the importance of the strike and dip of the mineralized structures) and erosion through time (Figure 55). The distance between the primary deposit in outcrop and the edge of the colluvial accumulation increases during the erosion process. Mapping of the stone lines and outcrops of ruby-bearing rocks could be an important tool for future ruby placer exploration in the Montepuez mining area.

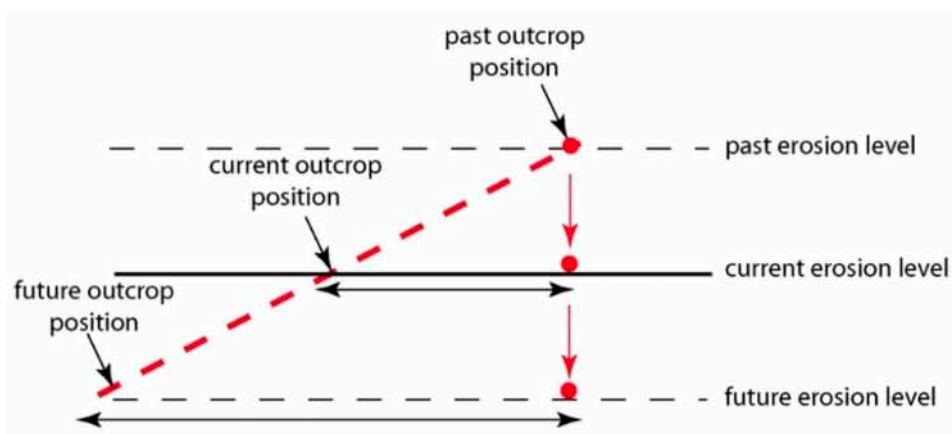


Figure 55. Schematic time-relationship of the formation and position of a colluvial placer through erosion of an angle-dipping primary deposit [25].

(2) Economic ruby placer deposits in marble environments of South-Eastern Asia (Figure 2).

In the Mogok Stone Track in Myanmar (Figure 56A), gem-bearing levels enriched in pebbles, sand, silt, clay, and iron oxides are called ‘byon’ [259,260] (Figure 56B,C).



Figure 56. Different aspects of the gem placers in the Mogok Stone Track, Myanmar (in January 2015). (A) Panoramic view of the primary deposits mined in marble on the flank of the hills (foreground view) and secondary deposits, i.e., placers, mined in the valley (background); (B) image of the gem-bearing material called ‘byon’ enriched in gravels and sand. The concentration of heavy minerals is visible and is composed of iron oxides, corundum, quartz, and pieces of marble; (C) concentration of gem minerals (ruby, spinel, and sapphire) in the pan of a miner; and (D) sedimentary breccia formed in a cave placer karst. The breccia formed from an argillite containing crystals of spinel, plates of graphite, and fragments of marble and quartz. Size of the breccia sample around 15 cm long. Photo: Gaston Giuliani.

Similar deposits are found at Namyá in the northern part of the country where the monsoon is an effective erosion mechanism in low-altitude environments [5,108,261]. The gem concentration is closely related to the formation of karst and chemical weathering of marble and associated rocks, i.e., schists, gneisses, and granitoids (Figure 56D). The cave placers in karst contain sedimentary breccias formed by argillites with ruby, sapphire, spinel, graphite, and fragments of marble and quartz. The ruby and other gems (sapphire and spinel) are trapped in eluvial, colluvial, alluvial, fracture-filling, and cave deposits (Figure 57) [29].

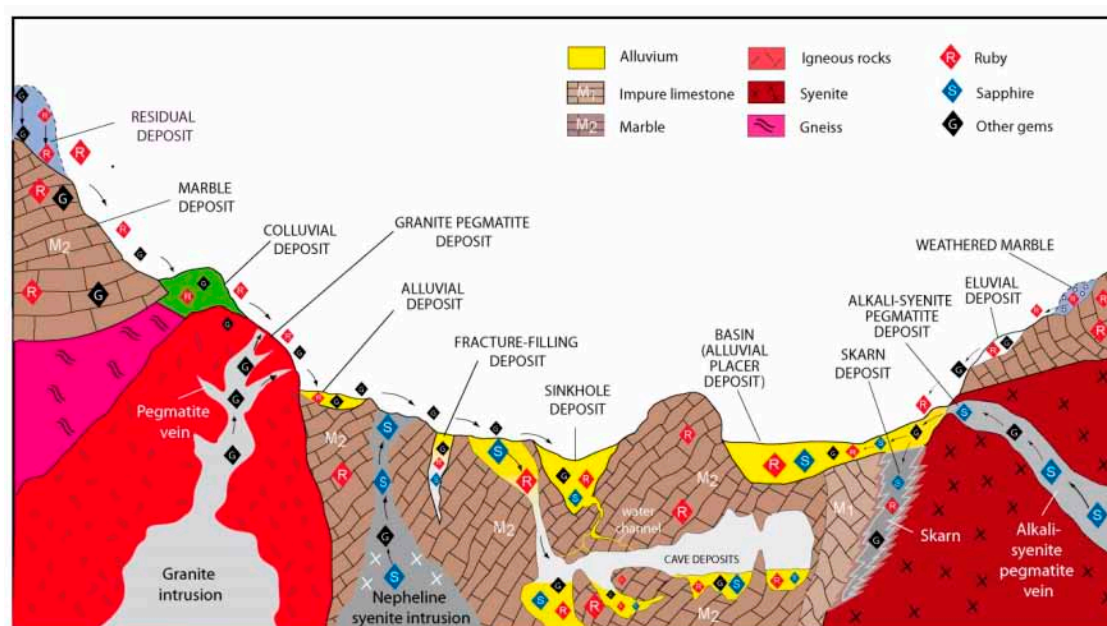


Figure 57. The main types of ruby-bearing placers in the Mogok Stone Track, Myanmar; modified from [29]. The primary ruby deposits are located in marble and the secondary deposits are residual, colluvial, alluvial, fracture-filling, and cave placers in karst morphologies. The figure represents the ruby deposit of Dattaw in marble (on the left) and the sapphire deposit of Thurein-taung (on the right). At Mogok, the different types of primary deposits of ruby and sapphires resulted in the mingling of gems from different sources in single secondary accumulations.

In Vietnam, the placers are proximal to the main primary deposits of ruby and colored sapphires in marble. They are located in the Luc Yen and Yen Bai provinces in the Red River shear zone area and in the Quy Chau ruby deposit (Nghe An province) in the Bu Kang metamorphic zone in Central Vietnam [98,210]. The placers are exploited at Luc Yen, An Phu, Khoang Thong, and Nuoc Ngap (Luc Yen district); at Truc Lau, Yen Thai, Tan Huong, Tan Dong, Hoa Cuong, and Tran Yen (Yen Bai district); and at Quy Hop and Quy Chau (Nghe An district). The paleoplacer at Truc Lau consists of 10 m of sediments overlying bedrock. The rubies and blue sapphires are contained in 5 m thick gravel layer overlain by a 3.5 m thick bed of Quaternary sediments and 1–1.5 m of soil. In 2002, up to two boulders (1–2 kg) of pink sapphire and star ruby were recovered every month in the paleoplacer. The placer deposits consist of gravel concentrations in karst pockets (Figure 58A) and alluvial fans (Figure 58B) found all over the Luc Yen region [261,262]. The gem-bearing valleys are often narrow and correspond to small depressions, which typically range in area from 2 to 3 km² (Figure 58D). These placers furnish a variety of gem-quality materials for a market, which has been open daily in Luc Yen city since 1987 (Figure 58C). The rubies in the placers have a proximal origin as confirmed by the oxygen isotopic values of the crystals: $\delta^{18}\text{O}$ ranges between 15.5‰ and 22.3‰, which overlaps the worldwide oxygen isotopic range (16–23‰) defined for ruby hosted in marble [40,93].

Mining is conducted on a small scale, from Bai Lai in the northeast of Luc Yen to the Na Ha area in the south, near the banks of Thac Ba Lake. The most active sites are along the streams of Cong Troi,

in Nuoc Ngap (An Phu area). Material is also removed from old mines in areas such as Minh Tien, Khoan Thong, and Bai Chuoi, where big companies mined the most accessible and profitable material, often missing areas between marble pinnacles (Figure 58E) that excavators could not easily reach. As a result, some gem-rich ground was left behind; this is now collected by locals with shovels and buckets.



Figure 58. Ruby-bearing placers hosted in marble from northern Vietnam (Luc Yen area; 2009). (A) Exploitation by locals of ruby-bearing gravel concentration in karst pockets; (B) artisanal exploitation of ruby-bearing alluvial fans concentrated in narrow valleys bordered by rice fields; (C) the famous gem market at Luc Yen city; authorization for the photograph of the Luc Yen market by filed gemmologist M. Shuan, and (D) the gem-bearing valleys are often narrow and correspond to small depressions, which typically range in area from 2 to 3 km². These valleys are defined by shear zones and faults that crosscut the marble units. The karst geomorphology is characterized by an alignment of marble domes forming cones and lines of karst hills; (E) excavation of ruby-bearing areas continued up to the marble pinnacles, but the missed gem areas between the pinnacles is exploited by locals with shovels, picks and buckets. Photos: Vincent Pardieu © GIA.

6.3.3. Sub-Type IIIC: Gem Placers with Ruby Originating from Multiple and Unknown Sources

Gem placers of economic interest are also found in Madagascar (Ilakaka, Andilamena, Bemainty, Didy, and Zahamena) and Tanzania (Tunduru, Songea, and Umba). The historical, geological, and mineralogical features of these deposits are described in different publications; see [5,19,20,108,161,164,263–266]. These placers contain ruby, sapphires, and other minerals (garnets, alexandrite, topaz, zircon, spinel, and tourmaline) that originate from multiple unknown sources. We can note that at Songea and Andilamena, corundum is found both in placers and in situ in highly weathered rocks.

In the Ilakaka area (see Figure 4), gem corundum is found at three gravel levels in two main alluvial terraces deposited on the Triassic Isalo sandstone [108]. The terraces are weakly consolidated, but correspond to paleoplacers. The terraces are the result of the erosion and stripping of the sandstones. The deposit is not well consolidated and is composed of quartz-rich sands containing pebbles of ferruginous laterite, rounded blocks of Isalo sandstone and quartz, and quartzite and schist pebbles.

The Ilakaka deposits produce very fine blue, blue-violet, violet, purple, orange, yellow, and translucent sapphire crystals along with pink corundum and rare rubies, zircon, alexandrite, topaz, garnet, spinel, andalusite, and tourmaline. In 2002, test mining by Gem Mining Resources Company over 38 days resulted in approximately 43 kilos of gems, comprising of 4% semi-precious stones, volcanic glasses, and ruby, and 96% sapphire comprising 58% pink gem corundum, 30% sapphire, and 8% other colors of sapphire (e.g., yellow, orange, padparadscha, and green). Microscopic examination of respectively 30 ruby and 58 blue sapphire crystals showed that all of the rubies have the same gemmological features, i.e., growth, twinning, color bands, and solid inclusions, but that the blue sapphires define two different mineralogical groups [40].

The ruby crystals have $\delta^{18}\text{O}$ values between 2.6‰ and 3.8‰ ($\delta^{18}\text{O}_{\text{mean}} = 3.5 \pm 0.5\text{‰}$, $n = 4$) that are within the isotopic range defined for primary ruby deposits in metamorphosed M-UMR from Southern Madagascar ($2.5\text{‰} < \delta^{18}\text{O} < 6.8\text{‰}$; [128]). The Phanerozoic sedimentary sequences and the Isalo Group cover the northern part of the Vohibory unit, where intercalations or complexes of M-UMR hosting ruby and pink corundum are common [164]. Erosion of the Vohibory unit during the Late Carboniferous to Middle Jurassic contributed to the concentration of ruby in the basin. A proximal source for ruby in Ilakaka from the Vohibory region is likely. Quaternary erosion remobilized paleoplacers.

In the eastern part of Madagascar, several ruby-bearing placers have been discovered over the last 20 years as the Vatomandry deposit [255] (see Figure 4). The ensuing rush of locals and immigrants opened up several mining zones in the areas of Andilamena (2000–2004), Andrebabe (2002), Moramanga (2010), Didy (2012), Zahamena (2015), and Bemainty (2016). The deposits are generally exploited by either unlicensed miners when working outside of protected areas or illegal miners when working inside the areas (Figure 59). The miners operate in quagmires with shovels and buckets, washing gravels in pans and removing the stones from the sieves by hand.



Figure 59. Placer deposits in the eastern part of Madagascar. (A) General view of the ruby and sapphire deposit in the jungle of Didy. Photo: Nirina Rakotosaona; (B) crystals of ruby and sapphires from the Didy deposit. The crystals are around 8 mm in size; photo: Vincent Pardieu © GIA; and (C) sapphire and pink corundum placer deposits in the jungle near Bemainty. Photo: Vincent Pardieu.

Ruby is generally associated with sapphires at Vatomandry [77,78], Didy [265] (Figure 59), and Bemainty [265] but is exploited as a main gem mineral from the Andilamena and Zahamena

deposits [266]. Up until the present, geological information is lacking, but visits to the mining district of Andilamena by V. Pardiou allowed him to observe the corundum host rocks, which were highly weathered. They comprised fuchsite-bearing altered mafic rocks, biotite schists, and kaolinite-bearing rocks. The rubies are found in mafic rocks and/or biotite schists. Sapphires are restricted to veins of quartz-free kaolinite-bearing rocks that crosscut the mafic rocks.

Debate on the geologic and geographic origins of rubies from Andilamena and Vatomandry involved:

(i) The chemistry of these rubies in the diagram $\text{FeO-Cr}_2\text{O}_3\text{-MgO-V}_2\text{O}_3$ versus $\text{FeO} + \text{TiO}_2 + \text{Ga}_2\text{O}_3$ is similar and characterized by an overlap of two chemical domains (bimodal distribution; see Figure 53). On the contrary, the diagram V versus Fe (Figure 60) shows a clear difference in the V contents of ruby for both deposits that allows the allocation of the geographic origin of the Vatomandry rubies relative to Andilamena and also the main ruby deposits worldwide;

(ii) The $\delta^{18}\text{O}$ values for rubies from the Vatomandry mining district span the range 2.7–6.7‰ ($n = 8$) with a mean value of $\delta^{18}\text{O} = 5.1 \pm 1.4\text{‰}$ ($n = 5$). Those for rubies from the Andilamena deposit are between 0.5‰ and 4‰ with a mean value of $\delta^{18}\text{O} = 2.9 \pm 1.5\text{‰}$ [128]. Both ranges of $\delta^{18}\text{O}$ values overlap and fit within the worldwide range defined for ruby in basaltic environments ($1.3\text{‰} < \delta^{18}\text{O} < 5.9\text{‰}$, mean $\delta^{18}\text{O} = 3.1 \pm 1.1\text{‰}$, $n = 57$); [80]) and ruby associated with metamorphosed M-UMR ($0.25\text{‰} < \delta^{18}\text{O} < 6.8\text{‰}$, $n = 19$). Both rubies are compatible with a metamorphic origin.

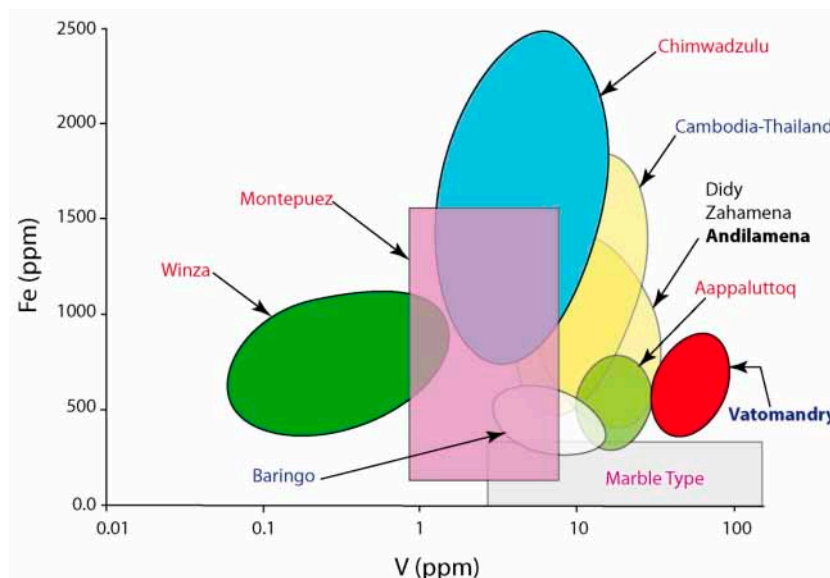


Figure 60. V versus Fe (in ppm) for the main ruby deposits of Madagascar (Vatomandry, Andilamena, Didy, Zahamena) and other deposits worldwide (Kenya, Baringo; Greenland, Aappaluttoq; Tanzania, Winza; Mozambique, Montepuez; Malawi, Chimwadzulu; Cambodia and Thailand; and finally deposits of marble type from Central and Southeastern Asia). Chemical data from [200,267] and Pardiou unpublished data. The chemical domain of ruby from Vatomandry is clearly separated from all the other ones and this parameter permits to precise its geographic origin. The name of ruby deposits related respectively, to M-UMR is written in red (Types IIA₁, IIB₁), to marble deposits in violet (Type IIB₂), to alkali-basalt in blue (Type IIIA), and to metamorphic environment in black (Type IIIB).

7. Conclusions and Perspectives

In the present paper, the ruby occurrences and deposits were classified into three main types: (Type I) magmatic-related, (Type II) metamorphic-related, and (Type III) sedimentary-related (Figure 61).

The economic ruby deposits, in terms of volume and quality, are the placers that in the new ruby deposits classification are called “Sedimentary-related (Type III)”. The hardness and density of ruby are the main physical parameters that enable it to survive the erosion of primary deposits, mechanical transport, and accumulation along slopes or sedimentation in basins. Today Africa is the

top gem ruby producer in the world, via secondary deposits in metamorphic environments (Sub-Type IIIB) resulting from the erosion of primary deposits in metamorphosed mafic and ultramafic rocks (M-UMR; Sub-Types IIA₁ and IIB₁).

Over the last decade the main discoveries of ruby have been in Mozambique and Madagascar. It is not the end but the beginning of a new era for understanding the formation of such primary deposits and prospecting their associated placers. At the Montepuez mining district, the colluvial deposits are highly economic and characterized by limited transport. Most of the mineralized horizons are stone lines but the placers are proximal to the primary deposits. The exploration scheme proposed by [25] for the colluvial deposits based on detailed mapping of the primary deposits and erosion through time is of high importance. It includes the study of the paleogeography of eroded areas (plateaux and basins) in Eastern Africa where ruby occurrences are known, and the geology of mineralized structures in metamorphic belts.

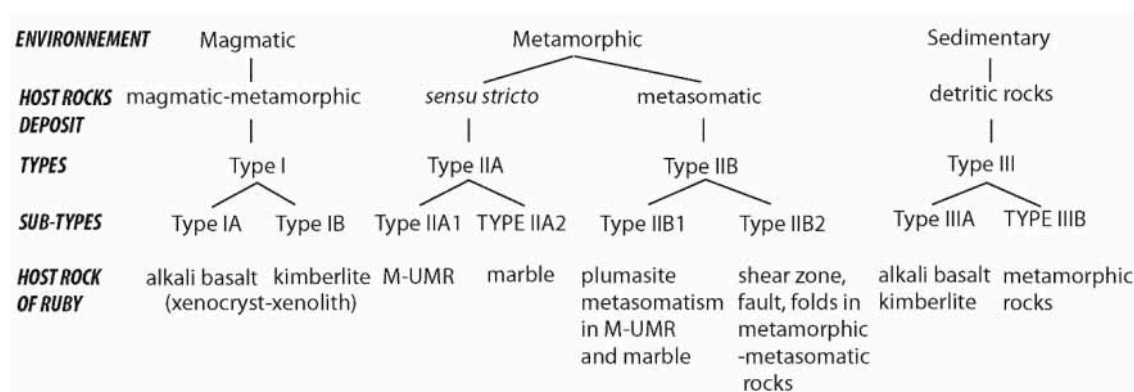


Figure 61. New typological classification for ruby occurrences and deposits worldwide. M-UMR = metamorphosed mafic-ultramafic rocks.

The extent of erosion through time can be assessed by dating the colluvial or alluvial material by measuring ¹⁰Be (cosmogenic isotope) in recent quartz-rich sediments or in pebbles of quartz (alluvial or not), which allows the quantification of mean denudation rates, in alluvial terraces and abrasion, across a watershed or an ancient basin. Cosmogenic isotopes are produced on the Earth's surface by the interaction of cosmic rays and their products with matter (¹⁰Be, T1/2 1.5 Ma). Such isotopes accumulate progressively in rocks near the surface, depending on altitude and erosion rates. The cosmogenic isotopic concentration of the sediment provides access to the average erosion rate of the watershed at its source. Fission track studies on zircon (and apatite) may be used in sediment provenance determination and in terms of the time of cooling below 300 °C in the zircon-bearing protolith before erosion.

The new and major discoveries of ruby and sapphire placers in Eastern Madagascar at Didy, Zahamena, and Bemainty, located in tropical forests, are economic. They were found by local people in areas, which are crosscut by numerous NE-SW faults separating small alluvial and diluvial basins. These zones are difficult to access and are protected forest areas; therefore prospecting has not been done but the combination of photosatellite images with geological maps, looking for metamorphic M-UMR formations, will help in the discovery of new placers.

Other ruby-bearing Neoproterozoic metamorphic M-UMR in East Africa have been productive and some of them still produce a few rubies as in Tanzania (Winza, Longido), Kenya (Mangare area, Kitui), Malawi (Chimwadzulu), and Southern Madagascar (Vohibory region). In 2005 these countries assumed most of the worldwide production. These primary deposits in M-UMR can be found in all metamorphosed volcano-sedimentary sequences from the Archean to the Cenozoic. The discovery and production of ruby at the Aappaluttoq deposit (south of Nuuk; Fiskensæst district) and the presence of new occurrences north of Nuuk (Kangerdluarssuk) is an excellent example that must encourage a better understanding of their formation and their prospecting as a function of the latitude of the different countries (tropical versus glacial and temperate climates).

The second important type of ruby deposit includes those located in marble (Sub-Type IIA₂) in Central and Southeastern Asia. These Cenozoic deposits are always one of the main worldwide sources of high quality ruby with intense color and high transparency, such as the famous Mogok pigeon blood rubies. The mining district of Mogok is rich in different types of gems including red spinel and ruby in marble. Genetic models are proposed for their genesis. They formed during the metamorphism, in the amphibolite facies, of carbonates interbedded with mudstone and evaporitic (salts and sulfates) intercalations. Lithological control of the mineralization is a function of the paleogeography of the carbonate platform environment before metamorphism. The role of evaporites is proposed as key for the genesis of ruby in marble but Al-enriched sediments such as metapelite or meta-bauxite intercalated in the marbles are in some cases also possible protolith for the ruby-parent rocks (Revelstoke and Snezhnoe deposits). The Mogok mining district remains a suitable site for developing further geological research considering the complexity of the relationships between the metamorphic rocks and granitoid intrusions. The formation of ruby-bearing skarns is possible, given the recrystallization of some carbonates, with crystals up to 10 cm across, present in the Dattaw mine. Multi-stage mineralization and telescoped episodes of thermal anomalies related to regional or contact metamorphism are highly probable. Future efforts will move towards developing more effective exploration guidelines that consider new geological factors responsible for the formation of ruby at Mogok and the timing of formation of these multi-stage gem deposits.

The timing between deformation, metamorphism, and ruby formation in these marble deposits is of importance, as shown in some deposits from Tanzania that are associated with folding, saddle-reef structure, and fluid circulation in zones of higher permeability. This scheme is applicable for all deposits, whatever their ages, but must be prospected in the Neoproterozoic Metamorphic Belt.

The classification proposed for ruby occurrences and deposits is a necessary step to build a new scheme for understanding ruby-mineralization from the field to the laboratory. The determination of the different sub-types based on the host rock of ruby and the knowledge on the genesis of most of the deposits will help us to understand the mineral associations and the chemistry of rubies. The combination of all these data linked to a specific type of deposit will serve as a basis for the determination of the geographical origin of rubies.

The diversification of known ruby sources in the world during these last two decades has increased considerably the challenge of gem ruby geographic origin determination [11–15]. The gemmological laboratories amassed rubies with samples obtained by professional field gemmologists [9,21,37,90,200]. The precise gem localization combined with accurate chemical analysis obtained by LA-ICP-MS calibrated by natural standards [92], enriched the collections of standard stones for different types of ruby deposits worldwide. The combination of inclusions and trace element chemistry makes the geographic origin determination more reliable currently, although it can remain inconclusive [11]. The case of ruby and sapphire in placers from basaltic environments is illustrative and the geographic origin is always matter of debate; the geologic origin is often confronted to different possible possibilities, i.e., metamorphic *sensu stricto*, metamorphic–metasomatic, and magmatic for gem material [11,268]. The V versus Fe diagram of ruby from several economic deposit (see Figure 60) confirms clearly the separation of the two main types of primary ruby deposits worldwide, i.e., those hosted in M-UMR (Types IIA₁ and IIB₁) and in marble (IIB₂), which are typically metamorphic. The origin of ruby from secondary deposits, i.e., placers in the alkali basalt environment (Type IIIA) is debatable because melt inclusions are present in some rubies from Thailand, Cambodia, and Montana. A magmatic origin is probable but the V versus Fe diagram shows that their chemical domain overlaps that of rubies from metamorphic origin. The discussion presented here provides a basis for further investigations into the origin of these rubies keeping in mind that they were incorporated by ascending basaltic magmas as xenocrysts from possible different geological sources.

Rubies are classified by most of the gemmological laboratories into two groups based on their trace element chemistry [11]: (i) low (below 200 pm) and high iron (above 400 ppm) rubies. The marble-hosted metamorphic rubies (Type IIA₂) have a very low Fe content when compared to all the other types

of rubies except those from the former John Saul mine (see Figure 19, e.g., plumasite of Type IIB₁). Nevertheless rubies in marble deposits have similar inclusion characteristics and their chemical domain overlap as well as their oxygen isotopic values. This remark opens the debate about the reality of determining the geographic origin of a gem when disconnected from its geological environment. Some stones and sometimes of top-quality are mingled with other ones and finally whenever the ruby is Fe-poor, the geographic determination is inconclusive. Myanmar stones are always highly prized on the market for their color and transparency. The Mogok and Mong Hsu rubies are identified based on their internal features and trace element profiles [11]. High-iron rubies (Thailand, Cambodia, Madagascar, Mozambique, Kenya, and Greenland) are usually basically identified by their inclusions and trace element profiles (V, Mg, and Fe but not Cr, see Figure 20; [11,82,83]). The main question of geographic attribution remains for rubies between these two ranges of Fe contents.

The new geological classification of ruby based on the geological environment and the gem host-rock proposed three main types and eight sub-types of deposits. The classification system reflects the interplay between tectonic with magmatic and metamorphic events during the history of the Earth, and through continental plate tectonics within Wilson cycles, over circa 150 millions of years. The final point concerns the basic erosion of ruby-bearing rocks at the surface, and the transport and sedimentation of the detrital material in basins. The different sub-types for primary deposits are based on the gem host-rock of ruby, which is different from place to place in the crust, the final petrographic product depending on the nature of the fluids, the timing of their circulation and the intensity of fluid–rock interaction. Desilication and/or metasomatism phenomena are effective processes able to extract not only the chromophores Cr, V, and Fe but also Al from M-UMR for the formation of ruby. The different sub-types of deposits will help either the geologist to understand the genesis of new deposits and to define zones of interest for exploration or the gemmologist for geographic origin determination.

Fingerprinting of ruby used by gemmologists is a tool derived from geological and mineralogical investigations: (i) Trace elements (V, Fe, Ga, and Mg) are used as previously reported. Ti is also an interesting element that can be used for determining the geological history of the gem-bearing sample as shown by [269] for corundum. The combination of different ratio such as Mg/Mg+Fe versus Cr/Cr+V will permit to trace the source of these elements, i.e., ultramafic versus mafic rocks as done for emerald by [270]; (ii) the combination of Fe, Ti, Ga, Cr, V, and Mg with oxygen isotope ratios of ruby provide a powerful tool for the determination of geologic origin [40,82,87,93,144,151,152]. The oxygen isotopes separate clearly three types of ruby deposits: (a) marble, (b) the John Saul mine type, and (c) metamorphosed M-UMR. The analysis of oxygen isotopes by SIMS is semi-destructive as is LA-ICP-MS for trace elements analysis but can be applied on cut and polished rubies; and (iii) inclusions are helpful in origin determination but similar geologic environments can produce gems of similar inclusion suites [269]. Determining the geological origin of corundum mingled in huge metamorphic placers remains a very difficult task, as for the Ilakaka deposit in Madagascar.

The objective geological criteria synthesized in the present review through scientific works and experience open a new framework for mineral exploration guidelines. The final conclusion is that the main economic ruby deposits are the result of continental plate tectonics. Ruby deposits are found where continental plate collision formed mountain ranges, as was the case in the Neoproterozoic with the Metamorphic Mozambican Belt, or with the Himalayas. Continental collision increases the thickness of the continental lithosphere, which is accompanied by an increase of pressure and temperature producing a zone of higher grade metamorphism (amphibolite to granulite facies), and sometimes melting rocks to form felsic magmas. Extensive deformation at high temperature with kilometer-scaled migration of material and fluids along shear zones (e.g., in the case either of the Red River shear zone in Southern China and Northern Vietnam or the Mogok Metamorphic Belt, where ruby is found in placers defining the trace of shear zones in Northern Vietnam) and faults results in the remobilization and precipitation of elements, and tectonic melange zones. These processes are heterogeneous, and proceed by dissolution and precipitation, as well as by fusion and crystallization,

where elements (such as chromium) are unusually concentrated in the crust. The return to isostatic equilibrium (30 km thick for the continental crust) and erosion processes through time brings to the surface the metamorphic roots (belts) of these ancient mountain chains. This is currently the case with the Mozambican metamorphic belt where high-temperature gems such as ruby, spinel, tsavorite, and other garnets are found.

The main production of gem ruby is provided by this Pan-African metamorphic belt. All ruby deposits are of metamorphic origin in the broad sense. These mineral deposits are associated either with regional metamorphism *sensu stricto* or through fluid–rock interactions accompanied by metasomatism, contemporary with, or slightly later than, metamorphism. Their dismantling by current erosion creates important reserves and the exploration of continental placers in tropical landscapes where regoliths have been present for several thousand years should be studied with new approaches.

Author Contributions: All the authors contributed with their field and laboratory work and experience, and the works of worldwide researchers for over one century with the first detailed description, at the beginning of the 20th century, of the Malagasy deposits by A. Lacroix (MNHN Paris), to the realization of this description of the state-of-the-art of the geology and genesis of ruby deposits worldwide. G.G., L.A.G. and V.P. collected the studied samples in the field as well as realized photographs on specific geological and gemmological cases. G.G. conducted geological mapping in several areas worldwide and G.G., L.A.G., I.P. and V.P. obtained and evaluated part of the mineralogical and geochemical data. I.P. conducted crystallography on corundum crystals as well as the study on trapiche rubies from different deposits. A.E.F. and G.G. obtained and evaluated the oxygen isotope data. V.P. obtained and evaluated part of the gemmological data. Investigations in the different specific domains were realized by the authors in their own laboratory. G.G. realized some software for corundum chemical analysis as well as the original draft preparation and the supervision of the paper project with approval of the co-authors. The writing was realized by all the authors in their area of competence with the supervision by G.G. and language corrections by A.E.F. Review and editing was done by G.G. All authors have read and agreed to the published version of the manuscript.

Funding: The present paper was realized without any direct funding. The work is based on the knowledge and funding obtained in the course of more than 30 years work on the geology of gems.

Acknowledgments: The authors want to thank the Editor of *Minerals* and Guest Editors, Frederick Lin Sutherland and Khin Zaw, for invitation to contribute in a special issue on “Mineralogy and Geochemistry of Ruby”, and for their valuable suggestions. We are also thankful to four anonymous reviewers for improving the text by pertinent and constructive comments on the article. The authors want also to thank D. Schwarz, E. Le Goff, C. Simonet for their discussion and collaborations on the scientific topic. G.G. wants to thank the Institut de Recherche pour le Développement (IRD, France) and the French CNRS and the Universities of Lorraine and Paul Sabatier (CRPG/CNRS-Université de Lorraine and GET/IRD-Université Paul Sabatier) for academic and financial support for research on the geology of gems over the past 30 years.

Conflicts of Interest: The authors declare no conflict of interest.

References

1. Eichholz, D.E. *Theophrastus, De Lapidibus*; Oxford Clarendon Press: Oxford, UK, 1965.
2. Littré, E. Tome Second. In *Histoire Naturelle de Pline*; Chez Firmin-Didot et Cie: Paris, France, 1877.
3. Ernault, L. *Marbode, Évêque de Rennes, Sa Vie et Ses Oeuvres*; Hte Cailleres: Rennes, France, 1890; pp. 1035–1123.
4. *Albertus Magnus Liber Mineralium*; Jacob Köbel: Oppenheim, Germany, 1518.
5. Hughes, R.W. *Ruby and Sapphire*; RWH Publishing: Boulder, CO, USA, 1997.
6. Pardieu, V. Thailand, the undisputed ruby kingdom: A brief history. *InColor* **2019**, *42*, 14–22.
7. Themelis, T. *The Heat Treatment of Ruby and Sapphire*; Gemlab Inc.: New York, NY, USA, 1992.
8. Shigley, J.E.; Dirlam, D.M.; Laurs, B.M.; Boehm, E.W.; Bosshart, G.; Larson, W.F. Gem localities of the 1990s. *Gems Gemol.* **2000**, *36*, 292–335. [[CrossRef](#)]
9. Dussart, S. The version of field gemologist Vincent Pardieu. *IGR It alian Gemol. Rev.* **2019**, *7*, 58–64.
10. Raden, A. *Stoned: Jewelry, Obsession, and How Desire Shapes the World*; Ecco: Manhattan, NY, USA, 2015.
11. Palke, A.C.; Saeseaw, S.; Renfro, N.D.; Sun, Z.; McClure, S.F. Geographic origin determination of ruby. *Gems Gemol.* **2019**, *55*, 580–612. [[CrossRef](#)]
12. Gübelin Gem Laboratory: The roots of origin determination. *Jewel. News Asia* **2006**, 52–62.
13. Gübelin Gem Laboratory: The limits of origin determination. *Jewel. News Asia* **2006**, 66–71.
14. Gübelin Gem Laboratory: A holistic method to determining gem origin. *Jewel. News Asia* **2006**, 118–126.
15. McClure, S.F.; Moses, T.M.; Shigley, J.E. The geographic origin dilemma. *Gems Gemol.* **2019**, *55*, 457–462.

16. Gübelin, E.J.; Koivula, J.I. *Photoatlas of Inclusions in Gemstones*; ABC Edition: Zurich, Switzerland, 1986.
17. Gübelin, E.J.; Koivula, J.I. *Photoatlas of Inclusions in Gemstones*; Opinio Publishers: Basel, Switzerland, 1985; Volume 3.
18. Sotheby's Magnificent Jewels and Noble Jewels, Auction 502. 2005. Available online: <http://www.sothebys.com> (accessed on 20 June 2020).
19. Pardieu, V. Ruby and Sapphire Rush near Didy, Madagascar. April–June 2012. Available online: <https://www.gia.edu/doc/Ruby-and-Sapphire-Rush-Near-Didy-Madagascar.pdf> (accessed on 20 June 2020).
20. Peretti, A.; Hahn, L. Record-breaking discovery of ruby and sapphire at the Didy mine in Madagascar: Investigating the source. *InColor* **2013**, *21*, 22–35.
21. Pardieu, V.; Jacquat, S.; Senoble, J.B.; Bryl, L.P.; Hughes, R.W.; Smith, M. Expedition Report to the Ruby Mining Sites in Northern Mozambique (Niassa and Cabo Delgado Provinces), Bangkok, GIA Laboratory. 2009. Available online: <https://www.gia.edu/doc/Expedition-report-Ruby-mining-sites-Northern-Mozambique> (accessed on 20 June 2020).
22. Pardieu, V.; Jacquat, S.; Bryl, L.P.; Senoble, J.B. Rubies from northern Mozambique. *InColor* **2009**, *12*, 32–36.
23. Pardieu, V.; Thanachakaphad, J.; Jacquat, S.; Senoble, J.B.; Bryl, L.P. Rubies from the Niassa and Cabo Delgado Regions of Northern Mozambique. A Preliminary Examination with an Updated Field Report Annex. Bangkok, GIA Laboratory. Available online: https://www.gia.edu/doc/Niassa_Mozambique_Ruby_September13_2009.pdf (accessed on 20 June 2020).
24. Pardieu, V. Gemfields' November 2017 ruby auction yields record results. *InColor* **2018**, *37*, 62–63.
25. Simonet, C. The Montepuez ruby deposits, what's next? *InColor* **2018**, *37*, 32–40.
26. Vertriest, W.; Saeseaw, S. A decade of ruby from Mozambique: A review. *Gems Gemol.* **2019**, *55*, 162–183. [[CrossRef](#)]
27. *A Competent Persons Report on the Montepuez Ruby Project, Mozambique*; SRK Consulting (UK) Limited: Cardiff, UK, 2015; 195p.
28. Yager, Y.G.; Menzie, W.D.; Olson, D.W. *Weight of Production of Emeralds, Rubies, Sapphires, and Tanzanite from 1995 through 2005. Open File Report 2008–1013*; USGS: Reston, VA, USA, 2008.
29. Themelis, T. *Gems and Mines of Mogok*; Ted Themelis: Bangkok, Thailand, 2008; ISBN 0940965-30-5.
30. Peretti, A.; Schmetzer, K.; Bernhardt, H.J.; Mouawad, F. Rubies from Mong Hsu. *Gems Gemol.* **1995**, *31*, 2–26. [[CrossRef](#)]
31. Streeter, E.W. *Precious Stones and Gems, Their History Sources and Characteristics*; George Bell & Son: London, UK, 1892.
32. Rohtert, W.; Ritchie, M. Three parageneses of ruby and pink sapphire discovered at Fiskenæsset, Greenland. *Gems Gemol.* **2006**, *42*, 149–150.
33. Fagan, A.J. True North Gems Greenland mining—The final lap. *InColor* **2015**, *29*, 36–49.
34. Fagan, A.J. The Ruby and Pink Sapphire Deposits of SW Greenland: Geological Setting, Genesis, and Exploration Techniques. Ph.D. Thesis, University of British Columbia, Vancouver, BC, Canada, 2018.
35. Smith, C.P.; Fagan, A.J.; Bryan, C. Ruby and pink sapphire from Aappaluttoq, Greenland. *J. Gemmol.* **2016**, *35*, 294–306. [[CrossRef](#)]
36. Lucas, A.; Palke, A.; Vertriest, W. Mining rubies in Greenland. The Aappaluttoq ruby mine. *InColor* **2018**, *37*, 42–52.
37. Vertriest, W.; Palke, A.C.; Renfro, N.D. Field gemology: Building a research collection and understanding the development of gem deposits. *Gems Gemol.* **2019**, *55*, 490–511. [[CrossRef](#)]
38. Cesbron, F.; Lebrun, P.; Le Cléac'h, J.M.; Notari, F.; Grobon, C.; Deville, J. Corindons et spinelles. In *Minéraux et Fossiles 15*; Editions CEDIM: Paris, France, 2002.
39. Bowles, J.F.W.; Howie, R.A.; Vaughan, D.J.; Zussman, J. *Rock-Forming Minerals. Non-Silicates: Oxides, Hydroxides and Sulfides*; The Geological Society: London, UK, 2011; Volume 5A.
40. Giuliani, G.; Ohnenstetter, D.; Fallick, A.E.; Groat, L.; Fagan, J. The geology and genesis of gem corundum deposits. In *Geology of Gem Deposits*; Groat, L.A., Ed.; Mineralogical Association of Canada: Tucson, AZ, USA, 2014; Short Course Series; Volume 44, pp. 29–112.
41. Bindeman, I.N.; Serebryakov, N.S. Geology, petrology and O and H isotope geochemistry of remarkably ¹⁸O depleted Paleoproterozoic rocks of the Belmorian belt, Karelia, Russia, attributed to global glaciation 2.4 Ga. *Earth Planet. Sci. Lett.* **2011**, *306*, 163–174. [[CrossRef](#)]

42. Grapes, R.; Palmer, K. (Ruby-sapphire)-chromian mica-tourmaline rocks from Westland, New Zealand. *J. Petrol.* **1996**, *37*, 293–315. [[CrossRef](#)]
43. Hutchinson, M.T.; Nixon, P.H.; Harley, S.L. Corundum inclusions in diamonds—discriminatory criteria and a corundum composition dataset. *Lithos* **2004**, *77*, 273–286. [[CrossRef](#)]
44. Perretti, A. The Making of an International Color Standard by GRS: “Pigeon’s Blood” and “Royal Blue”. Definitions, Retrospective and Future. 2015. Available online: <http://www.pigeonsblood.com> (accessed on 23 November 2019).
45. Smith, C.P.; Surdez, N. The Mong Hsu ruby: A new type of Burmese ruby. *Jewelsiam* **1994**, *5*, 82–98.
46. Sunagawa, I. *Crystals: Growth, Morphology and Perfection*; Cambridge University Press: Cambridge, UK, 2005.
47. Sunagawa, I.; Bernhardt, H.-J.; Schmetzer, K. Texture formation and element partitioning in trapiche ruby. *J. Cryst. Growth* **1999**, *206*, 322–330. [[CrossRef](#)]
48. Hänni, H.A.; Schmetzer, K. New rubies from the Morogoro Area, Tanzania. *Gems Gemol.* **1991**, *27*, 156–167. [[CrossRef](#)]
49. Sorokina, E.S.; Hofmeister, W.; Häger, T.; Mertz-Kraus, R.; Buhre, S.; Saul, J. Morphological and chemical evolution of corundum (ruby and sapphire): Crystal ontogeny reconstructed by EMPA, LA-ICPMS, and Cr³⁺ Raman mapping. *Am. Mineral.* **2016**, *101*, 2716–2722. [[CrossRef](#)]
50. McKague, H.L. Trapiche emeralds from Colombia. *Gems Gemol.* **1964**, *11*, 210–213.
51. Schmetzer, K.; Hänni, H.A.; Bernhard, H.J.; Schwarz, D. Trapiche rubies. *Gems Gemol.* **1996**, *32*, 242–250. [[CrossRef](#)]
52. Schmetzer, K.; Beili, Z.; Yan, G.; Bernhard, H.J.; Hänni, H.A. Element mapping of trapiche rubies. *J. Gemmol.* **1999**, *26*, 289–301. [[CrossRef](#)]
53. Win, K.K. Trapiche of Myanmar. *Austr. Gemmol.* **2005**, *22*, 269–270.
54. Schmetzer, K.; Bernhardt, H.J.; Hainschwang, T. Chemical and growth zoning in trapiche tourmaline from Zambia—A re-evaluation. *J. Gemmol.* **2011**, *32*, 151–173. [[CrossRef](#)]
55. Koivula, J.I.; Kammerling, R.C.; Fritsch, E. Gem News: “Trapiche” purple-pink sapphire. *Gems Gemol.* **1994**, *30*, 197.
56. Kiefert, L. Unusual trapiche sapphire. *Gems Gemol.* **2012**, *48*, 229.
57. Pignatelli, I.; Giuliani, G.; Morlot, C.; Pham, V.L. The texture and chemical composition of trapiche ruby from Khoan Thong, Luc Yen mining district, northern Vietnam. *J. Gemmol.* **2019**, *36*, 726–745. [[CrossRef](#)]
58. Garnier, V.; Ohnenstetter, D.; Giuliani, G.; Schwarz, D. Rubis trapiches de Mong Hsu, Myanmar. *Rev. Ass. Fr. Gemmol. AFG* **2002**, *144*, 5–12.
59. Garnier, V.; Ohnenstetter, D.; Giuliani, G.; Blanc, P.; Schwarz, D. Trace-element contents and cathodoluminescence of “Trapiche” rubies from Mong Hsu (Myanmar): Geological significance. *Miner. Petrol.* **2002**, *76*, 179–193. [[CrossRef](#)]
60. Peretti, A.; Mullis, J.; Mouawad, F. The role of fluoride in the formation of color zoning in rubies from Mong Hsu (Myanmar, Burma). *J. Gemmol.* **1996**, *25*, 3–19. [[CrossRef](#)]
61. Pignatelli, I.; Giuliani, G.; Ohnenstetter, D.; Agrosi, G.; Mathieu, S.; Morlot, C.; Branquet, Y. Colombian trapiche emeralds: Recent advances in understanding their formation. *Gems Gemol.* **2015**, *51*, 222–259. [[CrossRef](#)]
62. Giuliani, G.; Dubessy, J.; Pignatelli, I.; Schwarz, D. Fluid inclusions study of trapiche and non-trapiche rubies from Mong Hsu deposit, Myanmar. *Can. Mineral.* **2018**, *56*, 1–13. [[CrossRef](#)]
63. Giuliani, G.; Dubessy, J.; Banks, D.; Lhomme, T.; Ohnenstetter, D. Fluid inclusions in ruby from Asian marble deposits: Genetic implications. *Eur. J. Mineral.* **2015**, *27*, 393–404. [[CrossRef](#)]
64. Giuliani, G.; Dubessy, J.; Ohnenstetter, D.; Banks, D.; Branquet, Y.; Feneyrol, J.; Fallick, A.E.; Martelat, J.-E. The role of evaporites in the formation of gems during metamorphism of carbonate platforms: A review. *Mineral. Depos.* **2018**, *53*, 1–20. [[CrossRef](#)]
65. Garnier, V.; Giuliani, G.; Ohnenstetter, D.; Fallick, A.E.; Dubessy, J.; Banks, D.; Hoàng, Q.V.; Lhomme, T.; Maluski, H.; Pêcher, A.; et al. Marble-hosted ruby deposits from central and southeast Asia: Towards a new genetic model. *Ore Geol. Rev.* **2008**, *34*, 169–191. [[CrossRef](#)]
66. Garnier, V. Les Gisements de Rubis Associés aux Marbres de l’Asie Centrale et du Sud-est: Genèse et Caractérisation Isotopique. Ph.D. Thesis, University of Nancy, Nancy, France, 2003.
67. Muhlmeister, S.; Fritsch, E.; Shigley, J.E.; Devouard, B.; Laurs, B.M. Separating natural and synthetic rubies on the basis of trace-element chemistry. *Gems Gemol.* **1998**, *34*, 80–101. [[CrossRef](#)]

68. Sutherland, F.L.; Schwarz, D.; Jobbins, E.A.; Coenraads, R.R.; Webb, G. Distinctive gem corundum suites from discrete basalt fields: A comparative study of Barrington, Australia, and West Pailin, Cambodia, gemfields. *J. Gemmol.* **1998**, *26*, 65–85. [[CrossRef](#)]
69. Sutherland, F.L.; Coenraads, R.R.; Abduriyim, A.; Meffre, S.; Hoskin, P.W.O.; Giuliani, G.; Beattie, R.; Wuhler, R.; Sutherland, G.B. Corundum (sapphire) and zircon relationships, Lava Plains gem fields, NE Australia: Integrated mineralogy, geochemistry, age determination, genesis and geographic typing. *Mineral. Mag.* **2015**, *79*, 545–581. [[CrossRef](#)]
70. Peucat, J.J.; Ruffault, P.; Fritsch, E.; Bouhnik-Le Coz, M.; Simonet, C.; Lasnier, B. Ga/Mg ratios as a new geochemical tool to differentiate magmatic from metamorphic blue sapphires. *Lithos* **2007**, *98*, 261–274. [[CrossRef](#)]
71. Sutherland, F.L.; Abduriyim, A. Geographic typing of gem corundum: A text case from Australia. *J. Gemmol.* **2009**, *31*, 203–210. [[CrossRef](#)]
72. Giuliani, G.; Caumon, G.; Rakotosamizanany, S.; Ohnenstetter, D.; Rakotondrazafy, A.F.M. Classification chimique des corindons par analyse factorielle discriminante: Application à la typologie des gisements de rubis et saphirs. *Rev. Ass. Fr. Gemmol. AFG* **2014**, *188*, 14–22.
73. Sutherland, F.L.; Schwarz, D. Origin of gem corundums from basaltic fields. *Austr. Gemmol.* **2001**, *21*, 30–33.
74. Sutherland, F.L.; Hoskin, P.W.O.; Fanning, C.M.; Coenraads, R.R. Models of corundum origin from alkali basaltic terrains: A reappraisal. *Contrib. Mineral. Petrol.* **1998**, *133*, 356–372. [[CrossRef](#)]
75. Sutherland, F.L.; Coenraads, R.R.; Schwarz, D.; Raynor, L.R.; Barron, B.J.; Webb, G.B. Al-rich diopside in alluvial ruby and corundum-bearing xenoliths, Australian and SE Asian basalt field. *Mineral. Mag.* **2003**, *67*, 717–732. [[CrossRef](#)]
76. Abduriyim, A.; Kitawaki, H. Applications of laser ablation-inductively coupled plasma-mass spectrometry (LA-ICP-MS) to gemology. *Gems Gemol.* **2006**, *42*, 98–118. [[CrossRef](#)]
77. Rakotosamizanany, S.; Giuliani, G.; Ohnenstetter, D.; Rakotondrazafy, A.F.M.; Fallick, A.E.; Paquette, J.-L.; Tiepolo, M. Chemical and oxygen isotopic compositions, age and origin of gem corundums in Madagascar alkali basalts. *J. S. Afr. Earth Sci.* **2014**, *94*, 156–170. [[CrossRef](#)]
78. Arlabosse, J.-M.; Delaunay, A.; Lenne, N. Les rubis de Vatomandry—Madagascar. *Rev. Ass. Fr. Gemmol. AFG* **2018**, *203*, 6–15.
79. Uher, P.; Giuliani, G.; Szakall, S.; Fallick, A.E.; Strunga, V.; Vaculovic, D.; Ozdin, G.; Greganova, M. Sapphires related to alkali basalts from the Cerová Highlands, Western Carpathians (southern Slovakia): Composition and origin. *Geol. Carpathica* **2012**, *63*, 71–82. [[CrossRef](#)]
80. Giuliani, G.; Ohnenstetter, D.; Garnier, V.; Fallick, A.E.; Rakotondrazafy, A.F.M.; Schwarz, D. The geology and genesis of gem corundum deposits. In *Geology of Gem Deposits*; Groat, L.A., Ed.; Mineralogical Association of Canada: Yellowknife, NT, Canada, 2007; Short Course Series; Volume 37, pp. 27–78.
81. Sutherland, F.L.; Graham, I.T.; Harris, S.J.; Coldham, T.; Powell, W.; Belousova, E.A.; Martin, L. Unusual ruby-sapphire transition in alluvial megacrysts, Cenozoic basaltic gem field, New England, New South Wales, Australia. *Lithos* **2017**, *278–281*, 347–360. [[CrossRef](#)]
82. Sutherland, F.L.; Giuliani, G.; Fallick, A.E.; Garland, M.; Webb, G.B. Sapphire-ruby characteristics, West Pailin, Cambodia: Clues to their origin based on trace element and O isotope analysis. *Austr. Gemmol.* **2009**, *23*, 373–432.
83. Keulen, N.; Thomsen, T.B.; Schumacher, J.C.; Poulsen, M.D.; Kalvig, P.; Vennemann, T.; Salimi, R. Formation, origin and geographic typing of corundum (ruby and pink sapphire) from the Fiskenaæsset complex, Greenland. *Lithos* **2020**, *366–367*. [[CrossRef](#)]
84. Giuliani, G.; Pivin, M.; Fallick, A.E.; Ohnenstetter, D.; Song, Y.; Demaiffe, D. Geochemical and oxygen isotope signatures of mantle corundum megacrysts from the Mbuji-Mayi kimberlite, Democratic Republic of Congo, and the Changle alkali basalt, China. *C.R. Geosciences* **2015**, *347*, 24–34. [[CrossRef](#)]
85. Sutherland, F.L.; Khin, Z.; Meffre, S.; Giuliani, G.; Fallick, A.E.; Webb, G.B. Gem-corundum megacrysts from east Australian basalt fields: Trace elements, oxygen isotopes and origins. *Austr. J. Earth Sci.* **2009**, *56*, 1003–1022. [[CrossRef](#)]
86. Sutherland, L.; Graham, I.; Harris, S.; Khin, Z.; Meffre, S.; Coldham, T.; Coenraads, R.; Sutherland, G. Rubis australasiens. *Rev. Ass. Fr. Gemmol. AFG* **2016**, *197*, 13–20.
87. Khin, Z.; Sutherland, F.L.; Yui, T.F.; Meffre, S.; Thu, K. Vanadium-rich ruby and sapphire within Mogok gemfield, Myanmar: Implications for gem color and genesis. *Mineral. Depos.* **2015**, *50*, 25–39. [[CrossRef](#)]

88. Sutherland, F.L.; Khin, Z.; Meffre, F.; Thompson, J.; Goemann, K.; Kyaw, T.; Than, T.N.; Mhod, Z.M.; Harris, S.I. Diversity in ruby chemistry and its inclusions: Intra and inter-continental comparisons from Myanmar and Eastern Australia. *Minerals* **2019**, *9*, 28. [[CrossRef](#)]
89. Pardieu, V. Concise field report Volume 1: Pailin, Cambodia, Dec 2008–Feb 2009, Bangkok, GIA Laboratory. 2009. Available online: <https://www.gia.edu/doc/Field-ReportPailin.pdf> (accessed on 25 June 2020).
90. Pardieu, V. Field gemology. The evolution of data collection. *InColor* **2020**, *46*, 100–106.
91. Groat, L.A.; Giuliani, G.; Stone-Sundberg, J.; Sun, Z.; Renfro, N.D.; Palke, A.C. A review of analytical methods used in geographic origin determination of gemstones. *Gems Gemol.* **2019**, *55*, 512–535. [[CrossRef](#)]
92. Stone-Sundberg, J.; Thomas, T.; Sun, Z.; Guan, Y.; Cole, Z.; Equall, R.; Emmett, J.L. Accurate reporting of key trace elements in ruby and sapphire using matrix-matched standards. *Gems Gemol.* **2017**, *53*, 438–451. [[CrossRef](#)]
93. Giuliani, G.; Fallick, A.E.; Garnier, V.; France-Lanord, C.; Ohnenstetter, D.; Schwarz, D. Oxygen isotope composition as a tracer for the origins of rubies and sapphires. *Geology* **2005**, *33*, 249–252. [[CrossRef](#)]
94. Rakotosamizany, S. Les Corindons Gemmes Dans Les Basaltes Alcalins et Leurs Enclaves à Madagascar: Significations Pétrologique et Métallogénique. Ph.D. Thesis, Université Henri Poincaré, Nancy, France, 2009.
95. Voudouris, P.; Mavrogatos, C.; Graham, I.; Giuliani, G.; Melfos, V.; Karamelas, S.; Karantoni, V.; Wang, K.; Tarantola, A.; Khin, Z.; et al. Gem Corundum deposits of Greece: Geology, mineralogy and genesis. *Minerals* **2019**, *9*, 49. [[CrossRef](#)]
96. Fanka, A.; Sutthirat, C. Petrochemistry, mineral chemistry, and pressure-temperature model of corundum-bearing amphibolite from Montepuez, Mozambique. *Arab. J. Sci. Eng.* **2018**, *43*, 3751–3767. [[CrossRef](#)]
97. Morishita, T.; Arai, S.; Gervilla, F. High pressure aluminous mafic rocks from the Ronda peridotite massif, southern Spain: Significance of sapphirine- and corundum-bearing assemblages. *Lithos* **2001**, *57*, 143–161. [[CrossRef](#)]
98. Pham, V.L.; Hoàng, Q.V.; Garnier, V.; Giuliani, G.; Ohnenstetter, D. Marble-hosted ruby from Vietnam. *Can. Gemmol.* **2004**, *25*, 83–95.
99. Ishimaru, S.; Arai, S.; Miura, M.; Shmelev, V.; Pushkarev, E. Ruby-bearing feldspathic dyke in peridotite from Ray-Iz ophiolite, the Polar Urals: Implications for mantle metasomatism and origin of ruby. *J. Mineral. Petrol. Sci.* **2015**, *110*, 76–81. [[CrossRef](#)]
100. Andriamamonjy, S.A. Les corindons associés aux roches métamorphiques du Sud ouest de Madagascar: Le gisement de saphir de Zazafotsy. Master Thesis, Université d'Antananarivo, Tananarive, Madagascar, 2006.
101. Kongsomart, B.; Vertriest, W.; Weeramankhont, V. Preliminary observations on facet-grade ruby from Longido, Tanzania. *Gems Gemol.* **2017**, *53*, 472–473.
102. Krebs, M.Y.; Pearson, D.G.; Fagan, A.J.; Bussweiler, Y.; Sarkar, C. The application of trace elements and Sr–Pb isotopes to dating and tracing ruby formation: The Aappaluttoq deposit, SW Greenland. *Chem. Geol.* **2019**, *523*, 42–58. [[CrossRef](#)]
103. Harlow, G.E.; Bender, W. A study of ruby (corundum) compositions from the Mogok Belt, Myanmar: Searching for chemical fingerprints. *Am. Mineral.* **2013**, *98*, 1120–1132. [[CrossRef](#)]
104. Sorokina, E.S.; Litvinenko, A.K.; Hofmeister, W.; Häger, T.; Jacob, D.E.; Nasriddinov, Z.Z. Rubies and sapphires from Snezhnoe, Tajikistan. *Gems Gemol.* **2015**, *51*, 160–175. [[CrossRef](#)]
105. Palke, A.C.; Wong, J.; Verdel, C.; Avila, J.N. A common origin for Thai/Cambodian rubies and blue and violet sapphires from Yogo Gulch, Montana, USA? *Am. Mineral.* **2018**, *103*, 469–479. [[CrossRef](#)]
106. Graham, I.; Sutherland, L.; Khin, Z.; Nechaev, V.; Khanchuk, A. Advances in our understanding of the gem corundum deposits of the West Pacific continental margins intraplate basaltic fields. *Ore Geol. Rev.* **2008**, *34*, 200–215. [[CrossRef](#)]
107. Stern, R.J.; Tsujimori, T.; Harlow, G.; Groat, L. Plate tectonic gemstones. *Geology* **2013**, *41*, 723–726. [[CrossRef](#)]
108. Garnier, V.; Giuliani, G.; Ohnenstetter, D.; Schwarz, D. Saphirs et rubis. Classification des gisements de corindon. *Le Règne Minéral* **2004**, *55*, 4–47.
109. Emmett, J.L.; Stone-Sundberg, J.; Guan, Y.; Sun, Z. The role of silicon in the color of gem corundum. *Gems Gemol.* **2017**, *53*, 42–47. [[CrossRef](#)]
110. Simonet, C.; Fritsch, E.; Lasnier, B. A classification of gem corundum deposits aimed towards gem exploration. *Ore Geol. Rev.* **2008**, *34*, 127–133. [[CrossRef](#)]

111. Kissin, A.J. Ruby and sapphire from the southern Ural Mountains, Russia. *Gems Gemol.* **1994**, *30*, 243–252. [[CrossRef](#)]
112. Okrusch, M.; Bunch, T.E.; Bank, H. Paragenesis and petrogenesis of a corundum-bearing marble at Hunza (Kashmir). *Mineral. Depos.* **1976**, *11*, 278–297. [[CrossRef](#)]
113. Dzikowski, T.J.; Cempirek, J.; Groat, L.A.; Dipple, G.M.; Giuliani, G. Origin of gem corundum in calcite marble: The Revelstoke occurrence in the Canadian Cordillera of British Columbia. *Lithos* **2014**, *198–199*, 281–297. [[CrossRef](#)]
114. Balmer, W.A.; Hauzenberger, C.A.; Fritz, H.; Sutthirat, C. Marble-hosted ruby deposits of the Morogoro region, Tanzania. *J. Afr. Earth. Sci.* **2017**, *134*, 626–643. [[CrossRef](#)]
115. Litvinenko, A.K. Nuristan-South Pamir province of Precambrian gems. *Geol. Ore Depos.* **2004**, *46*, 263–268.
116. Garde, A.; Marker, M. Corundum crystals with blue-red color zoning near Kangerdluarssuk, Sukkertoppen district, West Greenland. *Rep. Gronl. Geol. Unders.* **1988**, *140*, 46–49.
117. Key, R.M.; Ochieng, J.O. The growth of rubies in south-east Kenya. *J. Gemmol.* **1991**, *22*, 484–496. [[CrossRef](#)]
118. Simonet, C. Géologie des Gisements de Saphir et de Rubis. L'exemple de la John Saul Mine, Mangari, Kenya. Ph.D. Thesis, Université de Nantes, Nantes, France, 2000.
119. Mercier, A.; Debat, P.; Saul, J.M. Exotic origin of the ruby deposits of the Mangari area in SE Kenya. *Ore Geol. Rev.* **1999**, *14*, 83–104. [[CrossRef](#)]
120. Schwarz, D.; Pardieu, V.; Saul, J.M.; Schmetzer, K.; Laurs, B.M.; Giuliani, G.; Klemm, L.; Malsy, A.K.; Hauzenberger, C.; Du Toit, G.; et al. Ruby and sapphires from Winza (Central Tanzania). *Gems Gemol.* **2008**, *44*, 322–347. [[CrossRef](#)]
121. Tenthorey, E.A.; Ryan, J.G.; Snow, E.A. Petrogenesis of sapphirine-bearing metatroctolites from the Buck Creek ultramafic body, southern Appalachians. *J. Metam. Geol.* **1996**, *14*, 103–114.
122. Nicollet, C. Sapphirine et staurotide riche en magnésium et chrome dans les amphibolites et anorthosites à corindon du Vohibory Sud, Madagascar. *Bull. Minéral.* **1986**, *109*, 599–612. [[CrossRef](#)]
123. Kröner, A. Late Precambrian plate tectonics and orogeny: A need to redefine the term Pan-African. In *African Geology*; Klerkx, J., Michot, J., Eds.; Tervuren, Musée Royal de l'Afrique Centrale: Tervuren, Belgium, 1984; pp. 23–28.
124. Le Goff, E.; Deschamps, Y.; Guerrot, C. Tectonic implications of new single zircon Pb-Pb evaporation data in the Lossogonoi and Longido ruby-districts, Mozambican metamorphic Belt of north-eastern Tanzania. *Comptes Rendus Geosci.* **2010**, *342*, 36–45. [[CrossRef](#)]
125. Jöns, N.; Schenk, V. Relics of the Mozambique Ocean in the central East African Orogen: Evidence from the Vohibory Block of Southern Madagascar. *J. Metam. Geol.* **2008**, *26*, 17–28. [[CrossRef](#)]
126. Bingen, B.; Jacobs, J.; Viola, G.; Henderson, I.H.C.; Skår, Ø.; Boyd, R.; Thomas, R.J.; Solli, A.; Key, R.M.; Daudi, E.X.F. Geochronology of the Precambrian crust in the Mozambique belt in NE Mozambique, and implications for Gondwana assembly. *Precambrian Res.* **2009**, *170*, 231–255. [[CrossRef](#)]
127. Paquette, J.L.; Nédelec, A.; Moine, B.; Rakotondrazafy, A.F.M. U-Pb single zircon Pb-evaporation and Sm-Nd isotopic study of a granulite domain in SE Madagascar. *J. Geol.* **1994**, *102*, 523–538. [[CrossRef](#)]
128. Giuliani, G.; Fallick, A.E.; Rakotondrazafy, A.F.M.; Ohnenstetter, D.; Andriamamonjy, A.; Rakotosamizanany, S.; Ralantoarison, T.; Razanatsheho, M.M.; Dunaigre, C.; Schwarz, D. Oxygen isotope systematics of gem corundum deposits in Madagascar: Relevance for their geological origin. *Mineral. Depos.* **2007**, *42*, 251–270. [[CrossRef](#)]
129. Sorokina, E.S.; Rošel, D.; Häger, T.; Mertz-Kraus, R.; Saul, J.M. LA-ICP-MS U-Pb dating of rutile inclusions within corundum (ruby and sapphire): New constraints on the formation of corundum deposits along the Mozambique belt. *Mineral. Depos.* **2017**, *52*, 641–649. [[CrossRef](#)]
130. Meert, J.G.; Van Der Voo, R.; Ayub, S. Paleomagnetic investigation of the Neoproterozoic Gagwe lavas and Mbozi complex, Tanzania and the assembly of Gondwana. *Precambrian Res.* **1995**, *74*, 225–244. [[CrossRef](#)]
131. Garnier, V.; Giuliani, G.; Maluski, H.; Ohnenstetter, D.; Phan, T.T.; Hoàng, Q.V.; Pham, V.L.; Vu, V.T.; Schwarz, D. Ar-Ar ages in phlogopites from marble-hosted ruby deposits in northern Vietnam: Evidence for Cenozoic ruby formation. *Chem. Geol.* **2002**, *188*, 33–49. [[CrossRef](#)]
132. Garnier, V.; Ohnenstetter, D.; Giuliani, G.; Maluski, H.; Deloule, E.; Phan, T.T.; Pham, V.L.; Hoang, Q.V. Age and significance of ruby-bearing marbles from the Red River shear zone, northern Vietnam. *Can. Mineral.* **2004**, *43*, 1315–1329. [[CrossRef](#)]

133. Garnier, V.; Maluski, H.; Giuliani, G.; Ohnenstetter, D.; Schwarz, D. Ar-Ar and U-Pb ages of marble hosted ruby deposits from central and south East Asia. *Can. J. Earth Sci.* **2006**, *43*, 1–23. [[CrossRef](#)]
134. Litvinenko, A.K.; Sorokina, E.S.; Häger, T.; Kostitsyn, Z.A.; Botcharnikov, R.E.; Somsikova, T.; Romashova, T.V.; Hofmeister, W. Petrogenesis of the Snezhnoe ruby deposit, Central Pamir. *Minerals* **2020**, *10*, 478. [[CrossRef](#)]
135. Khin, Z.; Sutherland, F.L.; Graham, I.; McGee, B. Dating zircon inclusions in gem corundums from placer deposits, as a guide to their origin. In Proceedings of the 33rd International Geological Congress (IGC), Oslo, Norway, 6–14 August 2008.
136. Sutherland, F.L.; Fanning, C.M. Gem-bearing basaltic volcanism, Barrington, New South Wales: Cenozoic evolution, based on basalt K-Ar ages and zircon fission track and U/Pb isotope dating. *Austral. J. Earth Sci.* **2001**, *48*, 221–237. [[CrossRef](#)]
137. Graham, I.T.; Sutherland, F.L.; Webb, G.B.; Fanning, C.M. Polygenetic corundums from New South Wales gemfields. In *Metallogeny of the Pacific Northwest: Tectonics, Magmatism and Metallogeny of Active Continental Margins*; Khanchuk, A.I., Gonevchuk, A.N., Mitrokhin, I.F., Simanenko, N.J., Cook, Seltmann, R., Eds.; Falnuka: Vladivostok, Russia, 2004; pp. 336–339.
138. Dill, H.G. Gems and placers—A genetic relationship par excellence. *Minerals* **2018**, *8*, 470–513.
139. Rhamdohr, R.; Milisenda, C.C. Neue Vorkommen von Saphir-Seifenlagerstätten auf Nosy-Bé, Madagaskar. *Z. Dt. Gemmol. Ges.* **2004**, *53*, 143–158.
140. Giuliani, G.; Groat, L. Geology of corundum and emerald gem deposits: A review. *Gems Gemol.* **2019**, *55*, 464–489. [[CrossRef](#)]
141. Ozerov, K. Form of corundum crystals as dependent upon chemical composition of medium. *Dolk. Akad. Nauk SSSR* **1945**, *XLVII*, 49–52.
142. Schwarz, D. Aus Basalten, Marmoren und Pegmatiten. Spezielle Ursachen formten in der Erdkruste edle Rubine und Saphire. In *Rubin, Saphir, Korund: Schön, Hart, Selten, Kostbar*; Weise, C., Ed.; ExtraLapis: München, Germany, 1998; Volume 15, pp. 5–9.
143. Kievenko, E.Y. *Geology of Gems*; Ocean Pictures Ltd.: Littleton, CO, USA, 2003.
144. Giuliani, G.; Ohnenstetter, D.; Fallick, A.E.; Groat, L.; Feneyrol, J. Geographic origin of gems linked to their geographical history. *InColor* **2012**, *19*, 16–27.
145. Sutthirat, C.; Saminpanya, S.; Droop, G.T.R.; Henderson, C.M.B.; Manning, D.A.C. Clinopyroxene-corundum assemblages from alkali-basalt and alluvium, eastern Thailand: Constraints on the origin of Thai rubies. *Mineral. Mag.* **2001**, *65*, 277–295. [[CrossRef](#)]
146. Saminpanya, S.; Sutherland, F.L. Different origins of Thai area sapphire and ruby, derived from mineral inclusions and co-existing minerals. *Eur. J. Mineral.* **2001**, *23*, 683–694. [[CrossRef](#)]
147. Baldwin, L.C.; Tomaschek, F.; Ballhaus, C.; Gerdes, A.; Fonseca, R.O.C.; Wirth, R.; Geisler, T.; Nagel, T. Petrogenesis of alkaline basalt-hosted sapphire megacrysts. Petrological and geochemical investigations of in situ sapphire occurrences from the Siebengebirge volcanic field, Germany. *Contrib. Mineral. Petrol.* **2017**, *172*. [[CrossRef](#)]
148. Promwongan, S.; Sutthirat, C. Mineral inclusions in ruby and sapphire from the Bo Welu gem deposit in Chanthaburi, Thailand. *Gems Gemol.* **2019**, *55*, 354–369.
149. Promwongan, S.; Sutthirat, C. An update on mineral inclusions and their composition in ruby from the Bo Rai gem field in Trat Province, eastern Thailand. *J. Gemmol.* **2019**, *36*, 634–645. [[CrossRef](#)]
150. Palke, A.C.; Hapeman, J.R. Rubies from Rock Creek, Montana. *Gems Gemol.* **2019**, *55*, 286–288.
151. Yui, T.F.; Khin, Z.; Limkatrun, P. Oxygen isotope composition of the Denchai sapphire, Thailand; a clue to its enigmatic origin. *Lithos* **2003**, *67*, 153–161. [[CrossRef](#)]
152. Yui, T.F.; Wu, C.-M.; Limkatrun, P.; Sricharn, W.; Boonsoong, A. Oxygen isotope studies on placer sapphire and ruby in the Chanthaburi-Trat alkali basaltic gemfield, Thailand. *Lithos* **2006**, *86*, 197–211. [[CrossRef](#)]
153. Vysotskiy, S.V.; Nechaev, V.P.; Kissin, A.Y.; Yakovenko, V.V.; Ignat'ev, A.V.; Velivetskaya, T.A.; Sutherland, F.L.; Agoshkov, A.I. Oxygen isotopic composition as an indicator of ruby and sapphire origin: A review of Russian occurrences. *Ore Geol. Rev.* **2015**, *68*, 164–170. [[CrossRef](#)]
154. Sutthirat, C.; Hauzenberger, C.; Chualaowanich, T.; Assawincharoenkij, T. Mantle and deep crustal xenoliths in basalts from the Bo Rai ruby deposit, eastern Thailand: Original source of basaltic ruby. *J. Asian Earth Sci.* **2018**, *164*, 366–379. [[CrossRef](#)]

155. Khin, Z.; Sutherland, F.L.; Dellapasqua, F.; Ryan, C.G.; Yui, T.Z.; Mernagh, T.P.; Duncan, D. Contrasts in gem corundum characteristics, eastern Australian basaltic fields: Trace elements, fluid/melt inclusions and oxygen isotopes. *Mineral. Mag.* **2006**, *70*, 669–687.
156. Vertriest, W.; Palke, A. Identification of opaque sulphide inclusions in rubies from Mogok, Myanmar and Montepuez, Mozambique. *Minerals* **2020**, *10*, 492. [[CrossRef](#)]
157. Limkatrun, P.; Khin, Z.; Ryan, C.G.; Mernagh, T.P. Formation of the Denchai gem sapphires, northern Thailand: Evidence from mineral chemistry and fluid/melt inclusion characteristics. *Mineral. Mag.* **2001**, *65*, 725–735.
158. Palke, A.C.; Renfro, N.D.; Berg, R.B. Melt inclusions in alluvial sapphires from Montana, USA: Formation of sapphires as restitic component of lower crustal melting? *Lithos* **2017**, *278–281*, 43–53. [[CrossRef](#)]
159. Herzberg, C.T. Pyroxene geothermometry and geobarometry: Experimental and thermodynamic evaluation of some subsolidus phase relations involving pyroxenes in the system CaO-MgO-Al₂O₃-SiO₂. *Geochim. Cosmochim. Acta* **1978**, *42*, 945–957. [[CrossRef](#)]
160. Irvin, A.J. Geochemical and high pressure experimental studies of garnet pyroxenite and pyroxene granulite xenoliths from the Delegate basaltic pipes, Australia. *J. Petrol.* **1974**, *15*, 1–40. [[CrossRef](#)]
161. Rakotosamizanany, S.; Giuliani, G.; Ohnenstetter, D.; Rakotondrazafy, A.F.M.; Fallick, A.E. Les gisements de saphirs et de rubis associés aux basaltes alcalins de Madagascar: Caractéristiques géologiques et minéralogiques. 1ère partie: Caractéristiques géologiques des gisements. *Rev. Assoc. Fr. Gemmol. AFG* **2009**, *169*, 13–21.
162. Rakotosamizanany, S.; Giuliani, G.; Ohnenstetter, D.; Rakotondrazafy, A.F.M.; Fallick, A.E. Les gisements de saphirs et de rubis associés aux basaltes alcalins de Madagascar: Caractéristiques géologiques et minéralogiques. 2ème partie: Caractéristiques minéralogiques. *Rev. Assoc. Fr. Gemmol. AFG* **2009**, *170*, 9–18.
163. Rakotosamizanany, S. Les corindons gemmes associés au magmatisme basaltique de Madagascar. In *Rapport Final du Projet de Gouvernance des Ressources Minérales (PGRM) de Madagascar*; PGRM: Antananarivo, Madagascar, 2008.
164. Rakotondrazafy, A.F.M.; Giuliani, G.; Fallick, A.E.; Ohnenstetter, D.; Andriamamonjy, A.; Rakotosamizanany, S.; Ralantoarison, T.; Razanatsheho, M.; Offant, Y.; Garnier, V.; et al. Gem corundum deposits in Madagascar: A review. *Ore Geol. Rev.* **2008**, *34*, 134–154. [[CrossRef](#)]
165. Promprated, P.; Taylor, L.A.; Neal, C. R Petrochemistry of mafic granulite xenoliths from the Chantaburi basaltic field: Implications for the nature of the lower crust beneath Thailand. *Int. Geol. Rev.* **2003**, *45*, 383–406. [[CrossRef](#)]
166. Kornprobst, J.; Piboule, M.; Roden, M.; Tabit, A. Corundum-bearing garnet clinopyroxenites at Beni Bousera (Morocco): Original plagioclase-rich gabbros recrystallized at depth within the mantle? *J. Petrol.* **1990**, *31*, 717–745. [[CrossRef](#)]
167. Chetouani, K.; Bodinier, J.-L.; Garrido, C.J.; Marchesi, C.; Amri, I.; Targuisti, K. Spatial variability of pyroxenite layers in the Beni Bousera orogenic peridotite (Morocco) and implications for their origin. *Comptes Rendus Geoscience* **2016**, *348*, 619–629. [[CrossRef](#)]
168. Matthey, D.; Lowry, D.; Macpherson, C.G. Oxygen isotope composition of mantle peridotite. *Earth Planet. Sci. Lett.* **1994**, *128*, 231–241. [[CrossRef](#)]
169. Watt, G.; Harris, J.W.; Harte, B.; Boyd, S.R. A high-chromium corundum (ruby) inclusion in diamond from the São Luiz alluvial mine, Brazil. *Mineral. Mag.* **1994**, *58*, 490–493. [[CrossRef](#)]
170. Hutchinson, M.T.; Hursthouse, M.B.; Light, M.E. Mineral inclusions in diamonds: Associations and chemical distinctions around the 670 km discontinuity. *Contrib. Mineral. Petrol.* **2001**, *142*, 119–126. [[CrossRef](#)]
171. Hutchinson, M.T. Constitution of the Deep Transition Zone and Lower Mantle shown by Diamonds and their Inclusions. Ph.D. Thesis, University of Edinburgh, Edinburgh, UK.
172. Pivin, M.; Femenias, O.; Demaiffe, D. Metasomatic mantle origin for Mbuji-Mayi and Kundelungu garnet and clinopyroxene megacrysts (Democratic Republic of Congo). *Lithos* **2009**, *112S*, 951–960. [[CrossRef](#)]
173. Pivin, M. La Suite Complexe des Mégacristaux des Kimberlites de Mbuji-Mayi en République Démocratique du Congo: Témoins du Métasomatisme dans le Manteau Lithosphérique Sous-Continental Archéen du Craton du Congo-Kasaï. Ph.D. Thesis, Université Libre de Bruxelles, Bruxelles, Belgique, 2012.
174. Ratrimo, V. Les indices à corindons gemmes du socle précambrien de Madagascar. In *Rapport Final du Projet de Gouvernance des Ressources Minérales (PGRM) de Madagascar*; PGRM: Antananarivo, Madagascar, 2008.

175. Zhang, R.Y.; Liou, J.G.; Zheng, J.P. Ultrahigh pressure corundum rich-garnetite in garnet peridotite, Sulu terrane, China. *Contrib. Mineral. Petrol.* **2004**, *147*, 21–31. [[CrossRef](#)]
176. Padovani, E.R.; Tracey, R. A pyrope-spinel (alkremite) xenolith from Moses Rock Dyke: First known North American occurrence. *Am. Mineral.* **1981**, *66*, 741–745.
177. Shirey, S.B.; Cartigny, P.; Frost, D.J.; Keshav, S.; Nestola, F.; Nimis, P.; Pearson, D.G.; Sobolev, N.V.; Walter, M.J. Diamonds and the geology of mantle carbon. *Rev. Mineral. Geochem.* **2013**, *75*, 355–421. [[CrossRef](#)]
178. Eggler, D.H.; McCallum, M.E.; Smith, C.B. Megacryst assemblage in kimberlite from Northern Colorado and Southern Wyoming: Petrology, geothermometry-barometry and areal distribution. In *The Mantle Sample: Inclusion in Kimberlites and other Volcanics*; Boyd, F.R., Meyer, H.O.A., Eds.; Books Series Special Publication; American Geophysical Union: Washington, DC, USA, 1979; pp. 213–226. ISBN 9780875902135. Online ISBN 9781118664858. [[CrossRef](#)]
179. Stachel, T.; Harris, J.W. The origin of cratonic diamonds—Constraints from mineral inclusions. *Ore Geol. Rev.* **2008**, *34*, 5–32. [[CrossRef](#)]
180. Giuliani, G.; Fallick, A.E.; Ohnenstetter, D.; Pégère, G. Oxygen isotopes of sapphire from the French Massif Central: Implications for the origin of gem corundum in basaltic fields. *Mineral. Depos.* **2009**, *44*, 221–231. [[CrossRef](#)]
181. Dirlam, D.M.; Misorowski, E.B.; Tozer, R.; Stark, K.B.; Bassett, A.M. Gem wealth of Tanzania. *Gems Gemol.* **1992**, *28*, 80–102. [[CrossRef](#)]
182. Le Goff, E.; Deschamps, Y.; Cocherie, A.; Guerrot, C.; Ketto, D. Structural, petrological and geochronological constraints of the Tanzanian ruby belt. In Proceedings of the 22ème RST Meeting Nancy. University of Nancy, Nancy, France, 21–24 April 2008.
183. Saul, J. Chronique de la découverte de trois mines historiques de gemmes en Afrique de l’Est. *Le Règne Minéral* **2013**, *2*, 89–92.
184. Haapala, I.; Siivola, J.; Ojanperä, P.; Yletyunen, V. Red corundum, sapphirine and kornerupine from Kittilä, Finnish Lapland. *Bull. Geol. Soc. Finland* **1971**, *43*, 221–231. [[CrossRef](#)]
185. Janardhanan, A.; Leake, B.E. Sapphirine in the Sittampundi complex, India. *Mineral. Mag.* **1974**, *39*, 901–902. [[CrossRef](#)]
186. Forestier, F.; Lasnier, B. Découverte de niveaux d’amphibolites à pargasite, anorthite, corindon et sapphirine dans les schistes cristallins du Haut-Allier. *Contrib. Mineral. Petrol.* **1969**, *23*, 194–235. [[CrossRef](#)]
187. Wang, K.; Graham, I.; Martin, L.; Voudouris, P.; Giuliani, G.; Lay, A.; Harris, J.H.; Fallick, A.E. Fingerprinting Paranesti rubies through oxygen isotopes. *Minerals* **2019**, *9*, 91. [[CrossRef](#)]
188. Barot, N.; Harding, R.R. Pink corundum from Kitui, Kenya. *J. Gemmol.* **1994**, *24*, 165–172. [[CrossRef](#)]
189. Andreoli, M.A.G. Petrochemistry, tectonic evolution and metasomatic mineralizations of Mozambique belt granulites from Malawi and Tete (Mozambique). *Precambrian Res.* **1994**, *25*, 161–186.
190. Henn, U.; Bank, H.; Bank, F.H. Red and orange corundum (ruby and padparadscha) from Malawi. *J. Gemmol.* **1990**, *22*, 83–89. [[CrossRef](#)]
191. McColl, D.; Warren, R.G. The first discovery of ruby in Australia. *Aust. Mineral.* **1979**, *26*, 121–125.
192. Mortimer, G.E.; Cooper, J.A.; James, P.R. U-Pb and Rb-Sr geochronology and geological evolution of the Harts Range ruby mine area of the Arunta Inlier, central Australia. *Lithos* **1987**, *20*, 445–467. [[CrossRef](#)]
193. Aboosally, S. Update on production in Pakistan, Afghanistan. *Jew. News Asia* **1999**, *1*, 60–64.
194. Morishita, T.; Kodera, T. Finding of corundum-bearing gabbro boulder possibly derived from the Horoman peridotite complex, Hokkaido, northern Japan. *J. Mineral. Petrol.* **1998**, *93*, 52–63. [[CrossRef](#)]
195. Pratt, J.H. The occurrence and distribution of corundum in the United States. *Geol. Surv. Bull.* **1901**, *180*, 98.
196. Senoble, J.B. An expedition to Tanzania’s new ruby deposit in Winza. *InColor* **2008**, 44–45. Available online: <https://www.gemstone.org/incolor/Incolor07/index.html#44> (accessed on 27 June 2020).
197. Peretti, A.; Peretti, F.; Kanpraphai, A.; Bieri, W.; Hametner, C.; Günther, D. Winza rubies identified. *Contrib. Gemol.* **2008**, *7*, 1–97.
198. Pardieu, V.; Chauviré, B. Les rubis du Mozambique. *Le Règne Minéral* **2013**, *2*, 101–108.
199. Nicollet, C. Crustal evolution of the granulites of Madagascar. In *Granulites and Crustal Evolution*; Vielzeuf, D., Vidal, P., Eds.; Springer: Berlin, Germany, 1990; pp. 291–310.
200. Pardieu, V.; Sangsawong, S.; Chauviré, B.; Massi, L.; Sturman, N. Rubies from the Montepuez area (Mozambique), Bangkok, GIA Laboratory. 2013. Available online: https://www.gia.edu/doc/GIA_Ruby_Montepuez_Mozambique.pdf (accessed on 25 June 2020).

201. Vertriest, W.; Pardieu, V. Update on gemstone mining in northern Mozambique. *Gems Gemol.* **2016**, *52*, 404–409. [[CrossRef](#)]
202. Norconsult Consortium Mineral Resources Management Capacity Building Project, Republic of Mozambique; Component 2: Geological Infrastructure Development Project, Geological Mapping Lot 1; Geophysical Interpretation; Report no. B4; National Directorate of Geology: Maputo, Republic of Mozambique, 2007.
203. Norconsult Consortium Mineral Resources Management Capacity Building Project, Republic of Mozambique; Component 2: Geological Infrastructure Development Project, Geological Mapping Lot 1; Sheet Explanation: 32 sheets; Scale: 1: 250000; Report no. B6.f; National Directorate of Geology: Maputo, Republic of Mozambique, 2007.
204. Boyd, R.; Nordgulen, O.; Thomas, R.J.; Bingen, B.; Bjerkgard, T.; Grenne, T.; Henderson, I.; Melezhik, V.A.; Often, M.; Sandstad, J.S.; et al. The geology and geochemistry of the East African Orogen in Northeastern Mozambique. *S. Afr. J. Geol.* **2010**, *113*, 87–129. [[CrossRef](#)]
205. Viola, G.; Henderson, I.H.C.; Bingen, B.; Thomas, R.J.; Somethurst, M.A.; de Azavedo, S. Growth and collapse of a deeply eroded orogen: Insights from structural, geological and geochronological constraints on the Pan-African evolution of NE Mozambique. *Tectonics* **2008**, *27*, 1–31. [[CrossRef](#)]
206. Stern, R.J. Arc assembly and continental collision in the Neoproterozoic East African Orogen: Implications for the consolidation of Gondwanaland. *Annual Rev. Earth Planet. Sci.* **1994**, *22*, 319–351. [[CrossRef](#)]
207. Smith, C.P.; Gübelin, E.J.; Bassett, A.M.; Manandhar, M.N. Rubies and fancy-color sapphires from Nepal. *Gems Gemol.* **1997**, *33*, 24–41. [[CrossRef](#)]
208. Bowersox, G.W.; Foord, E.E.; Laurs, B.M.; Shigley, J.E.; Smith, C.P. Ruby and sapphire from Jegdalek, Afghanistan. *Gems Gemol.* **2000**, *36*, 110–126. [[CrossRef](#)]
209. Pêcher, A.; Giuliani, G.; Garnier, V.; Maluski, H.; Kausar, A.B.; Malik, R.M.; Muntaz, H.R. Geology and Geochemistry of the Nangimali ruby deposit area, Nanga-Parbat Himalaya (Azad Kashmir, Pakistan). *J. Asian Earth Sci.* **2002**, *21*, 265–282. [[CrossRef](#)]
210. Pham, V.L.; Pardieu, V.; Giuliani, G. Update on gemstone mining in Luc Yen, Vietnam. *Gems Gemol.* **2014**, *49*, 233–245.
211. Dunn, P.; Frondel, C. An uncommon margarite/corundum assemblage from Sterling Hill, New Jersey. *Mineral. Rec.* **1990**, *21*, 425–427.
212. Dzikowski, T.J.; Groat, L.A.; Dipple, G.M.; Marshall, D. Origin of the Revelstoke carbonate-hosted gem corundum occurrence, British Columbia, Canada. In Proceedings of the International Mineralogical Association Conference, Budapest, Hungaria, 21–27 August 2010.
213. Kyaw, T. The Igneous Rocks of the Mogok Stone Tract: Their Distributions, Petrography, Petrochemistry, Sequence, Geochronology and Economic Geology. Ph.D. Thesis, University of Yangon, Yangon, Myanmar, 2007.
214. Garnier, V.; Ohnenstetter, D.; Giuliani, G. L'aspidolite fluorée: Rôle des évaporites dans la genèse du rubis des marbres de Nangimali (Azad-Kashmir, Pakistan). *Comptes Rendus Geoscience* **2004**, *336*, 1245–1253. [[CrossRef](#)]
215. Gordon, S.G. Desilicated pegmatites. *Proc. Acad. of Nat. Sci. Phila.* **1921**, *73*, 169–192. Available online: <https://www.jstor.org/stable/4063801> (accessed on 17 May 2020).
216. Lawson, A.C. Plumasite, an oligoclase corundum rock, near Spanish Peak, California University of California. *Pub. Geol. Sci.* **1903**, *3*, 219–229.
217. Seifert, A.V.; Hyrsl, J. Sapphire and garnet from Kalalani, Tanga Province, Tanzania. *Gems Gemol.* **1999**, *35*, 108–120. [[CrossRef](#)]
218. Meng, F.; Shmelev, V.R.; Kulikova, K.V.; Ren, Y. A red-corundum-bearing vein in the Rai-Iz ultramafic rocks, Polar Urals, Russia: The product of fluid activity in a subduction zone. *Lithos* **2018**, *320–321*, 302–314. [[CrossRef](#)]
219. Simonet, C. Geology of the Yellow Mine (Taita-Taveta District, Kenya) and other yellow tourmaline deposits in East Africa. *J. Gemmol.* **2000**, *27*, 11–29. [[CrossRef](#)]
220. Terekhov, E.N. REE distribution in corundum-bearing and other metasomatic rocks during the exhumation of metamorphic rocks of the belmorian belt of the Baltic Shield. *Geochem. Int.* **2007**, *45*, 364–380. [[CrossRef](#)]
221. Bindeman, I.N.; Schmitt, A.K.; Evans, D.A.D. Origin of the lowest-known $\delta^{18}\text{O}$ silicate rock on Earth in Paleoproterozoic Karelian rift. *Geology* **2010**, *38*, 631–634. [[CrossRef](#)]
222. Vysotskiy, S.V.; Ignat'ev, A.V.; Levitskii, V.I.; Nechaev, V.P.; Velivetskaya, T.A.; Yakovenko, V.V. Geochemistry of stable oxygen and hydrogen isotopes in minerals and corundum-bearing rocks in northern Karelia as an indicator of their unusual genesis. *Geochem. Int.* **2014**, *52*, 773–782. [[CrossRef](#)]

223. Spiridonov, E.M. Gemstone deposits of the former Soviet Union. *J. Gemmol.* **1998**, *26*, 111–124. [[CrossRef](#)]
224. Walker, R.J.; Prichard, H.M.; Ishiwatari, A.; Pimentel, M. The osmium isotopic composition of convecting upper mantle deduced from ophiolite chromites. *Geochim. Cosmochim. Acta* **2002**, *66*, 329–345. [[CrossRef](#)]
225. Vakhrusheva, N.V.; Ivanov, K.S. The nature and age of plagioclases in the ultrabasic Rai-Iz massif (Polar Urals). *Dokl. Earth Sci.* **2018**, *480*, 587–590. [[CrossRef](#)]
226. Giuliani, G.; Groat, L.; Marshall, D.; Branquet, Y. Emerald deposits: A review and enhanced classification. *Minerals* **2019**, *9*, 105. [[CrossRef](#)]
227. Glodny, J.; Austrheim, H.; Molina, J.F.; Rusin, A.; Seard, D. Rb/Sr record of fluid-rock interaction in eclogites: The Marun-Keu complex, Polar Urals, Russia. *Geochim. Cosmochim. Acta* **2003**, *67*, 4353–4373. [[CrossRef](#)]
228. Bryanchaninova, N.I.; Makeev, A.B.; Zubkova, N.V.; Filipov, N.V. Sodium-strontium mica $\text{Na}_{0.50}\text{Sr}_{0.25}\text{Al}_2(\text{Na}_{0.25}\square_{0.75})\text{Al}_{1.25}\text{Si}_{2.75}\text{O}_{10}(\text{OH})_2$ from Rubinovyi Log. *Dokl. Earth Sci.* **2004**, *395*, 260–265.
229. Korzhinskii, D.S. *Theory of Metasomatic Zoning*; Clarendon Press: Oxford, UK, 1970.
230. Lacroix, A. *Les Gisements de Phlogopites de Madagascar et les Pyroxénites qui les Renferment: Ann. Géol. Serv. Min.*; Imprimerie officielle: Tananarive, Madagascar, 1941.
231. Lacroix, A. *Minéralogie de Madagascar, tome 1*; Challamel A.: Paris, France, 1922.
232. Raith, M.M.; Rakotondrazafy, R.; Sengupta, P. Petrology of corundum-spinel-sapphirine-anorthite rocks (sakenites) from the type locality in Southern Madagascar. *J. Metam. Geol.* **2008**, *26*, 647–667. [[CrossRef](#)]
233. Devouard, D.; Raith, M.M.; Rakotondrazafy, R.; El-Ghozzi, M.; Nicollet, C. Occurrence of musgravite in anorthite-corundum-spinel-sapphirine rocks (sakenites) from south Madagascar: Evidence for a high-grade metasomatic event. In Proceedings of the 18th General Meeting of the International Mineralogical Association, Edinburgh, Scotland, 1–6 September 2002.
234. Keulen, N.; Kokfelt, T.F. The Homogenization Team. A Seamless, Digital, Internet-Based Geological Map of South-West and Southern West Greenland, 1:100,000, 61. Geological Survey of Denmark and Greenland. 2011, pp. 300–364. Available online: <http://geuskort.geus.dk/gisfarm/svgrl.jsp> (accessed on 5 September 2018).
235. Keulen, N.; Schumacher, J.C.; Næraa, T.; Kokfelt, T.F.; Scherstén, A.; Szilas, K.; van Hinsberg, V.J.; Schlatter, D.M.; Windley, B.F. Meso- and Neoproterozoic geological history of the Bjørnesund and Ravns Storø Supracrustal Belts, southern West Greenland: Settings for gold enrichment and corundum formation. *Precambrian Res.* **2014**, *254*, 36–58. [[CrossRef](#)]
236. Polat, A.; Fryer, B.J.; Appel, P.W.U.; Kalvig, P.; Kerrich, R.; Dilek, Y.; Yang, Z. Geochemistry of anorthositic differentiated sills in the Archean (~2970 Ma) Fiskensæset Complex, SW Greenland: Implications for parental magma compositions, geodynamic setting, and secular heat flow in arcs. *Lithos* **2011**, *123*, 50–72. [[CrossRef](#)]
237. Yakymchuk, C.; Szilas, K. Corundum formation by metasomatic reactions in Archean metapelite, southern West Greenland—Identification of exploration vectors for ruby deposits within high-grade greenstone belts. *Geosci. Front.* **2018**, *9*, 727–749. [[CrossRef](#)]
238. Appel, C.C.; Appel, P.W.U.; Rollinson, H.R. Complex chromite textures reveal the history of an early Archean layered ultramafic body in West Greenland. *Mineral. Mag.* **2002**, *66*, 1029–1041. [[CrossRef](#)]
239. Poulsen, M.D.; Paulick, H.; Rosa, D.; van Hinsberg, V.J.; Petersen, J.; Thomsen, L.L. Follow-up on Ujarassiorit mineral hunt finds and outreach activities, South-East Greenland. In *Review of Survey Activities 2014*; Bennike, O., Garde, A.A., Watt, W.S., Eds.; Geological Survey of Denmark and Greenland Bulletin: Greenland, Denmark, 2015; Volume 33, pp. 53–56. Available online: www.geus.dk/publications/bull (accessed on 25 June 2020).
240. Ralantoarison, L.T. Les Corindons Associés aux Roches Métamorphiques du Sud de Madagascar: Le Gisement de Saphirs de Sahambano (Sud-Est d’Ihosy). Master’s Thesis/Mémoire de DEA, Université d’Antananarivo, Antananarivo, Madagascar, 2006.
241. Ralantoarison, T.; Offant, Y.; Andriamamonjy, A.; Giuliani, G.; Rakotondrazafy, A.F.M.; Ohnenstetter, D.; Schwarz, D.; Fallick, A.E.; Razanatsheho, M.; Rakotosamizanany, S.; et al. Les saphirs multicolores de Sahambano et Zazafotsy, région granulitique d’Ihosy, Madagascar. *Rev. Assoc. Fr. Gemmol. AFG* **2006**, *158*, 4–13.
242. Andriamamonjy, S.A. Importance des fluides sur la métallogénie des gisements de saphirs et de rubis dans le domaine granulitique de haute température du Sud de Madagascar: Cas de Zazafotsy et d’Ambatomena. Ph.D. Thesis, Université d’Antananarivo, Antananarivo, Madagascar, 2010.

243. Andriamamonjy, A.; Giuliani, G.; Ohnenstetter, D.; Rakotondrazafy, A.F.M.; Ralantoarison, T.; Ranatsenho, M.M.; Rakotosamizanany, S.; Fallick, A.E. Les corindons d'âge néoproterozoïque de Madagascar. *Le Règne Minéral* **2013**, *2*, 109–117.
244. Feneyrol, J.; Giuliani, G.; Ohnenstetter, D.; Fallick, A.E.; Martelat, J.-M.; Monié, P.; Dubessy, C.; Rollion-Bard, C.; Le Goff, E.; Malisa, E.; et al. Worldwide tsavorite deposits: New aspects and perspectives. *Ore Geol. Rev.* **2013**, *53*, 1–25. [CrossRef]
245. Malik, R.H. *Geology and Ressource Potential of Kashmir Ruby Deposits*; Unpublished Report; Azad-Kashmir Mineral and Industrial Development Corporation: Muzaffarabad (Azad-Kashmir), Pakistan, 1994.
246. Ray, H.N.; MacRae, G.P.; Cain, L.J.; Malloch, K.R. *New South Wales Industrial Minerals Data Base*, 2nd ed.; Geological Survey of New South Wales: Sydney, Australia, 2013.
247. Oakes, G.; Barron, L.M.; Lishmund, S.R. Alkali basalts and associated volcanoclastic rocks as a source of sapphire in Eastern Australia. *Aust. J. Earth Sci.* **1996**, *43*, 289–298. [CrossRef]
248. Sutherland, F.L.; Coenraads, R.R. An unusual ruby-sapphire-sapphirine-spinel assemblage from the Tertiary Barrington volcanic province, New South Wales. *Austr. Mineral. Mag.* **1996**, *60*, 623–638. [CrossRef]
249. Webb, G.; Sutherland, F.L. Gemstones of New England. *Austr. J. Mineral.* **1998**, *4*, 115–121.
250. Abduryiyim, A.; Sutherland, F.L.; Coldham, T. Past, present and future of Australian gem corundum. *Austr. Gemmol.* **2012**, *24*, 234–242.
251. Vichit, P.; Vudhichatvanich, S.; Hansawek, R. The distribution and some characteristics of corundum-bearing basalts in Thailand. *J. Geol. Soc. Thailand* **1978**, *M4*, 1–27.
252. Liu, Y.; Lu, R. Ruby and sapphire from Muling, China. *Gems Gemol.* **2016**, *52*, 98–100.
253. Sutherland, F.L.; Graham, I. *Geology of the Barrington Tops Plateau; It s Rocks, Minerals and Gemstones, New South Wales, Australia*; The Australian Museum Society: Sydney, Australia, 2003; p. 56.
254. Birch, W.D. Gem corundum from the St Arnaud district, western Victoria, Australia. *Austr. J. Mineral.* **2008**, *14*, 73–78.
255. Schwarz, D.; Schmetzer, K. Rubies from the Vatomandry area, eastern Madagascar. *J. Gemmol.* **2001**, *27*, 409–416. [CrossRef]
256. Rasimanana, G. Caractérisations Géochimiques et Géochronologiques de Trois Épisodes Magmatiques (Crétacé, Miocène Terminal et Quaternaire) à Madagascar Liés aux Phénomènes de Rifting. Ph.D. Thesis, Université d'Orsay, Paris, France, 1996.
257. Chapin, M.; Pardieu, V.; Lucas, A. Mozambique: A ruby discovery for the 21st century. *Gems Gemol.* **2015**, *51*, 44–54. [CrossRef]
258. Hsu, T.; Lucas, A.; Pardieu, V. Mozambique: A Ruby Discovery for the 21st Century. GIA Research News. 2014. Available online: <https://www.gia.edu/gia-news-research-mozambique-expedition-ruby-discovery-new-millennium> (accessed on 25 June 2020).
259. Kane, R.E.; Kammerling, R.C. Status of ruby and sapphire mining in the Mogok Stone Tract. *Gems Gemol.* **1992**, *28*, 152–174. [CrossRef]
260. Kammerling, R.C.; Scarratt, K.; Bosshart, G.; Jobbins, E.A.; Kane, R.E.; Gübelin, E.J.; Levinson, A.A. Myanmar and its gems-an update. *J. Gemmol.* **1994**, *24*, 3–40. [CrossRef]
261. Garnier, V.; Giuliani, G.; Ohnenstetter, D.; Schwarz, D.; Kausar, A.B. Les gisements de rubis associés aux marbres de l'Asie centrale et du Sud-est. *Le Règne Minéral* **2006**, *67*, 17–48.
262. Kane, R.E.; McClure, S.F.; Kammerling, R.C.; Khoa, N.D.; Mora, C.; Repetto, S.; Khai, N.D.; Koivula, J.I. Rubies and fancy sapphires from Vietnam. *Gems Gemol.* **1991**, *27*, 136–155. [CrossRef]
263. Keller, P. *Gemstones of East Africa*; Geoscience Press: Phoenix, AZ, USA, 1992.
264. Henn, U.; Milisenda, C.C. Neue Edelsteinvorkommen in Tansania: Die region Tunduruzongea. *Z. Deut. Gemmol. Gesell.* **1997**, *46*, 29–43.
265. Pardieu, V.; Vertriest, W.; Weeramonkhonlert, V.; Raynaud, V.; Atikarnsakul, U.; Perkins, R. Sapphires from the Gem Rush Bemainty Area, Ambatondrazaka (Madagascar). GIA Research News. 2017. Available online: <https://www.gia.edu/gia-news-research/sapphires-gem-rushbemainty-ambatondrazaka-Madagascar> (accessed on 20 June 2020).
266. Pardieu, V.; Sangsawong, S.; Detroyat, S. Gem News International: Rubies from a new deposit in Zahamena National Park, Madagascar. *Gems Gemol.* **2015**, *51*, 454–456.

267. Thirangoon, K. Ruby and Pink Sapphire from Aappaluttoq, Greenland: Status of Ongoing Research, GIA, Bangkok, Thailand. 2009. Available online: <https://www.gia.edu/gia-news-research-nr32309> (accessed on 20 June 2020).
268. Palke, A.C. Coexisting rubies and blue sapphires from major world deposits: A brief review of their mineralogical properties. *Minerals* **2020**, *10*, 472. [[CrossRef](#)]
269. Palke, A.C.; Breeding, C.M. The origin of needle-like inclusions in natural gem corundum: A combined EPMA, LA-ICP-MS, and nanoSIMS investigation. *Am. Mineral.* **2017**, *102*, 1451–1461. [[CrossRef](#)]
270. Franz, G.; Vyshnevskiy, O.; Taran, M.; Khomenko, V.; Wiedenbeck, M.; Schiperski, F.; Nissen, J. A new emerald occurrence from Kruta Balka, Western Peri-Azovian region, Ukraine: Implications for understanding the crystal chemistry of emerald. *Am. Mineral.* **2020**, *105*, 162–181. [[CrossRef](#)]



© 2020 by the authors. Licensee MDPI, Basel, Switzerland. This article is an open access article distributed under the terms and conditions of the Creative Commons Attribution (CC BY) license (<http://creativecommons.org/licenses/by/4.0/>).